AASERT Contract F49620-95-1-0386
AFOSR Contract F49620-95-1-0132

DEVELOPMENT OF A CUMULUS PARAMETERIZATION SUITABLE FOR USE IN MESOSCALE THROUGH GCM-SCALE MODELS

by Scot C. R. Rafkin

William R. Cotton, P.I.

Colorado State University

DEPARTMENT OF ATMOSPHERIC SCIENCE

PAPER NO. 611

DEVELOPMENT OF A CUMULUS PARAMETERIZATION SUITABLE FOR USE IN MESOSCALE THROUGH GCM-SCALE MODELS

by

Scot C. R. Rafkin

Department of Atmospheric Science

Colorado State University

Fort Collins, CO 80523

Research Supported by

Augmentation Awards for Science and Engineering Research Training

under Contract F49620-95-1-0386

Air Force Office of Scientific Research

under Contract F49620-95-1-0132

June 11, 1996

Atmospheric Science Paper No. 611

ABSTRACT

DEVELOPMENT OF A CUMULUS PARAMETERIZATION SUITABLE FOR USE IN MESOSCALE THROUGH GCM-SCALE MODELS

A cumulus parameterization is described and implemented into the Regional Atmospheric Modelling System (RAMS). Although specifically formulated for use in mesoscale model applications, it can be applied with equal validity in larger-scale models. The new cumulus parameterization is a hybrid mass flux and adjustment scheme. The mass flux component closely follows the theory developed in the Arakawa-Schubert parameterization to describe the change in the cloud environment due to cumulus induced subsidence and detrainment. However, the cloud-base mass flux is computed using a prognostic cumulus kinetic energy equation. The adjustment component describes the change in the grid average property due to the expansion or contraction of cloud area. Unlike most adjustment schemes, the adjustment time scale is not the lifetime of convection, but the growth rate of convective area. Therefore, the adjustment term can either nudge the grid average property toward the cloud profile or toward the environment value. The major benefit of this parameterization is that it is designed to be valid over scales ranging from meso-γ (5 km) to GCM scale (200 km) grid spacings. Comparison of explicitly simulated convection at a horizontal grid resolution of 1.5 km with parameterized simulations at 20 km, 12 km and 6 km are made. Comparisons to the Kuo parameterization are also discussed. Results indicate

that the new parameterization does a good job at reproducing the effects of convection as simulated in the cloud resolving simulations, and performs immensely better than the Kuo parameterization.

ACKNOWLEDGEMENTS

The completion of this work would not have been possible without the help of an enormous number of people. First and foremost, I would like to thank my wife, Gina, who has given me unending moral support and understanding. She has more than graciously handled what often seemed like a never ending process and for this I will always be grateful. I also need to thank my adviser, William Cotton, who took me on as a last minute Ph.D. student when this whole thing started back in 1993. He has always had confidence in my abilities and given me encouragement on the "down days". Instead of just being a boss, he has treated me as a peer—an admirable quality which seems to be on the decline in this department. Finally, Bill has been a friend with whom I have enjoyed running, backpacking and flying. Hopefully there is more to come! I am grateful to my committee for their insight, comments and suggestions during the preparation of this dissertation. Many others have spent what have probably added up to hundreds of hours discussing my research. In particular, I would like to acknowledge Hongli Jiang, Robert Walko, Michael Meyers and Peter Olsson for unselfishly yielding their time to my interruptions and rambling, verbal brain storms. Brenda Thompson and Abby Hodges have been indispensable and always seemed to be able to help me work through the department paperwork and politics. Countless other friends and family have contributed in one way or another to this dissertation or helped me maintain my sanity, and I hope they will forgive me for not explicitly mentioning their names. Last, but certainly not least, I would like to thank my Grandmother, Zelda and my late Grandfather, Sol, who have always been there for me no matter what the circumstances. This research was

supported by Augmentation Awards for Science and Engineering Research Training under Contract F49620-95-1-0386 and Air Force Office of Scientific Research under Contract F49620-95-1-0132

LIST OF FIGURES

LIST OF TABLES

Chapter 1

INTRODUCTION

1.1 Motivation and Objectives

This dissertation describes the development and implementation of a cumulus parameterization scheme designed explicitly for mesoscale models, although it may be applied with equal validity in larger-scale models. The rise of mesoscale and regional numerical models over the last decade necessitates the development of parameterizations for atmospheric convective phenomena which are not completely resolved. Schemes valid at scales from roughly five to one hundred kilometers are few in number (Kreitzberg and Perkey (1976); Fritsch and Chappel (1980); Weissbluth and Cotton (1993a)), and have generally been applied only in situations with strongly forced, quasi-steady convection. The ability of these schemes to account for less organized and weakly forced convection has not been widely investigated with the exception of perhaps Weissbluth and Cotton (1993b). Furthermore, many of these parameterization schemes use assumptions with questionable validity as the grid spacing is reduced. Even worse, cumulus parameterizations designed for large-scale models with grid spacings on the order of hundreds of kilometers such as Kuo (1965), Arakawa and Schubert (1974), Betts (1986), and Betts and Miller (1986), are often applied at the finer grid spacings despite the potentially increasing errors in assumptions as the horizontal grid dimensions are reduced.

One reason cumulus parameterization in mesoscale models is particularly challenging is because convection may already be partially resolved. This problem is

not encountered in large-scale models; there is a clear scale separation between the resolved large-scale energy associated with atmospheric circulations and the unresolved energy associated with convection. Therefore, in a large-scale model there is no danger in parameterizing a convective phenomena which may be partially or completely resolved. The possibility of *double counting* in a mesoscale model is significant. In some way, a convective parameterization in a mesoscale model must begin to shutdown as the model begins to resolve the phenomena.

Another desirable feature of a mesoscale convective parameterization would be its ability to reduce to a large-scale parameterization when grid spacings become large, and bypass the problem of having to decide, usually somewhat arbitrarily, when to switch from one parameterization scheme to another. This raises the question as to whether or not there exists a smooth transition from the non-deterministic view of convection at GCM-like scales to the deterministic view typically taken at so-called cloud resolving scales. The answer to this question will be discussed in a later chapter.

Using the nomenclature of Arakawa and Schubert (1974; hereafter AS74), the parameterization described in this manuscript consists of three parts: feedback, static control, and dynamic control. The feedback loop determines how the cumulus affect the model resolved prognostic variables. Essentially, this amounts to specifying the form of the cumulus eddy flux divergence. The static control is a cumulus ensemble model. Here, the resolved properties are used to determine the in-cloud properties of a spectrum of clouds which could exist in the given environment. The dynamic control is synonymous with the parameterization closure. Rather than the quasi-equilibrium assumption proposed by AS74, a prognostic cumulus kinetic energy equation (Randall and Pan 1993) is used to obtain the cloud base mass flux for each ensemble. The feedback, static control and dynamic control will be discussed in more detail in Chapter 2.

The major original scientific contribution of the convective parameterization presented in this paper is that it addresses the issue of grid-scale flexibility. Therefore, the parameterization is a unifying theory, since it is valid from the GCM-like scales to the mesoscale. Another significant contribution is the departure from the mesoscale convective parameterization paradigm. In the past, parameterizations designed for mesoscale models typically followed this basic recipe: 1) conditional instability; 2) trigger function; 3) cloud model; 4) feedback. This class of parameterizations has been successful under many circumstances. However, the return per unit effort following the standard parameterization paradigm is decreasing. We have tried to take a step back and re-examine the parameterization problem with an open mind; sometimes it is hard to see the forest for the trees. The outcome of this research is a new mesoscale parameterization philosophy, method, framework and design.

1.2 A New Paradigm

The previous section of this chapter posed the rhetorical question "is there a smooth transition from the deterministic view of convection taken at cloud-resolving scales to the non-deterministic view of convection taken at large, GCM-like scales?" In order to address this question, we will first define some terminology. Throughout the rest of this manuscript we will define the *cloud ensemble* to be the set of all *possible* types of clouds which *could* exist in a given environment. The *active cloud population* or just *active population* is defined as the subset of the ensemble which *actually* exists in a given area.

In some cases the active population will be the cloud ensemble. This is what is assumed in the Arakawa-Schubert parameterization. The set of all possible clouds is defined as a collection of cloud types defined by the single entrainment parameter, and all the cloud types contribute (*i.e.*, they exist) to the net cumulus flux. This of course seems reasonable since we might imagine that a GCM-sized grid box could be large enough to physically contain so many potential clouds. This is also consistent

with one of the primary assumptions of AS74: that the area over which it is applied is large enough to encompass an ensemble of clouds. Another assumption, however, which has never been explicitly stated, although has certainly been applied, is that all the clouds in the ensemble exist in the given area.

1.2.1 Philosophical Continuum

Consider a hypothetical grid box and examine the ensemble and active population as the area of the box shrinks (Fig. 1.1). If the environment confined within the box does not change then the ensemble does not change; the environment determines the set of possible clouds. Therefore, the ensemble is *independent* of the grid spacing or model resolution. The active cloud population however is dependent on the grid spacing. As the grid becomes significantly smaller than a GCM-sized box, we imagine that some cloud types will not be represented within the sample of clouds in the box. If we still wish to apply a convective parameterization that utilizes a cloud model to determine convective fluxes it is necessary to know what the active population is. To do this, we define a probability density function (PDF) for the cloud types.

Let $P(\lambda)d\lambda$ be the probability of sampling cloud types which have entrainment values in the interval $[\lambda, \lambda + d\lambda]$. If we integrate over the whole ensemble then we must have

$$\int_0^\infty P(\lambda)d\lambda = 1. \tag{1.1}$$

For the sake of discussion, assume that $P(\lambda)$ is graphically given by Fig. 1.2. Cloud types with small entrainment values (big clouds) are not as common as the smaller cloud types with larger entrainment values. From a statistical standpoint, if the grid box is too small to contain the entire ensemble, we can certainly make a reasonable guess at which ones will and will not be represented in our sample. As an example, suppose our box was only big enough to contain one cloud (or one cloud type), and we had to place a bet on what the one cloud (the active population) was. The

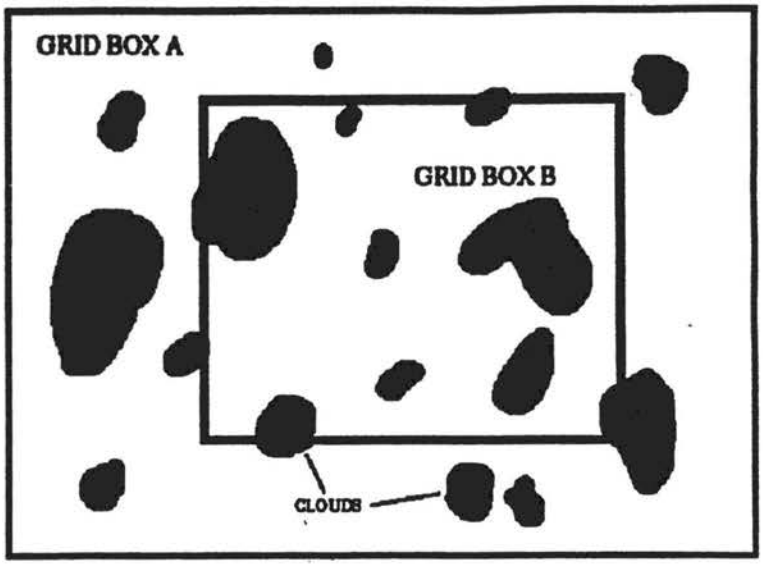

Figure 1.1: Hypothetical grid boxes A and B. The cloud ensemble is a function of the environment, but the active population is determined by the size of the grid box. The grid box A is large enough so that the active population is identical to the ensemble. The smaller grid box B can not physically contain the ensemble. The active population in grid Box B is a subset of the ensemble.

smart money would have to be on the most likely cloud to be found in the given environment: the smallest cloud type. In a larger box which might contain n cloud types, we would chose the n most likely clouds. Of course, we will occasionally be wrong and choose an incorrect active population. For example, you may run the risk of not including or sampling large cumulonimbi even though the CAPE is large and the Richardson Numbers is small. Another possibility—and the one used in this parameterization—is to partition your money so that you bet on all cloud types, but weight your bet according to $P(\lambda)$. This method allows all possible cloud types to exist to some degree; the PDF determines the relative activity of each type.

The AS74 parameterization does not require a PDF since it assumes that all possible clouds exist. Equivalently, if a PDF for the ensemble were defined, AS74 would take infinite samples to determine the active population which by definition would then be equivalent to the ensemble itself.

Unlike AS74, many parameterization schemes use only a single cloud type for the active population (Weissbluth (1991); Fritsch and Chappel (1980); Kreitzberg

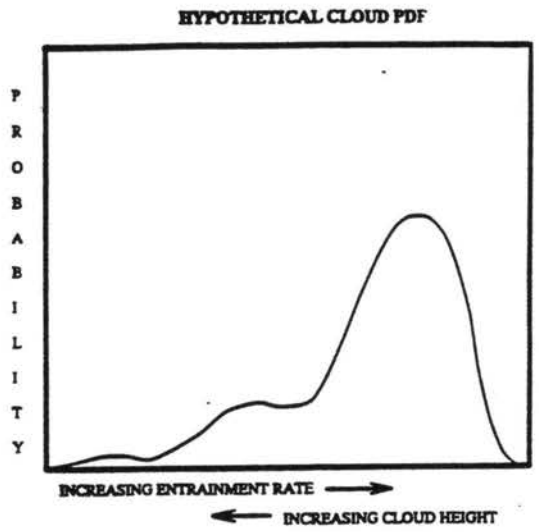

Figure 1.2: A hypothetical cloud probability density function. The smaller clouds (large entrainment) are more likely than the taller clouds (small entrainment). The PDF should be used to determine what fraction of sub-ensembles are in the active population.

and Perkey (1976); Kuo (1965)). This would perhaps be acceptable as long as the single cloud type was the most probable cloud type (or nearly so). It would also be sufficient if the single cloud could capture the characteristics of all possible clouds. Unfortunately, there is no reason to believe that this would be the case.

Recently, another class of cloud models used in parameterizations has appeared: buoyancy sorting models (Kain and Fritsch 1990; Emanuel 1991). The basic idea is to allow fractions of an ascending parcel to mix with different quantities of environmental air to produce sub-parcels with a spectrum of buoyancies. These sub-parcels are then allowed to ascend or descend to levels in the environment with the same corresponding buoyancy. The collection of the sub-parcels determines the cloud profile. Therefore, these types of cloud models represent single clouds with multiple drafts. While the buoyancy sorting model probably represents an improvement over single cloud/single draft models, it is not entirely clear that they are significantly different from multiple cloud/single draft models, for example AS74. It may be that a collection of clouds with single drafts produces nearly identical results to a single

cloud with multiple drafts. The major difference seems to be that the multiple cloud models allow cloud mass fluxes which are independent while the mass flux associated with the sub-parcels of the buoyancy sorting models are inherently connected. In this sense, the multiple cloud models seem to have an advantage, but it all remains to be seen.

To illustrate the potential hazards of using a single cloud type, consider the experience we have had using the Weissbluth convective parameterization in a Florida sea-breeze simulation (Weissbluth and Cotton 1993b). Observations and explicit modelling have demonstrated that there are two modes of convection. The first mode consists of transient cumulonimbi and smaller towering cumuli occurring prior to the collision of the inland propagating east and west coast sea-breezes. The second mode consists of deep, long-lived cumulonimbi which fire after the two sea breezes collide in the region of strong convergence.

During the parameterized simulation, deep, long-lived cumulonimbi were parameterized to provide the cumulus fluxes. This was by design, since the cloud model used in the parameterization was only capable of producing a single, deep and steady-state cloud type. Unfortunately, it was not the most likely cloud type for the given environment, and the predicted grid-scale cumulus tendencies were much too strong and resulted in excessive stabilization (warming and drying) of the atmosphere. When the sea-breezes finally collided, the parameterization failed to produce the strong cumulus forcing which was expected based on the observations and explicit modelling. This was attributed to the exhausting of boundary layer energy by the earlier parameterized convection. Had the parameterization been able to model different cloud types and choose transient towering cumuli as the most probably cloud type during the first mode of convection, and deep, steady-state cumulonimbi during the second mode, the parameterized solution would have likely been quite good. In fact, a simulation in which convection was explicitly simulated up to the point of sea-breeze

collision and then used to initialize a parameterized simulation produced encouraging results. This shows that choosing the correct active population is quite important.

1.2.2 Spatial Continuity from Cloud Resolving to the Large-scale

When modelling at the cloud resolving scale (on the order of a kilometer or smaller) convection is sometimes considered (perhaps incorrectly) deterministic and other times not. The first view is taken when an individual cloud is simulated. Often the modeller will attempt to compare the simulated cloud with observations. The second view is taken in cumulus ensemble simulations. Here, the modeller makes no effort to compare individual clouds to observed clouds; only statistics from the entire population are examined. These two views, however, are not necessarily in opposition to one another.

Consider two types of cloud resolving simulations of an individual cloud. The first type is typically performed by applying large scale convergence, or a thermal or moisture perturbation to initiate the convection. The second type is performed by beginning at a synoptic-like scale and nesting down to the cloud resolving scale over a limited area. In the first case the modeller forces the solution to a particular cloud type. Typically, a strongly buoyant bubble or increasingly stronger convergence will create deeper convection. In fact, the simulation is often tuned to observations by varying these parameters to produce the most optimal results. The cloud that is simulated should be considered one realization, or one probable solution out of all possible solutions in the given environment. Hopefully, the initial conditions are chosen so that the model correctly models the active cloud which was observed. The simulation, however, should not be considered deterministic; the modeller imposes conditions which select the desired solution from a wide range of possibilities. In the second case of nesting, the interpretation is slightly more complex. Here, the modeller does not artificially impose a solution, although by nesting, the forcing can be focused so that convection may preferentially occur in the region with the nest.

Nonetheless, the simulated clouds seldom match observations either temporally or spatially, but the types of clouds in the given region often do. We discuss a cloud resolving sea-breeze simulation to illustrate this point.

In the sea-breeze simulation the model is initialized according to observations prior to the onset of convection. Upon integration, the model produces convection along the inland propagating sea-breeze which matches in character the observed convection. However, no attempt is made to exactly match individual convective elements to observations. For example, if we were to use the simulation as a forecast model, it would not be wise to predict that Orlando, Florida would experience a thunderstorm exactly of the same type and at same time that was simulated by the model. However, we might forecast that a region around Orlando might experience a thunderstorm similar to the one modelled around a similar time. The simulation should be considered as one possible realization. If we wanted a probability forecast, we would have to run many simulations with slightly varying initial conditions to generate an ensemble of realizations. We could then statistically determine the most probable scenario as is done in ensemble forecasting. In either case it would appear that the modelled cloud should not be considered deterministic. Rather, it should be considered as one realization of all possible scenarios. Hopefully, it is the most probable one in the case of a forecast model, or the one which most closely matches observation.

A cumulus ensemble model representing a non-deterministic viewpoint is almost like running many explicit simulations simultaneously. Under similar environmental conditions and forcing, a population of different cloud types is allowed to develop. Therefore, the cloud ensemble simulation contains many simultaneous realizations. Statistics from the cumulus ensemble determines what the average (or most probable) effect the population has on its environment.

Based on the preceding discussion, there is now a basis upon which we can philosophically describe the smooth transition of cumulus parameterization from just

beyond cloud resolving scales, through the mesoscale, up to GCM-like grid scales. In no situation should the clouds be regarded as being deterministic from a modelling standpoint. A cumulus parameterization that operates just beyond the resolved scale should provide fluxes from the most probable cloud type or from fluxes normalized by a cloud PDF. As the scale increases and more than one cloud can physically fit within a grid box, the parameterization should consider the effect of the most probable set of cloud types. Finally, at large GCM-like scales, the parameterization should consider all cloud types, even the most unlikely. Of course, at the cloud-resolving scale and smaller, a parameterization is not needed at all.

1.2.3 Temporal Continuity from Cloud Resolving to the Large-scale

At large scales, there is assumed to be enough clouds of a particular cloud type so that we do not need to consider the temporal evolution of the clouds. Instead, we only need to consider the average effect over the lifetime of the clouds. As the grid spacing decreases, there may not be enough clouds of a given type to make this assumption.

In a manner similar to what has been done with the selection of cloud types using a PDF, it may be possible to define another PDF which provides the probability of finding a particular cloud type in a given stage of its life-cycle. Then we could select the most probable stage for each member of the active population. Of course, this requires a cloud model which is capable of determining in-cloud properties which are a function of cloud type and time.

Adding time dependence to a cloud model is not trivial. This is especially true if the code must be numerically efficient. We have made the assumption that a time independent cloud model will accurately represent a cloud over its lifetime. This assumption does not discount the possibility of transient convection. The only requirement is that

$$\frac{1}{\tau}\int_0^\tau \chi(t)dt \approx \chi(t) \tag{1.2}$$

where χ is some cloud property and τ is the lifetime of the cloud. There is clearly room for improvement, but this will undoubtedly require significantly more memory since in-cloud properties would have to be carried around for at least two model timesteps.

Chapter 2

CUMULUS PARAMETERIZATION FRAMEWORK

This chapter provides the theoretical framework upon which the cumulus parameterization is based. The description of the parameterization is separated into three components: feedback, static control and dynamic control. Although the components are described somewhat independently, only together do they constitute a complete parameterization.

2.1 Feedback: The Cumulus Eddy Fluxes

The effect of unresolved convection on model resolved variables can be expressed as the divergence of the cumulus eddy flux. For example, the tendency of model variable $\overline{\chi}$ due to unresolved cumulus activity is

$$\frac{\partial \overline{\chi}}{\partial t} = -\frac{1}{\rho} \nabla \cdot \overline{w' \chi'}. \tag{2.1}$$

There are basically two ways to determine the cumulus eddy flux divergence. The first method is to determine the cumulus fluxes and then take a vertical derivative. The second method is to provide the eddy flux divergence directly; the need for an exact form of the flux is eliminated and only its derivative is required. Experience has shown that the first method produces results which are generally only capable of drying and heating the free atmosphere. This is acceptable for large-scale models where the moist cumulus contribute negligibly to the grid average. Examples of this method include the Arakawa-Schubert parameterization where the flux of a conservative scalar quantity χ is

$$\overline{\omega' \chi'} = M_c \bar{\chi} \tag{2.2}$$

and M_c is the cumulus mass flux. If we imagine a non-entraining cloud (constant mass flux as a function of height) then the cumulus will heat the free atmosphere whenever the local atmospheric stability is positive and dry the atmosphere whenever total water mixing ratio decreases with height.

Once the cumulus occupy a significant portion of a model grid box, as they might in a mesoscale model, the cumulus must be able to contribute to the moisture and heat content of the atmosphere by virtue of the warm and moist clouds replacing the drier and cooler environmental air as they expand in area. This can easily be accomplished by specifying the flux divergence (method two). Since we wish the parameterization to function at all scales, we will take a hybrid approach of determining the tendency partly from a specified eddy flux and partly from an eddy flux divergence

Deriving a suitable form of cumulus eddy flux divergence is straight forward. Using subscripts u and d to denote updraft and downdraft cloud properties, respectively, and a tilde to denote properties in the cloud environment, the grid average property denoted by an overbar is constructed as

$$\bar{\chi} = \sum_{clouds} \sigma_u^i \chi_u^i + \sum_{clouds} \sigma_d^i \chi_d^i + (1 - \sigma_c)\tilde{\chi}. \tag{2.3}$$

The superscript i refers to the cloud type and summations are over all cloud types. The total cloud fractional area is σ_c and $\tilde{\chi}$ represents the environment value.

We now take the total derivative of Eq. 2.3 and make a steady-state assumption for the clouds. The motivation for doing this is two-fold. First, if we were to leave in the time rate of change of cloud properties than we would need to develop a time-dependent cloud model–not an easy task. Second, and perhaps more importantly, even if we had a time dependent cloud model, the amount of memory required to store the cloud values from the previous time step for every cloud at every level over the entire model domain is prohibitive. Therefore,

$$\frac{\partial \bar{\chi}}{\partial t} = \sum_{clouds} \left[(\chi_u^i - \tilde{\chi}) \frac{D\sigma_u^i}{Dt} \right] + \sum_{clouds} \left[(\chi_d^i - \tilde{\chi}) \frac{D\sigma_d^i}{Dt} \right] + (1 - \sigma_c)\frac{\partial \tilde{\chi}}{\partial t} - \vec{V} \cdot \nabla \sum_{clouds} (\sigma_u^i \chi_u^i + \sigma_d^i \chi_d^i). \tag{2.4}$$

The first two terms in Eq. 2.4 are adjustment terms. The third term is an environmental subsidence term and the fourth is an advective term. The adjustment terms differ from the those typically used in other parameterizations (Kuo 1965; Weissbluth and Cotton 1993a) in that the timescale of adjustment is not the average lifetime of the cloud but the rate of change of fractional cloud area. Under most circumstances the result will be to nudge the average property toward the in-cloud property if the cloud area is growing or toward the environment value if the cloud area is shrinking. The adjustment process is illustrated in Fig. 2.1 for a growing cloud fractional area.

Generally, the adjustment terms are locally non-conservative. By this we mean that a vertical integration of the adjustment terms over the depth of the cloud will generally be non-zero. A good example is to consider a growing cloud which by definition is moister than the environment; there is a net moisture source over the depth of the cloud. Clearly there must be mass and energy conservation and as we will see, the last term in Eq. 2.4, the advection term, will pick up the slack and provide the necessary conservation.

The third term in Eq. 2.4 is an environmental subsidence term analogous to that derived by AS74. If we make the small cloud fractional area assumption and neglect horizontal eddy convergence we arrive at exactly the same form of the flux given by Eq. 2.2. We close this term as AS74 did and as discussed in a later section. Unlike the adjustment terms and the advection term, the vertical integration of the subsidence term is conservative in a grid column. This is by definition since the cloud mass flux goes to zero below and above the cloud.

Finally, we examine the advection term. This term will cause the grid average value to change by allowing a net convergence or divergence of the cloud property by both resolved and unresolved convective circulations. Because we require the vertically-integrated grid tendency to be zero and the subsidence term is by definition, the net increase or decrease of $\bar{\chi}$ in a column from the adjustment term must be

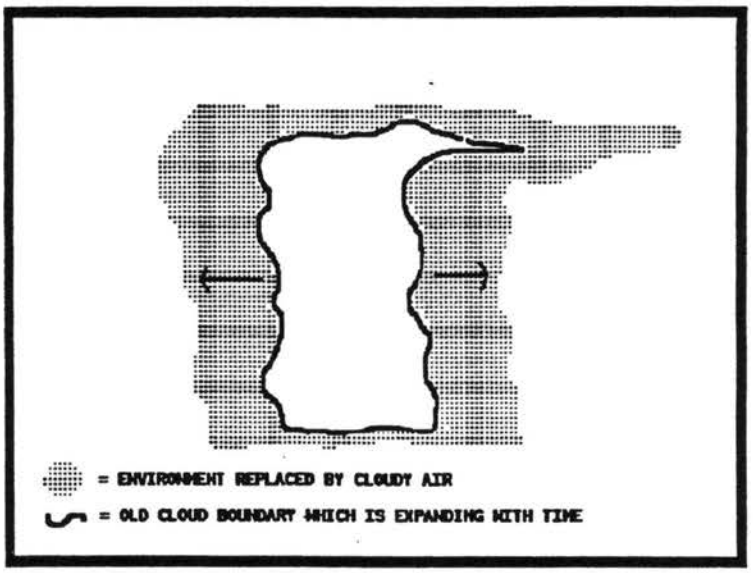

Figure 2.1: The effect of the adjustment term on the resolved grid value depends on the rate of change of cloud fractional area. If the clouds are growing in area, there is less environment to contribute to the grid average. Consequently, the grid average becomes more cloud-like. The opposite occurs when the cloud area shrinks.

accounted for in the advection term. For illustrative purposes let χ be total water. If the adjustment term causes net column moistening (as it would if the cloud area was growing) then this moisture must come from advection of moisture from within the PBL below the cloud or from other grid columns as shown in Fig. 2.2.

The closure of the four terms in Eq. 2.4 will require updraft and downdraft properties, the cloud-base mass flux and the cloud fractional area of the active cloud population within the grid box. In the following sections we describe the cumulus ensemble model which provides the in-cloud properties and the prognostic cumulus kinetic energy (CKE) closure which provides the cloud-base mass flux. The cloud fractional area is obtained using information from both the cumulus model and CKE closure.

2.2 Static Control: Cumulus Ensemble Model

The cumulus ensemble model provides the cloud updraft and downdraft properties. Cloud types, or *sub-ensembles* are distinguished from one another by the

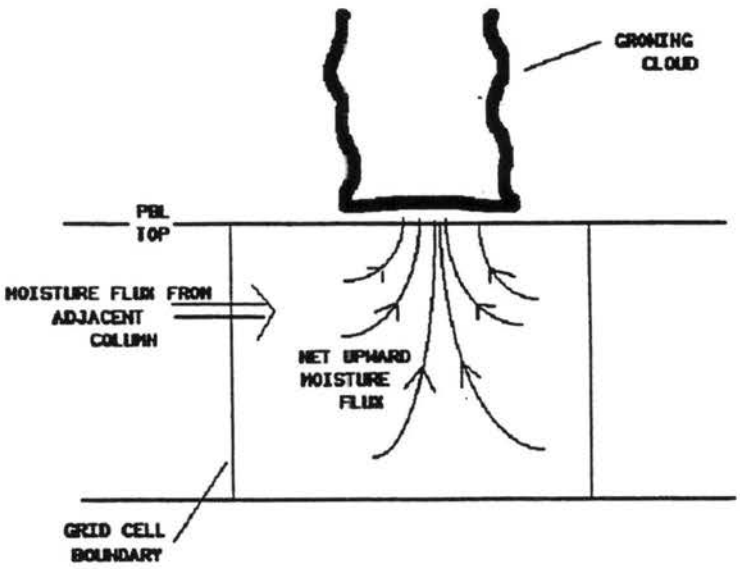

Figure 2.2: In a growing cloud, the adjustment term will cause net moistening. The excess water mass must be provided by the advection term which will dry the PBL or other grid columns. When a cloud shrinks, the excess drying in the free atmosphere will appear as moistening in the PBL or other columns.

single parameter λ which, following AS74, is the fractional entrainment rate. Each cloud of type λ is considered representative of clouds with entrainment in the interval $[\lambda, \lambda + \Delta\lambda]$.

2.2.1 Cloud Updrafts

For cloud i with entrainment $\lambda(i)$, the updraft normalized mass flux (η_u), potential temperature (θ_u), total water (q_u), and microphysical species (q_u^j) are described by

$$\frac{\partial}{\partial z}\eta_u(z,i) = \lambda(i)\eta(z,i), \tag{2.5}$$

$$\frac{\partial}{\partial z}[\eta_u(z,i)\theta_u(z,i)] = \lambda(i)\eta_u(z,i)\theta_u(z,i) + \frac{L_{lv}}{C_pT}C_u(i) + \frac{L_{il}}{C_pT}F_u(i), \tag{2.6}$$

$$\frac{\partial}{\partial z}[\eta_u(z,i)q_u(z,i)] = \lambda(i)\eta_u(z,i)q_u(z,i) - D_u(z,i) - R(z,i), \tag{2.7}$$

$$\frac{\partial}{\partial z}[\eta_u(z,i)q_u^j(z,i)] = \lambda(i)\eta_u(z,i)q_u^j(z,i) - D_u^j(z,i) - S_u(z,i) + C_u^j(z,i) + F_u^j(z,i). \quad (2.8)$$

Although we can construct equations for all the microphysical species in RAMS we choose to do so only for three: cloud water, rain and total ice. There are several reasons for this. First of all, carrying around additional scalars can become numerically expensive and we wish to be as frugal as possible. Second, only very crude parameterizations of microphysical interactions between the species would be possible, and the gain in doing so would likely be minimal. Finally, RAMS will perform more accurate microphysics once microphysical species are on the resolved grid. With only three species in the cloud model we need only worry about conversion of cloud water to rain, freezing of rain to ice and melting of ice to rain. We do not allow cloud water to freeze unless it is below $-40°$C at which point it freezes instantaneously.

Liquid water is condensed from vapor in the amount exceeding the saturation mixing ratio and is denoted by C_u in Eq. 2.6 and releases latent heat into the updraft. At temperatures below freezing, some water may also freeze in amount equal to F_u and provide an additional heat source. The constants L_{lv} and L_{il} are the latent heat of vaporization and sublimation, defined positive for condensation and freezing. The conversion of cloud water (q^c) to rain (q^r) is obtained from a simple auto-conversion formula:

$$q^r = a(q^c - q_*^c) \quad (2.9)$$

where $a = .25$ and $q_*^c = 1 \times 10^{-3}$ is a critical cloud water mixing ratio. The equation is only applied once the calculated cloud water content exceeds the critical amount, and is intended to model the warm rain collision and coalescence process.

Once the updraft temperature falls below freezing, ice processes become active. Ice is formed from the freezing of rain and is parameterized as a linear function of

temperature. All rain is assumed to freeze at temperatures below −20°C. Cloud water does not freeze until a temperature of −40°C is reached as previously stated. Neglect of cloud water freezing will slightly reduce the potential cloud buoyancy since the additional latent heating is not realized.

Total water substance may change through entrainment of environmental air, by the transfer of amount D_u to the downdraft or through removal via convective precipitation. Only rain and ice are affected by transfer to the downdraft and precipitation removal R. The amount of transfer to the downdraft is parameterized as a constant fraction of the updraft condensate:

$$D^j_{u(z,i)} = c_o q^j_{u(z,i)}. \tag{2.10}$$

We have chosen $c_o = 0.25$. Rain and ice are parameterized to fall out of the updraft and contribute directly to surface precipitation following the method of AS74 and Hack *et. al.* (1984; hereafter H84). For simplicity, we have chosen a constant auto-conversion factor for all cloud types even though as pointed out by H84 this may overestimate rainfall from shallow clouds. Currently, we use a value of $2.0 \times 10^{-3}\ m^{-1}$ for this coefficient.

Cloud top is defined as the level at which the cloud buoyancy is equivalent to the the environmental value, including virtual and buoyancy loading effects. Since the clouds generally lose buoyancy between the discrete model levels, the actual cloud top is obtained through linear interpolation and used in all ensuing calculations.

Choosing the origin and initial properties of the cloud updraft parcel is a problem which is not encountered in GCM models with a PBL parameterization. In GCM models the clouds start at the top of the PBL with the well mixed properties of the PBL. RAMS and most other mesoscale models do not contain an explicit PBL parameterization. Therefore, we must decide where the clouds originate and with what properties. Originally, we had tried starting the clouds at the lowest model level. We soon discovered that this was inappropriate. As a general rule, the lowest

model level tended to moisten rapidly over water and moist soil causing the convective available potential energy (CAPE) for that parcel to grow rapidly. However, once the sub-grid scale mixing processes began, the CAPE would be rapidly removed from that layer. Even though the net entropy of the PBL was going up, the CAPE of our low level parcel was going down! Through trial and error, we discovered that starting the parcel at approximately 1 km AGL with a mass weighted mixture of the properties below provided satisfactory results; the CAPE followed the more typical and expected diurnal trend due to large scale forcing from surface fluxes.

The numerical clouds must be physically realistic. Therefore, we impose the following logical constraints:

- The cloud work function, A, must be positive where

$$A(\lambda) = \int_{z_o}^{z_t} \eta(z,\lambda) B(z,\lambda) dz. \tag{2.11}$$

  B is the local buoyancy including virtual and precipitation loading and the integral is from cloud base to cloud top. This is a general criteria for convective instability.

- There must be condensate and the cloud must be saturated at cloud top. This rules out clouds which have entrained so heavily that they are dry.

- The clouds must be at least three model levels deep. This is necessary in order to compute fluxes and tendencies from the clouds. Clouds which are only two model levels deep are assumed to be handled by the sub-grid mixing parameterization.

2.2.2 Determining Updraft Vertical Velocity

Following Simpson and Wiggert (1969), the vertical distribution of kinetic energy of the sub-ensemble updrafts is

$$\frac{1}{2}w^2(\lambda,z) = w_o^2 + \int_{z_b}^{z}[\frac{gB}{1+\beta} - \lambda w^2]dz. \tag{2.12}$$

The arbitrary additive constant w_o^2 is determined by requiring that the updraft always have positive vertical velocity. Typically, the cloud will be negatively buoyant in the lowest layers requiring an initial kinetic energy in order to penetrate to the level of free convection. We have arbitrarily selected the initial kinetic energy to be enough so that the kinetic energy at any cloud level never falls below 1.0 $m^2s^{-2}+TKE$. Here, TKE is the average value of TKE in the PBL as obtained following the Mellor-Yamada (1974) closure currently implemented in RAMS. Sensitivity studies show that varying the initial vertical velocity within reasonable values does not noticeably change the solution.

2.2.3 Cloud downdrafts

The downdrafts are modelled using the ideas proposed by Johnson (1976) and Betts and Silva Dias (1977). The downdraft is assumed to have the same entrainment rate as the corresponding updraft. The budget equations for the downdraft normalized mass flux, theta, total water and microphysical species are

$$\frac{\partial \eta_d(z,i)}{\partial z} = \lambda(i)\eta_d(z,i), \tag{2.13}$$

$$\frac{\partial}{\partial z}[\eta_d(z,i)\theta_d(z,i)] = \lambda(i)\eta_d(z,i)\theta_d(z,i) - \frac{L_{lv}}{C_p}C_d(z,i) - \frac{L_{il}}{C_p}F_d(z,i), \tag{2.14}$$

$$\frac{\partial}{\partial z}[\eta_d(z,i)q_d(z,i)] = \lambda(i)\eta_d(z,i)q_d(z,i) + D_u(z,i), \tag{2.15}$$

$$\frac{\partial}{\partial z}[\eta_d(z,i)q_d^j(z,i)] = \lambda(i)\eta_d(z,i)q_d^j(z,i) - S_d(z,i) + C_d^j(z,i) + F_d^j(z,i). \quad (2.16)$$

The notation is the same as described for the updrafts, but terms C and F represent evaporation and melting.

Downdrafts are assumed to start at cloud top. This is in contrast to other downdraft models which often assume that the downdraft originates at the level of free sink or at some specified fraction of the updraft height or pressure level. The current formulation was necessary in order to preserve mass balance between the updraft and downdraft. If we wanted to start the downdraft at some specified fraction of the updraft depth, we would need to know *a priori* the depth of the updraft. This is impossible without iteration since the cloud top depends on the cloud buoyancy which in turn depends on the downdraft condensate transfer rate.

The initial property of the downdraft is obtained by assuming that the mixing ratio of rain and ice in the updraft is ejected into the environment to produce an evaporatively and sublimatively cooled parcel which is 0.1°K colder than the environment, *i.e.,* just enough to start a negatively buoyant descent. Subsequent evaporation or sublimation is parameterized using the evaporative pressure scale proposed by Betts and Silva Dias (1977). Typically the value is between 50 to 150 mb. Melting of ice occurs instantaneously.

The downdrafts terminate at the level at which they become neutrally buoyant or at the ground, whichever comes first. Like the updraft, the actual level is obtained via linear interpolation since the downdrafts generally end between the discrete model levels. If condensate is present at the ground level, it assumed to fall completely to the ground and contribute to the convective precipitation.

2.3 Dynamic Control: Prognostic Cumulus Kinetic Energy Closure

Randall and Pan (1993; hereafter RP93) relaxed the equilibrium closure assumption used in AS74 to determine the cloud-base ($z = z_o$) mass flux which is defined as

$$M_B = \rho(z_o)w(z_o)\sigma_*(z_o). \tag{2.17}$$

The sub-ensemble fractional area (σ_*) is defined over an area which is large enough to contain the ensemble of clouds, but small enough so as to cover only a fraction of a large-scale disturbance. The closure begins with the cumulus kinetic energy budget equation for a sub-ensemble as discussed by Lord and Arakawa (1980). We re-write it here using slightly different notation:

$$\frac{\partial}{\partial t}CKE(\lambda) = M_B(\lambda)A(\lambda) - D(\lambda). \tag{2.18}$$

The cumulus kinetic energy, CKE, is the vertically-integrated kinetic energy of the sub-ensemble in the interval $[\lambda, \lambda + d\lambda]$ per unit area. The area over which CKE is integrated is the same as the cloud-base mass flux. CKE includes both the horizontal and vertical components of kinetic energy. The rate at which CKE is dissipated per unit cloud-base mass flux is given by D. Shear production terms have been neglected. Since CKE is a vertically-integrated quantity, vertical transport terms such as those involving vertical velocity, or advection of CKE by the cloud do not appear. However, horizontal advection by the mean wind over the depth of the sub-ensemble λ remains. Throughout the rest of this chapter we will drop the explicit notation of λ, however it should be remembered that there exists as many equations as there are sub-ensembles.

Closure involves relating CKE to the cloud-base mass flux according to

$$CKE = \alpha M_B^2, \tag{2.19}$$

as first proposed by Arakawa and Xu (1990) and Xu (1991). Also, the dissipation is modelled in a simple way:

$$D = \frac{CKE}{\tau_D}, \tag{2.20}$$

where τ_D is a dissipation time scale. Substituting Eqs. 2.19 and 2.20 into Eq. 2.18 yields a linear prognostic equation for the cloud-base mass flux:

$$\frac{\partial M_B}{\partial t} = \frac{A}{2\alpha} - \frac{M_B}{2\tau_D}. \tag{2.21}$$

We note that a similar equation could also be derived for the CKE.

Given α and τ_D, the sub-ensemble cloud-base mass flux can now be determined. However, the mass flux in Eq. 2.21 is the mass flux averaged over a large scale area. The large-scale area might be more properly defined as the area which encompasses the subsident inflow and outflow circulations of the convection in the ensemble. If we let this area be $\mathcal{A}$, then the area covered by convective cores is $a = \sigma_* \mathcal{A}$. The fraction of the sub-ensemble (σ) we expect in a grid box smaller than $\mathcal{A}$ of size Δ_{xy} is

$$\sigma = \frac{\sigma_* \mathcal{A}}{\Delta_{xy}^2}. \tag{2.22}$$

There are several observational studies which show that $\mathcal{A}$ is a function of the Richardson Number (Weissman and Klemp 1982). Since the computation of R_i is somewhat numerically intensive, we have fixed $\mathcal{A}$ at a value consistent (about 100 km^2) with the environment of the parameterized simulations that will be discussed later. A formulation for $\mathcal{A}$ such as that used by Weissbluth (1991) can be added in the future with little trouble although it will impact the efficiency of the code.

We require that the total grid fractional area be invariant to the number of sub-ensembles (number of different entrainment values) chosen to represent the ensemble. This is done simply by normalizing the fractional area of each sub-ensemble by the total number of sub-ensembles with cloud tops (detrainment levels) at the same model level. Consequently, if we decrease $\Delta\lambda$, although we will have more clouds detraining in any given model level, the total fractional area will remain independent of the discretization of the ensemble.

We also require that the total cloud fractional area in a grid remain less than or equal to unity. If the total cloud area exceeds the grid area we may interpret this to mean that the grid is completely covered by the ensemble, and that only a fraction of the ensemble mass flux is contained within the grid box.

Obviously, the cloud-base mass flux in a model grid is adjusted so as to be consistent with the grid fractional area. In summary, the grid fractional area σ is given by

$$\sigma(\lambda) = \frac{f}{N(\lambda)} \frac{\sigma_* \mathcal{A}}{\Delta_{xy}^2} \tag{2.23}$$

where σ_* is computed directly from Eq. 2.17, $\mathcal{A}$ is either a fixed area or computed as a function of R_i and $N(\lambda)$ is the number of sub-ensembles which detrain in the same model level as sub-ensemble λ. The variable f is unity as long as the total ensemble cloud area remains below the grid area Δ_{xy}^2. If the cloud area is greater than the grid area, f is a normalization factor such that $\sum \sigma(\lambda) = 1$.

By definition then, the cloud-base mass flux in the grid box (not in the large-scale environment) is

$$M_B^G(\lambda) = \sigma(\lambda)\rho(z_o)w(z_o). \tag{2.24}$$

The method for obtaining w was discussed in a preceding section. For simplicity, all future references to the grid cloud-base mass flux will be notationally given by M_B rather than M_B^G and we will reserve M_B^* for the large-scale, cloud-base mass flux. The grid fractional area of sub-ensembles will be donated by $\sigma(\lambda)$ and $\sigma_*(\lambda)$ will be used for the environmental large-scale fractional area. The reader should take careful note of this notational change to avoid later confusion.

The expression for $\sigma(\lambda)$ is the PDF we use to obtain the active population from the ensemble. Note that if the total fractional area of the ensemble is less than unity, and if there is only one λ type cloud detraining at each level, the active population is the ensemble. In all other cases, each λ type cloud is allowed to exist, but only a

fraction of its mass flux will be represented. The fraction is dependent on the total area of the ensemble and the number of similar λ-clouds which detrain at identical model levels.

2.3.1 Determining α

As shown by Xu (1991) and Xu and Arakawa (1992), the contribution to CKE from the updraft and downdraft structure of the convection is almost completely manifested in the vertical kinetic energy, $k_z = \frac{1}{2}\rho\overline{w'w'}$. Mesoscale organization and circulations primarily contribute to CKE in the form of kinetic energy of the horizontal wind. Therefore, it appears convenient to define a partition parameter

$$\epsilon \equiv \frac{K_z}{CKE} \tag{2.25}$$

where K_z is the vertically-integrated vertical variance k_z which can be written

$$k_z = \int_{z_b}^{z_t} \rho\overline{(w'w')}dz. \tag{2.26}$$

Pan (1995) attempts to use a grid average definition of the vertical variance in order to write α as

$$\alpha = \frac{1}{2\epsilon}\int_{z_s}^{z_t} \frac{\eta^2}{\rho\sigma(1-\sigma)}. \tag{2.27}$$

However, it appears that he has been inconsistent with the definition of cloud-base mass flux. He uses the following definition in deriving an expression for α:

$$k_z = \frac{M^{*2}_B\eta^2}{2\rho\sigma^*(1-\sigma^*)} \tag{2.28}$$

while using $M^*_B = \rho w\sigma_*$ elsewhere. These expressions are not equivalent in any obvious way.

One of the major disadvantages to using the prognostic CKE equation is that it becomes a function of the unknown parameter α. Perhaps it is not so surprising since the CKE equation is in essence a turbulent kinetic energy (TKE) equation.

The TKE equation cannot be closed without the introduction of a constant which relates terms of order n to terms of order $n+1$. We should not expect any different behavior from the CKE equation. At some point, it may be possible to develop a prognostic equation for α, but this will depend on other unknowns which will have to be set equal to a constant or parameterized in some way. RP93 have set α equal to a constant; a zeroth order closure.

RP93 claim that α should be a function of the number of sub-ensembles that are used. Their reasoning is that as the number of sub-ensembles increases (by decreasing $\Delta\lambda$), we would expect the fractional area occupied by each sub-ensemble to also decrease, which should in turn cause α to decrease. This obviously can not happen if we fix α. They then formulate α to be inversely proportional to $\Delta\lambda$. Their reasoning, however, is based upon their inconsistent definition of the cloud-base mass flux, and it is not entirely clear whether this analysis is valid.

We prefer a slightly different interpretation on this matter. Since we have normalized the cloud-base mass flux and sub-ensemble fractional area by the number of sub-ensembles which detrain at similar levels, we find that the total ensemble cloud-base mass flux and fractional area are independent of the entrainment interval chosen. Therefore, we do not expect α to depend on the number of sub-ensembles.

Scaling arguments of RP93 demonstrate that α should range between 10^7 and 10^9. In practice, we have found that α should be much more narrowly defined at around 10^8. Values greater than this result in convection which is incapable of removing any significant part of the CAPE generated by external forcing while values significantly less generate explosive convection which consumes not only CAPE generated by external forcing, but any background CAPE as well. We will discuss the sensitivity of the parameterization to α in the next chapter.

2.4 Cumulus Eddy Flux Closure

With the exception of the advection term, we now have all the information we require to formulate expressions for the terms in Eq. 2.4. However, there is no information in Eq. 2.4 which tells what fraction, if any, of the four terms are explicitly resolved and what fraction must be parameterized. In the case of the subsidence term, it appears to have a built in shutdown mechanism as the clouds take up more of the grid column. The factor $(1-\sigma_c)$ will go to zero linearly as $\sigma_c \rightarrow 1$. Nonetheless, this term may result in double counting since part of the box may be taken up by resolved subsidence. In the case for the adjustment term it will continue to operate as long as the clouds occupy an area less than the grid area. Therefore, even if the clouds occupy 99% of the grid box—at which point the clouds are most likely resolved—we will see an adjustment tendency. The advection term is the most difficult to deal with since it can include effects from other columns.

To remediate potential double counting we propose the linear filter given by

$$\mathcal{F}(\Delta_{xy}^2) = 2.52 \times 10^{-3}\Delta_{xy}^2 - 8 \times 10^{-3} \tag{2.29}$$

to determine the fraction of unresolved convection (Δ_{xy} in km^2). This function is intuitively based and may be regard somewhat as an *ad hoc* approach. The value of $\mathcal{F}$ is zero at some critical grid spacing where convection is completely resolved. As the grid spacing increases the fraction of unresolved convection increases linearly until another critical grid spacing is reached and all convection is completely unresolved. Once the grid tendencies are computed from Eq. 2.4, the tendencies are multiplied by $\mathcal{F}$ to separate out the unresolved component. In other words, if we decompose the grid tendency due to convection into contributions from resolved and unresolved convection

$$\left(\frac{\partial \bar{\chi}}{\partial t}\right)_{cu} = \left(\frac{\partial \bar{\chi}}{\partial t}\right)_{resolved} + \left(\frac{\partial \bar{\chi}}{\partial t}\right)_{unresolved}, \tag{2.30}$$

then

$$\left(\frac{\partial \bar{\chi}}{\partial t}\right)_{unresolved} = \mathcal{F}(\Delta_{xy}^2)\left(\frac{\partial \bar{\chi}}{\partial t}\right)_{cu}. \tag{2.31}$$

We now have the information we require to construct the equations for the subsidence term, adjustment terms and advection term which comprise Eq. 2.4.

2.4.1 Subsidence Term

AS74 presented a well recognized theory on how cumulus interact with the large-scale environment. However, unlike AS74 we are not interested in deriving an expression for the the time rate of change of the combined environment and cloudy air—a derivation which requires the "small sigma" approximation. We are interested only in the change of the environment. Therefore, we may use their equation for the change in the environment property without approximation. For dry static energy and total water the tendency of the environment due to convection is

$$\frac{\partial \tilde{s}}{\partial t} = \sum_{det} D_i[(s_c - L_l q_l - L_i q_i) - (\tilde{s} - L_l \tilde{q}_l - L_i \tilde{q}_i)] + M^* \frac{\partial \tilde{s}}{\partial z} \tag{2.32}$$

and

$$\frac{\partial \tilde{q}}{\partial t} = \sum_{det} D_i[(q + \tilde{q} + q_l - \tilde{q}_l + q_i - \tilde{q}_i)] + M^* \frac{\partial \tilde{q}}{\partial z}. \tag{2.33}$$

The summations are over all sub-ensembles which detrain at the level z, and q, q_l and q_i refer to mixing ratios of vapor, liquid and ice. The environment values are obtained by inverting Eq. 2.3 given the model grid value and the cloud properties obtained from the cumulus model. Note that the tendency to the environment is independent of the grid spacing.

If we were to vertically-integrate Eqs. 2.32 and 2.33 from cloud base to cloud top, and include convective precipitation, we would find the value is zero. This is necessary since the mass flux goes to zero below and above the cloud. The contribution of the environment tendency to the grid average is obtained by multiplying by $(1 - \sigma_c)$ as in Eq. 2.4.

2.4.2 Adjustment Term

The closure of the adjustment terms require the time rate of change of sub-ensemble grid fractional area and the cloud and environment properties. The environment property is obtained by the same method as was used for the subsidence term. Since the grid fractional area is computed each time the parameterization is called, we could directly compute the time rate of change. However, this is numerically expensive since we must store in memory the fractional area of each sub-ensemble at every level over the entire domain. Consequently, we obtain the tendency of the fractional area indirectly by taking the time derivative of Eq. 2.24, and assuming a steady state updraft. Then

$$\frac{\partial \sigma(z)}{\partial t} = \frac{\eta(z)}{\rho(z) w(z)} \frac{\partial M_B}{\partial t} \tag{2.34}$$

This method does not require any additional memory over the amount already used to retain the cloud-base mass flux for use in the prognostic CKE closure. Given the tendency of the cloud fractional area and the environment and cloud property, the adjustment term is closed.

2.4.3 Advection Term

If we vertically-integrate the tendencies obtained from the subsidence and advection terms after being run through the filter function, the result will generally be non-zero. This means there is net column heating, moistening, *etc.* in the grid column. If mass and energy are conserved then the integration of the filtered advection term must provide the necessary balance. The problem is that the integration boundary is unknown.

As a first guess, we assumed that the horizontal limits of integration were the local grid column walls and that the surface and top of the PBL were the vertical limits. In other words, if there was net column moistening over the cloud depth, the PBL below the cloud and in the column provided that moisture. This assumption

worked well at very large grid spacings. However, by the time we reached a 20km grid spacing we found that requiring the PBL to dry an amount necessary to provide mass balance resulted in an almost immediate loss of convective instability. Apparently, the moisture should not be coming exclusively from the local PBL, but from other grid columns as well. In retrospect this makes sense. We know from everyday experience that a typical cumulonimbus can feed upon air which is located many kilometers away. Larger storms may draw upon air 100 km away, or more.

It seems that to properly close the advection term, the parameterization must become horizontally non-local, and we must also somehow decide from what columns to take mass and energy and in what amounts. This is not an easy problem! We gave this problem extensive thought and did not come up with any workable solution. Fortunately, we can circumvent the whole issue.

We were curious how much of a problem the mass and energy imbalance was, so we ran the parameterization and completely neglected any contribution from the advection term. Each time the parameterization provided tendencies, we computed a domain integration of sensible and latent energy, and total water to test just how "leaky" the scheme was. To our surprise, it was hardly noticeable. The error or residual was on the order of $10^{-4}\%$ of the total domain value. So, running the parameterization for 10 hours only results in an error on the order of 1.0%. This is nice, but why is this?

The answer appears to be quite simple. First of all we note that most of the error comes from the adjustment term; it will usually only moisten or dry, or heat or cool the entire column. The subsidence term is nearly conservative causing heating and drying through the depth of the cloud and moistening and cooling at detrainment level. At large grid spacings, the adjustment term does not do much since the clouds typically occupy only a small fraction of the grid. We are then left with the rather small error introduced by the subsidence term. Using only the local PBL to account for this difference does not do much since the amount is small. Also,

the large grid spacing means it is unlikely that the clouds are drawing upon other columns for source air. This explanation also holds for smaller grid spacings near initialization time (when the clouds start of with zero area) or anytime clouds are nearly steady-state with respect to cloud area (the adjustment term is zero). When the grid spacing decreases, the adjustment term starts to dominate since there is less and less environment in the grid column. Imagine in a given grid column that there exists a growing cloud and consider the following chain of events:

- The growing cloud will cause heating and induce a positive vertical velocity perturbation on the resolved grid.
- The upward motion on the resolved grid will in turn cause resolved subsidence (primarily in the form of gravity waves) which affect other columns.
- The subsidence will result in a decrease in the cloud work function in those columns leading to a weakening of parameterized convection.
- The weakening of the convection is realized as a decrease in the mass flux and a negative tendency of the cloud fractional area.
- The negative cloud fractional area tendency results in drying and cooling in that column.

Therefore, when one cloud grows and causes an imbalance, other clouds feel the effect and respond in an opposite sense to offset that imbalance. This is great! It appears that we can let the resolved physics deal with the adjustment term. The gravity waves propagating away from the growing cloud will determine which columns and clouds within those columns will feel the convective influence. The effect can be seen in the parameterized heating and moistening rates, and we will illustrate this when we discuss the parameterization performance.

Based on the above discussion, our approach to the closure of the advection term is to simply ignore it. We keep track of domain integrated values to insure that we do not develop any significant imbalances in mass or energy. As of yet, we have not seen any which warrant concern.

2.5 Parameterization Summary

For clarity, we will now summarize the parameterization and present an overview of its implementation. The description applies to a single model column, and computations are carried out once for each grid column in the model domain.

The steps listed below are carried out every CONFRQ seconds where CONFRQ is the host model convective update cycle. Typically in mesoscale modes this is on the order of 450 seconds. The user may call this part of the parameterization as frequently as desired for presumably better results. However, due to the numerical complexity, model efficiency will be sacrificed.

1. Run the cumulus updraft model N times, where N is the number of desired possible clouds (Eq. 2.6 - Eq. 2.8).
   (a) Cloud type i will have the entrainment rate of $i\lambda_{max}N^{-1}$ where λ_{max} is the maximum allowable entrainment rate and i is an integer from 0 to $N-1$.
   (b) Clouds originate at approximately 1 km AGL and are a mass weighted mixture of the properties below.
2. Calculate the cloud top of each potential cloud by finding the equilibrium buoyancy level including virtual and precipitation loading effects.
3. Compute the cloud work function (Eq. 2.11).
4. Disregard any non-physical clouds. Must have:
   (a) Cloud work function greater than zero.

(b) Condensate and saturation at cloud top.

(c) Cloud top at least three model levels deep.

5. Compute the updraft vertical velocity profiles for all viable clouds.

   (a) Adjust the profiles so that $w \geq (1.0ms^{-1} + TKE)$ at all levels.

6. Using the (large-scale) cloud-base mass flux from the previous model time, construct the (large-scale) cloud fractional area for each cloud at each level. The method of obtaining the cloud-base mass flux is discussed further below.

7. Construct the downdraft profile corresponding to each updraft profile Eq. 2.13- Eq. 2.16.

8. Compute the convective fluxes and tendencies.

   (a) The first component of the subsidence term is given by Eq. 2.32 and Eq. 2.33.

      i. The environment value (tilde) is obtained by inverting Eq. 2.3.

      ii. The value σ_c is the total normalized cloud fractional area given by Eq. 2.23.

   (b) The result obtained from above is multiplied by $(1 - \sigma_c)$ as in Eq. 2.4 to obtain the complete subsidence term.

   (c) Using the current and previous value of the cloud-base mass flux, the rate of change of cloud fractional area is obtained from Eq. 2.34. Note this is the normalized cloud fractional area and cloud-base mass flux.

   (d) The above result is multiplied by the difference between the in-cloud properties and the environment as in Eq. 2.4. The adjustment term is now completely computed.

   (e) The advection term is neglected.

(f) Run the sum of the adjustment and subsidence tendency through the filter function to obtain the total unresolved cumulus tendency.

9. Update the host model tendencies.

The time integration of the cloud-base mass flux (Eq. 2.21) is carried out every host model time step using the value of the cloudwork function obtained from the last call to the cumulus parameterization. Let t be the current time, $t+1$ be the time in one host model timestep and A be the value of the cloudwork function obtained from the last call to the parameterization. The value of the cloud-base mass flux at time $t+1$ is computed from a discretized forward time difference equation:

$$\frac{M_B^{*t+1} - M_B^{*t}}{\Delta t} = \frac{A}{2\alpha} - \frac{M_B^{*t+1}}{2\tau_D} \tag{2.35}$$

The mass flux tendency equation could be solved explicitly, but the solution involves an exponential function which is numerically expensive. Consequently, we use the discretized rather than the analytical form.

After the local time change is computed, advection by the mean wind over the depth of the cloud is computed. We have adapted the RAMS fourth order scalar advection routine to suit our needs. This routine is used as a black box. The reader should refer to RAMS documentation for a detailed explanation of the numerics of the advection operator.

The mass flux tendency equation uses a very small value (10^{-7} $kg\text{-}m^2s^{-1}$) as an initial condition for each cloud type. If M_B^* falls below this value during integration or advection, it is reset to the small value.

Chapter 3

PARAMETERIZATION PERFORMANCE

The use of a numerical data set to examine and develop parameterizations for atmospheric processes is a widely accepted tool in boundary layer meteorology. Large eddy simulations (LES) explicitly resolve the boundary layer eddies which are responsible for mixing and transport. Statistics from an ensemble of eddies, or examination of individual eddies provide guidance for parameterization closures and also as a data set by which parameterizations can be evaluated. Observational data with the temporal and spatial coverage of an LES do not exist, so the LES is an essential tool. If the validity of the LES is accepted, then it is easy to extend the concept to cloud-resolving models (CRMs). In these cases, most of the mixing and transport is associated with moist convection, and with sufficiently small grid spacing, the individual convective elements are resolved. Once again, the CRM provides data at spatial and temporal coverage which is simply not possible with observational data sets. In most cases the LES or CRM results are compared to observation as much as possible in order to substantiate their use as credible data sets.

The performance of the convective parameterization is evaluated by running a variety of simulations at various grid spacings in two and three dimensions, and comparing the results to a simulation in which convection is explicitly resolved. Our cloud-resolving simulations are idealized and we can not directly make comparisons with observations, but we will show that the data from the cloud-resolving simulations are consistent with numerous observational and numerical studies of similar convective situations. The configuration of the two-dimensional simulations is an idealized

sea-breeze scenario consisting of a 200 km wide piece of land surrounded by 200 km of water on either side. This configuration crudely represents the Florida Peninsula. The two-dimensional simulations are primarily used for sensitivity studies; they run fast, take up little disk space and are much more straight forward to evaluate. The three-dimensional simulations are more realistic, but take longer to run, take up significant amounts of disk space, and the analysis becomes much more complicated because of the additional degree of freedom. The 3-D simulations are all configured with a 120 km wide strip of land with water on either side. The length of the strip and amount of adjacent water was constrained by the 128 megabytes of computer memory. The exact configurations will be discussed in detail when the individual simulations are investigated.

All the simulations are initialized with the sounding shown in Fig. 3.1. The sounding is similar to that used by Weissbluth (1991) and Nicholls et al. (1991), and characteristic of the Type I sounding described by Blanchard and Lopez (1984). Comparisons of the parameterized simulations will be made with data from cloud resolving simulations which have been averaged to the resolution of the parameterized simulations. Consequently, we take a moment to discuss the technique by which we average the explicit simulation.

3.1 Averaging Techniques

We state from the very beginning that averaging a high resolution simulation to a different, coarser resolution is somewhat arbitrary. For example, if we want to know how convection would appear on a twenty kilometer Δ_x model grid, should we average the convection to Δ_x? Or, is $2\Delta_x$ more appropriate? Some would argue that the minimum resolvable model feature is $4\Delta_x$. Also, how should we average the data? One possibility is to sample the high resolution data set at the desired frequency. This method produces different answers depending on where we start the sampling, and also potentially aliases the location and magnitude of maxima and

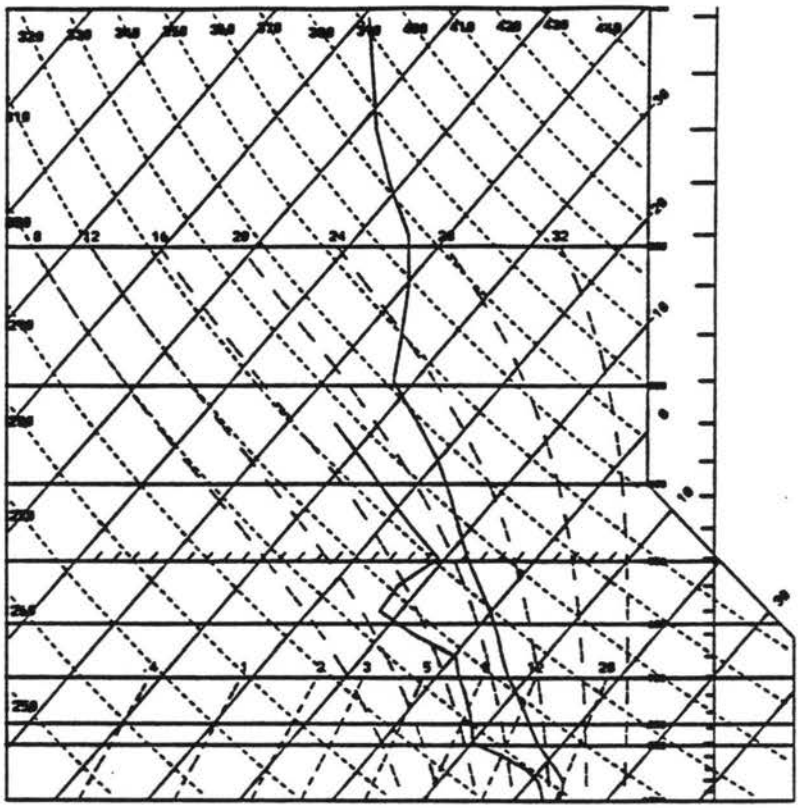

Figure 3.1: All the sea-breeze simulations were initialized with the above sounding. It is representative of the Type I sounding described by Blanchard and Lopez (1984) and similar to the one used by Nicholls et al. (1991) and Weissbluth (1991).

minima in the data. Another possibility, and the one we choose to use, is to take a running average, also known as windowing the data.

The choice of a windowing function is almost as arbitrary as the choice of averaging technique. Because of its simplicity, our first choice of a windowing function was the so-called "top hat". This function is unity in the desired averaging interval and zero elsewhere. We soon discovered this function generates severe noise when the high resolution data has a small spatial wavelength. As a simple exercise, the reader might try to construct a drawing of a two-dimensional narrow updraft with narrow downdrafts on both sides. Now imagine what the top-hat average of the drawing looks like. You should have come up with a broad updraft with a double maximum and small downdrafts on both sides. We want the parameterized simulation to represent a blurred picture of the explicit simulation, but a windowing function which creates two updrafts from one is not the kind of blurry picture we are after.

The noise we encounter from the top hat windowing function can be reduced by introducing a windowing function which rolls off as we move away from the center of the average (Press et al. 1995). Many complex windowing functions which do this have been described, but we are interested in something simple. Therefore, our next attempt at a windowing function was a triangle-like function. This function had a maximum at the center of the average and decreased linearly to zero at some desired distance away from center. Of course, we normalized the function. This simple function seemed to do the trick. When we averaged the updraft-downdraft scenario described above, we ended up with a broad updraft surrounded by broad downdrafts, all of which were reduced in magnitude. This is the blurry picture of the explicitly simulated convection we expect!

The last thing we need to do is determine how broad the triangle window function should be. Once again, this is somewhat arbitrary. We found that a triangle which was about 70% broader than the scale to which we wanted to average seemed to produce results which were objectively consistent with what we expected. In other

words, if we wanted to average the explicit simulation to 20 km, we would use a triangle which was 34 km wide at the base. The only reason for this choice was that the explicit convection averaged this way seemed to look like what we might expect at 20 km. We cannot emphasize strongly enough that the choice of the windowing function is somewhat arbitrary. Nevertheless, we do expect the parameterized simulations to compare to some reasonable degree in magnitude and spatial scale to the averaged explicit simulation.

3.2 Convective Heating and Moistening: Q_1 and Q_2

Virtually every convective parameterization described in the literature uses convective heating and moistening (Yanai et al. 1973) as part of the evaluation. This is a reasonable and well accepted procedure, but it is only truly applicable when there is a scale separation between the resolved and convective energy. In fact, the scale separation assumption goes into the derivation of $Q1$ and $Q2$. Even though this parameterization provides heat and moisture tendencies they should not be regarded as begin equivalent in any way, shape or form to the total convective tendencies if convection is being partially resolved. In other words, the host model (RAMS) will, in addition to the parameterized tendencies, produce heating and moistening tendencies which are associated with the resolved adiabatic heating and cooling as well as resolved condensation. For example, the parameterization may cause heating in a grid column which will in turn cause resolved vertical motion (partially resolved convection) which will offset some of that heating through adiabatic expansion, and possibly increase the heating through resolved latent heating. In short, $Q1$ and $Q2$ are not derivable properties in parameterizations which operate at grid spacings where convection is partially resolved.

The major problem with the loss of $Q1$ and $Q2$ as viable evaluation tools, is that it is quite difficult to find acceptable, alternative quantitative measures. One simple measure is surface precipitation, but this alone does not constitute a means

for accepting or rejecting a parameterization. The best method for evaluation seems to be to directly compare total water, vertical velocity, condensate fields, etc. with either observations or a CRM data set instead of trying to indirectly infer convective effects via $Q1$ and $Q2$. After all, $Q1$ and $Q2$ are simply residual terms obtained from budget equations. Why not examine the convection directly? This evaluation clearly becomes more objective and qualitative. However, it is quite easy to see when the parameterization is performing acceptably and when it is not, even if it is hard to quantify.

A discussion of standard techniques by which to validate convective parameterizations at the mesoscale would be a welcome sight in the literature. As of yet there is none. Consequently, we will do the best we can, primarily through direct comparisons with CRM data and precipitation records.

3.3 Overview of the 2-D Cloud Resolving Simulation

Since we are going to use the data from the cloud resolving simulation (hereafter referred to as Experiment E2DA) to evaluate the parameterization, it seems reasonable to briefly discuss the character and nature of the explicitly resolved convection. As in the explicit simulation carried out by Weissbluth (1991), two distinct modes of convection were exhibited. The first was a transient mode where short-lived, towering cumuli and cumulonimbi were triggered along and between the inland propagating sea-breezes. The second mode developed when the sea-breezes collided. It consisted of a multi-cellular storm with a lifetime two to three times longer than the convection in the transient mode. Strong convection dissipated several hours after the sea-breezes collided.

The simulation was started at 1200 UTC. Deep convection first appeared around 1730 UTC along the east coast sea-breeze. Small storms then proceeded to break out in a westward moving fashion, perhaps excited by gravity waves produced from the original east coast storm, until reaching the west coast where a large cell developed

around 1930 UTC. A convectively quiescent period, characterized by towering cumuli over the land dominated the period from about 2045 UTC through 2145 UTC. The sea-breezes collided during this time and produced a multi-cellular storm around 2200 UTC which had a lifetime of about one and one-half hours. We have refrained from displaying figures from the simulation since they will be shown later when comparisons with the parameterization are made.

Because of the ambient easterly wind, the east coast sea-breeze propagated inland at a much faster rate than the west coast sea-breeze. Consequently, the sea-breeze collision occurred west of the center of the land mass. We also note that dry (no condensation) sensitivity runs at various grid resolutions produced sea-breezes which propagated at different speeds. In general, the larger the horizontal grid spacing the slower the sea-breezes propagated, and the more diffuse the sea-breeze fronts appeared. The slowed propagation may be related in some sense to the diffuse sea-breeze front. If we regard the sea-breeze as a density current, the contrast in the air masses determines the speed of propagation. The sharper the gradient, the faster the boundary moves. Geisler and Bretherton (1969) and Pielke (1974) found the sea-breeze may be more closely related to an undular bore. In either case, the propagation of the sea-breezes has important implications for the convective parameterization since it ultimately must respond to the model resolved fields. We can not expect the parameterization operating at 20 km grid spacing to trigger the long-lived, multi-cellular convection at the same time as in the explicit simulation if the sea-breezes have not yet collided.

The evolution of the sea-breezes and associated convection is consistent with the observational studies of Pielke (1973), Burpee (1979), Blanchard and Lopez (1984), the preliminary observations from the Convective and Precipitation Experiment (Williams et al. 1992), and numerous numerical modelling studies (Pielke 1974; Pielke and Mahrer 1978; Gannon 1978; McCumber 1980; Burpee and Lahiff 1983; Dalu and

Pielke 1989; Nicholls et al. 1991). Blanchard and Lopez (1984) examined data collected during the Florida Area Cumulus Experiment (FACE) and noted that "Type I convection is characterized by early development of convection within the east coast sea-breeze convergence zone, followed some time later by convection within the west coast sea-breeze convergence zone. Both sea-breezes advance inland; however, the east coast sea-breeze moves faster than the west coast sea-breeze. Merger of these two sea-breezes usually takes place inland in the center or to the west of the center of the peninsula. The strongest convection, in the interior of the peninsula, finally begins to diminish during the early evening." These observations are consistent with the evolution of the sea-breezes and convection in the cloud-resolving simulation and provide confidence in using the numerical data as a synthetic or surrogate to an observational data set.

Until recently, the microphysical structure of Florida sea-breeze convection has primarily been obtained from instrumented aircraft penetrations through the tops of growing towering cumuli at temperatures warmer than $-15°C$ (Sax and Keller 1980; Keller and Sax 1980; Hallet et al. 1978). The rise of multi-parameter radars over the last decade has provided a means for indirectly inferring the microphysical structure within mature thunderstorms which are generally not penetrated by aircraft. Caylor et al. (1993), Bringi et al. (1993a,b;1995) and Liu et al. (1993) have examined several case studies from the Convective and Precipitation Electrification Experiment (CAPE) which took place in the vicinity of the Kennedy Space Center in Florida. Individual convective cells embedded in nearly identical environments were found to have widely varying mass and concentrations of hydrometeors. However, the basic structure and evolution of the cells inferred from radar were similar, and also agreed well with the earlier aircraft observation studies. During the growing stages of the towering cumuli and cumulonimbi, warm rain processes dominate the precipitation production. Once the cloud tops penetrate approximately the $-10°C$ level, some of the rain drops freeze and mixed phase precipitation production becomes important.

The main focus of this dissertation is not cloud resolving simulations. Consequently, we will not go into any more detail describing and verifying the CRMs against what are still sparse observational data sets. We assert that the data from the CRMs (2-D and 3-D) are in excellent agreement with the body of observational data which is available in the literature. More importantly, we claim that CRMs we have conducted are a valid data set for the purposes of evaluating convective parameterizations, particularly at mesoscale grid spacings. As a final argument for the credibility of the CRMs, we note that RAMS has been successfully used to explicitly supercell thunderstorms and their associated tornadoes (Grasso 1995), precipitating and non-precipitating stratocumulus topped boundary layers (Stevens et al. 1996), Eastern Pacific (Alexander 1995; Alexander and Cotton 1996a,b) and middle latitude (Olsson and Cotton 1996) mesoscale convective complexes. To some degree, this constitutes proof by induction.

Since we only carried out a single, explicit, two-dimensional, cloud-resolving simulation, we should regard the output as only a single realization. Small changes in initial conditions may have produced convection which triggered at different times and at different locations. The basic structure and characteristic of the storms should, however, be similar in any simulation we undertake. We should, for example, see the two modes of convection. We should also expect vertical velocity within the clouds, and the scalar transport done by the clouds to be similar. Also, we expect the microphysical and dynamical structure to be consistent with in situ and remotely sensed observations. In short, we do not expect the parameterization to exactly reproduce clouds or cloud effects whenever and wherever they were found in the CRM, but we do expect similar end results. It is in this spirit that we analyze and evaluate the parameterization.

3.4 Parameterization at Twenty, Twelve and Six Kilometers in Two Dimensions

Because of the transient nature of the simulated convection in both the CRM and the parameterized experiments prior to the collision of the sea-breezes, it is inherently difficult to capture the evolution of the convection without showing an enormous amount of figures. An animated sequence of the simulations would be useful, and this technique was employed during the defense of this research. However, animation is clearly not a viable alternative in a text. As a compromise, we will show a series of snapshots in time from the CRM and parameterized simulations which embodies the characteristics of the transient convection (typically a convective life-cycle), but which do not cover the entire time-span over which the transient convection was active. Because the appearance of individual, transient, convective cells, the CRM and parameterized simulations do not correspond exactly in time, and the sequence of snapshots in time from the CRM and parameterized experiments will typically be offset by an hour or more. The inability of the parameterized simulations to exactly reproduce convection at the same time and place as seen in the CRM should not be regarded as a failure of the parameterization. Instead, the CRM should be regarded as only one possible realization. What is important is that the parameterization produce transient convection when the CRM indicates this convective mode. Also, it is important that the strongest parameterized convection be collocated with the sea-breeze fronts, that weaker convection occur over land, between the sea-breezes, and that no convection is present over the water; all of these characteristics were found in the CRM. Once the sea-breezes collide and the convection becomes more steady-state, the characteristics of the convection is well represented by a snapshot at a single time. Therefore comparison between the CRM and the parameterizations becomes straight forward.

Snapshots of vertical velocity, total water and condensate from E2DA averaged to 20 km resolution are shown in Fig. 3.2a at fifteen minute intervals over a one

hour period from 1915-2000 UTC. The transient nature of the convective cell along the west coast sea-breeze is apparent. In Fig. 3.3a, a set of corresponding data are displayed from a 20 km parameterized simulation (hereafter Experiment P2DB) for a parameterized, transient convective cell also along the west coast over the period 1930-2015 UTC. The parameterization configuration of Experiment P2DB, along with all the other forthcoming experiments is summarized in Table 3.1. We note that the parameterized convection decays by 2030 UTC (not shown), so it is indeed transient, although slightly longer lived than its CRM counterpart. Also apparent is the development of a transient cell along the east coast sea-breeze. The vertical velocity fields compare well with peak values in E2DA and P2DB of approximately 2.0 ms^{-1}. The total water fields compare reasonably well; the most obvious difference is the parameterized simulation is about 1.0 $g\ kg^{-1}$ too moist in the PBL over land. Also, it appears that the CRM convection transports more water to the upper troposphere. Examination of the condensate field shows that some of the excess PBL moisture should probably be transported aloft and converted to condensate in the process. This is based on the depth and magnitude of the condensate column of E2DA at 1945 and the lack of an equal column in P2DB. The peak values of condensate magnitudes of the condensate fields are comparable in P2DB and E2DA.

What is not apparent from Fig. 3.3a is that convection triggers in P2DB nearly an hour and one-half after it is observed in E2DA. This may be related to the slow development and propagation of the sea-breeze at the 20 km grid spacing. We also note that both the east and west coast sea-breezes in P2DB are often active simultaneously; a feature not seen the in the explicit simulation. Some of the discrepancies are likely related to the choice of the windowing function and others, as we have previously stated, are probably a result of the poor resolution of the sea-breeze fronts. Even if this were not the case, we do not expect that the parameterization would have performed perfectly.

Experiment	Type	Δ_{xy} (km)	No. Pts.	α $(kg\ m^{-4})$	$\sqrt{\mathcal{A}}$ (km)	$\mathcal{F}$
E2DA	E	1.5	600	-	-	-
P2DA	P	20	31	10^8	100	1.0
P2DB	P	20	31	10^8	120	1.0
P2DC	P	20	31	10^8	160	1.0
P2DD	P	12	50	10^8	120	0.354
P2DE	P	12	50	10^8	160	0.354
P2DF	P	12	50	10^8	100	0.354
P2DH	P	6	100	10^8	100	0.083
P2DI	P	6	100	10^8	120	0.083
P2DJ	P	6	100	10^8	160	0.083
P2DK	K	6	100	-	-	-
P2DL	P	12	50	5×10^8	120	0.354
P2DM	P	12	31	10^7	120	0.354
P2DN	K	6	100	-	-	-
P2DO	K	12	50	-	-	-
P2DP	K	20	31	-	-	-
P2DQ	P	12	50	5×10^8	120	0.354
P2DR	P	12	50	5×10^7	120	0.354
P2DS	P	12	50	8.33×10^7	120	0.354
P2DT	P	12	50	1.25×10^8	120	0.354
P2DU	P	6	100	8.33×10^7	120	0.083
P2DV	P	6	100	1.25×10^8	120	0.083
P2DW	P	20	31	8.33×10^7	120	1.0
P2DX	P	20	31	1.25×10^8	120	1.0
P2DY	P	20	31	10^8	120	0.80
P2DZ	P	6	100	10^8	120	0.066
P2DAA	P	6	100	10^8	120	0.099
P2DAB	P	12	50	10^8	120	0.283
P2DAC	P	12	50	10^8	120	0.426

Table 3.1: A summary of the experiment nomenclature and values of disposable parameters in the two-dimensional simulations. Type E simulations are explicit (CRM); K are parameterized with the Kuo parameterization and P with the new parameterization.

The timing of the convection does not concern us too greatly. We believe that the late appearance of the convection is more closely tied to the slow development of the sea-breeze forcing. We are also not too concerned with the simultaneous appearance of east and west coast convection. In the explicit simulation, the east and west convection were observed to be active within an hour or so of each other, and a different realization may have produced simultaneously occurring convection.[1]

Of greater concern is that too much water seems to remain aloft. This becomes particularly obvious at later times when well developed anvils are found in P2DB and not in E2DA. Possible causes of this are that the parameterization is a) not removing enough precipitation via convective precipitation; b) producing too much cloud water, instead of heavier rain and ice which sediment out; or c) simply be transporting too much water upward. The middle option (b) seems to be the culprit. We noted earlier that while the total water transport seemed reasonable, there was a deficiency of condensate at upper levels. Therefore, we can assume that the parameterization is leaving too much water in the form of vapor upon which RAMS converts to the lighter species of cloud water and pristince ice, neither of which have a fall velocity. As a consequence, extensive anvils develop.

We next examine the quasi-steady-state mode of convection which occurs after the sea-breezes have collided. This convective mode is actually a multi-cellular storm with a lifetime of about two hours, and is composed of individual convective cells with much shorter lifetimes that rise in succession. Comparisons of vertical velocity, total water, and total condensate are shown in Fig. 3.4 for E2DA and P2DB at 2230 UTC. In P2DB we can see a cell ascending through the middle troposphere and another cell developing in its wake. The storm in E2DA only reveals a single cell at this time. The peak vertical velocities compare well, although the parameterized simulation appears

---

[1]Simultaneous east and west coast sea-breeze convection was observed in the three-dimensional, cloud resolving simulation.

slightly too strong. Also clearly evident by this time, is the accumulated effect of too much water remaining aloft in the parameterized simulation. The total amount of water is too high, and the host model (RAMS) has caused what was once excess water vapor to condense and nucleate into cloud water and pristine ice. If not for the extensive anvil in P2DB, the condensate fields would compare favorably.

The total precipitation from E2DA (averaged appropriately) and P2DB are displayed in Fig. 3.5. First, note that the basic structure of the the plots are the same. In particular there is a bimodal type structure which appears at later times in both simulations near the center of the domain. Overall, the magnitudes appear reasonable, but P2DB has somewhat lower values than expected (with the exception of the east coast spike). This is further evidence that a larger fraction of water should appear as large condensate which can fall instead of water vapor.

Having dispensed with most of the items that went wrong, let us take a look at what went right with this simulation. First and foremost, we can conclude that the basic premise and theory behind the parameterization seems to produce reasonable, albeit not perfect results–at least at a 20 km grid spacing. The parameterization has produced transient convection along the sea-breeze fronts, and longer-lived, multicellular convection at the boundary marking the sea-breeze collision. *This was done without the use of a trigger function.* We did not arbitrarily decide when to turn the parameterization on or off; if conditionally instability was present, the parameterization was operational. If we examine the magnitude of vertical velocity in E2DA and P2DB we see that the values are within reason. Turning to the condensate fields we find that the multiple maxima which appear in E2DA are also reproduced in P2DB. Cloud tops and lifetimes also compare favorably.

Fig. 3.6a and 3.7a are from E2DA averaged to a 12 km resolution (1915-2000 UTC) and from a similar transient event (1800-1845) in the 12 km parameterized simulation (P2DD), respectively. The figures are analogous to the fields previously discussed for the twenty kilometer simulation. The lifetime of the convective cell

in both simulations is comparable as are the values of vertical velocity. The water transport also appears to be within reason and the excessively moist PBL seen in P2DB is not as obvious in P2DD. A major feature of P2DD which is not seen in E2DA is the strong subsident drying west of the west coast sea-breeze. This feature is not a direct result of the parameterization, but an indirect consequence. The host model is concentrating the resolved compensating subsidence from the west coast convection within a narrow region, thereby producing the excessively strong subsident drying. It is not clear why this is happening, but it may be due to the inability of the model to propagate the subsidence over a larger area via gravity-waves as effectively as it is done in the CRM. Similar to what was seen in P2DB there is evidence that not enough water is being partitioned into the heavier hydrometeors which can precipitate out.

The precipitation record (Fig. 3.8) from P2DD is in excellent agreement with E2DA. The narrowness of the bimodal precipitation structure seen along the west coast in P2DD is due to the different propagation speeds of the sea-breeze fronts. Basically, the west coast sea-breeze penetrated farther inland in E2DA, and the proceeding collision produced a peak in precipitation farther east (grid point 178 in E2DA).

The timing of the onset of convection in this simulation is much better than in P2DB. The east coast sea-breeze is the first to trigger around 1730 UTC followed immediately by the west coast sea-breeze at 1745 UTC. Longer-lived convection triggers at the sea-breeze collision boundary around 2200 UTC, and exhibits a multicellular structure. The better timing of convection is likely related to the increased resolution and propagation speeds of the sea-breezes. Vertical velocity, total water and total condensate are shown in Fig. 3.9. The most obvious deficiency of the parameterization is, once again, the appearance of an excessively thick anvil.

Overall however, the simulation does quite well. Convection coincides nicely in space and time with the what we would expect based on the explicit simulation. P2DD

suffers from convection which appears somewhat too strong, although the surface precipitation compares favorably. The condensate field also shows that the anvil clouds become too well developed just as they did in P2DB. Although not perfect, the results are encouraging since it seems that the parameterization is basically working at the mesoscale grid spacings for which it was intended.

The last resolution at which we ran the parameterization was at six kilometers (Experiment P2DI). Just as we did for the 12 and 20 km simulations, we present snapshots in time of E2DA (1915-2000 UTC) averaged to six kilometers and P2DI (1800-1845 UTC) in Fig. 3.10a and 3.11a. In most respects the parameterization performs adequately, but suffers from many of the problems previously outlined at the larger grid spacing. In particular, too much vapor and small condensate (cloud water and pristine ice) remains aloft and creates too thick of an anvil and stratiform cloud layer. Also, unlike P2DB and P2DD, the sea-breeze collision and associated steady state convection occur farther west than found in E2DA. The precipitation record (Fig. 3.12) shows the basic structure seen in all the simulations. There is a bimodal peak on the west side of the land mass and a small hump indicating the east coast convection. Examination of P2DI during the steady-state mode basically shows the same strengths and weaknesses seen at the other grid spacings. Consequently, we omit these figures.

To summarize this simulation, the east coast sea-breeze develops before convection on the west coast, and initiates approximately one-half hour later than in E2DA. There is good agreement between the peak values of condensate and vertical velocity in E2DA and P2DI, and the life cycle of the transient cells is captured. The steady-state convective mode appears somewhat too weak in the parameterized simulation, although it is long-lived. The precipitation record also compares favorably with the cloud resolving simulation. As in the previous cases, the parameterization correctly placed and developed convection in a manner consistent with expectations, and did so without the use of a trigger function.

3.4.1 Mass and Energy Conservation

We will now revisit the issue of the non-conservative or "leaky" parameterization. We claimed that there should not be local column mass and energy balance since unresolved transport from other columns is possible, and in fact necessary to sustain convection. We also stated that over the model domain as a whole, mass and energy were nearly conserved. To illustrate this, we show the total water and ice-liquid potential temperature tendency at 1930 UTC from experiments P2DB, P2DD and P2DI (Fig. 3.13). In each case, we have convection which is growing in area and creating regions of positive total water and heating anomalies. There are also regions where convection is dissipating or decreasing in intensity resulting in drying and cooling. In all cases, it appears that the effects nearly offset each other. A domain wide budget of mass and energy confirm this.

3.4.2 Comparison with Kuo Parameterization

Before moving on to sensitivity studies, it is appropriate to compare the new parameterization with the Kuo parameterization. The Kuo scheme is the only convective parameterization currently implemented in RAMS. It is designed primarily for large-scale simulations, but is currently used at scales as small as 16 km in the case of the real-time forecasting model (Gaudet 1996). Gaudet found that the Kuo scheme was responsible in large part for many of the busted forecasts during the convective season over the Colorado Front Range foothills and plains.

We ran the Kuo scheme at twenty, twelve and six kilometers, and we set the vertical velocity cloud-base trigger to 0.02 ms^{-1}, 0.09 ms^{-1} and 0.25 ms^{-1} respectively. The values were chosen based on the cloud resolving simulation E2DA. In every simulation, the Kuo scheme failed miserably. Convection initially triggered in the right places at approximately the right time, but everything went downhill from there. As a quick, overall summary of the Kuo simulations we show vertical velocity, total water and condensate fields at 2000 UTC and 2300 UTC in Fig. 3.14 and 3.15

from experiment P2DO (Kuo at 12 *km* grid spacing). These should be compared to the corresponding fields in E2DA and P2DI. Simulations with the Kuo parameterization at six and twenty kilometers are similar to P2DO and the corresponding figures are not shown. The precipitation record is also shown in Fig. 3.16 for the Kuo parameterization simulations at three different grid spacings.

Major deficiencies of the Kuo scheme appear to be grossly underestimated precipitation, vertical velocity and total condensate. Even at six kilometers, where convection should be nearly resolved, the Kuo scheme rarely produces vertical velocity in excess of 75 $cm\ s^{-1}$. The condensate field does not give any indication of convection and total water transport is clearly underestimated.

In an effort to try and improve the simulations using Kuo, we lowered the threshold of vertical velocity required to trigger the parameterization. The reasoning was that this should cause the parameterized convection to become more active, produce more precipitation, transport more water and perhaps generate some semblance of resolved convection. Actually, we found that the simulation was worse. It appears that the decreasing trigger threshold approaches the magnitude of the velocity perturbations associated with the convectively-generated gravity waves. The result is a wave-CISK-like (Raymond 1975) simulation with convection firing at one point and spreading at gravity wave speed throughout the domain. After a while, convection appears almost random, firing over land and water with no regard to what the ambient sea-breeze circulation is doing.

Despite some of the inadequacies of our parameterization, it is clearly superior to the Kuo scheme under the conditions of these idealized, two-dimensional sea-breeze simulations. The added expense in running the new scheme appears worthwhile, especially after carrying out the head-to-head competition.

3.5 Sensitivity Experiments in Two-Dimensions

There are only a few parameters which we intend to be adjustable or variable within the parameterization, and we will focus on these when designing the sensitivity experiments. The first parameter we will examine is α which relates the cloud-base mass flux to CKE. Second, we will examine the sensitivity of the parameterization to the cloud influence area $\mathcal{A}$. Finally the filter function $\mathcal{F}(\Delta_{xy}^2)$ will be investigated. The reader is directed once again to Table 3.1 for a summary of the simulations.

3.5.1 Sensitivity to α

We can perhaps anticipate how changes in α will affect the parameterization before conducting any sensitivity studies. For simplicity, if we neglect the dissipation term in Eq. 2.21 we see that the cloud base mass flux will grow exponentially on the time scale of $(2\alpha)^{-1}$. It is now clear why the range of α between 10^7 and 10^9 suggested by PR93 is much too broad. The lower value causes the cloud base mass flux to explode at rates which are physically unrealistic and the higher value barely allows the convection to respond to the cloud work function. We feel it is more appropriate to test the sensitivity of the parameterization to α using values that augment the growth rate by $\pm 20\%$.

Small values of α should cause the cloud-base mass flux to grow fast. Therefore, for a given cloud work function, the cloud fractional area will be large, and the growth rate of the cloud fractional area will be large. This in turn means that the ratio of the adjustment tendency term to the subsidence tendency term will be larger than usual. Consequently, for a growing cloud we should see less subsidence drying and warming, and more adjustment moistening and warming. The opposite should occur when α is increased. The simulations bare this out.

Rather than presenting an enormous amount of figures from the α sensitivity studies, we will show the only the surface precipitation record The precipitation

record can be used to get an idea of convective intensity and location. The basic evolution of the convection is all very similar to the control runs P2DB, P2DD and P2DI. We conducted two simulations each at horizontal grid spacings of 6 km, 12 km and 20 km. The first set used $\alpha = 1.25 \times 10^8$, and $\alpha = 8.33 \times 10^7$ in the second. These values give growth rates which are within $\pm 20\%$ of the growth rate given by the control value of 10^8.

As expected we see that the parameterization produces more vigorous convection with a small value of α and more subdued convection with the larger value. The 12 km simulations (PT2DS and PT2DT) were least affected by the variation of α; total precipitation varied by approximately 15%. The 6 km and 20 km simulations did show reasonably strong sensitivity to α. In the case of the P2DW, total precipitation nearly doubled over the west-coast region.

Another interesting aspect which we did not anticipate is the weakening, and in some cases near disappearance of the steady-state convective mode when α was decreased. We are not sure of the precise cause, but it appears to be similar to the effect seen in Weissbluth (1991). Apparently, the transient convection is parameterized too strongly and this results in excessive stabilization of the atmosphere. When the sea-breezes finally collide, the convection is unable to sustain itself. Associated with the weakening of the steady-state mode was the weakening of the bimodal precipitation structure on the western half of the peninsula. The western most precipitation peak was caused by the initial convection along the sea-breeze while the peak further inland was due to the convection initiated along the convergence boundary of the sea-breeze collision. The loss of the bimodal peak seems to be due to an increase in the strength of the west coast sea-breeze and a decrease of the steady-state mode along the collision boundary.

Overall, increasing α had less of an impact than decreasing it. We are not sure why. Unfortunately, the parameterization seems fairly sensitive to this parameter.

This is perhaps not surprising since it appears as an exponent in the analytical solution to the prognostic CKE equation. Ideally, we would like to develop a diagnostic or prognostic equation for α which will free the user from having to prescribe a value. This will be relegated to future research, but will be among the top priorities.

3.5.2 Sensitivity to $\mathcal{A}$

As in the case of α sensitivity, it is possible to anticipate how the parameterization will respond to changes in $\mathcal{A}$. Given a fixed, large-scale cloud-base mass flux, the grid cloud-base mass flux will increase as $\mathcal{A}$ increases. The total cloud fractional area will also increase. The increasing fractional area should cause the contribution from the subsidence term to become weaker. At the same time, the contribution from the adjustment should increase. Unlike α, $\mathcal{A}$ does not affect the growth rate of the CKE. Also, it is a linear factor rather than exponential.

Simulations with $\sqrt{\mathcal{A}} = 100$, 120 and 160 km were conducted holding all other parameters fixed. This gives a total of nine simulations at grid spacings of six, twelve and twenty kilometers. As we expected, the simulations with higher values tended to produce stronger convection. The effect was more noticeable as the grid spacing decreased. Once again we show only the precipitation history from the simulations in Fig. 3.18.

Variations of $\mathcal{A}$ have much less impact than α variations. In the case of P2DA and P2DC, the bimodal precipitation feature along the west coast seems to be lost. The east coast maximum is also lost in P2DA, but over-exaggerated in P2DC. Because we have only shown a single time from each of the simulations, it may appear in some cases that the vertical velocity fields do not agree well (P2DC for example). This is not a real deficiency; it is due only to the single sampling time and the transient nature of the convection. The basic results are all very similar.

At some point in the near future, we will begin diagnosing $\mathcal{A}$ from the Richardson Number. Since this will only be a crude parameterization at best, we felt we were

justified to see how sensitive the parameterization was to this parameter. It seems that as long as we can get $\mathcal{A}$ within $\pm 40\%$, we should be able to get reasonable results.

3.5.3 Sensitivity to the Filter Function

The final set of sensitivity tests we conducted were on the filter function. A total of eight simulations were conducted—three each at 6 km and 12 km and two at 20 km. We did not run the 20 km simulation with an increased value of $\mathcal{F}$ since it is already unity at that grid spacing. $\mathcal{F}$ was allowed to vary at $\pm 33\%$ of the original value as given by Eq. 2.29. $\mathcal{F}$ is a linear factor like $\mathcal{A}$ so we expected similar behavior. The difference between the two is that the filter function is applied after the adjustment and subsident tendencies are calculated.

The surface precipitation record is shown in Fig. 3.19. The overall solutions are basically the same, and show many of the same sensitivities as seen with $\mathcal{A}$. All of the simulations looked reasonable and seemed to capture the convective features exhibited in the explicit simulation.

3.5.4 Summary of Sensitivity Experiments

The overall results from the sensitivity experiments indicate that the parameterization is most sensitive to α and less sensitive to $\mathcal{A}$ and $\mathcal{F}$. We more or less expected this since α appears as an exponential growth rate while the other parameters only have a linear effect. In almost all cases, the sensitivity studies gave reasonable results. In all cases, the solution was significantly better than those given by Kuo. More than anything, the sensitivity studies show that the parameterization is robust. As long as parameters are specified within reasonable values, we get reasonable results with the simulations generally being more similar than dissimilar. This is an encouraging finding.

Since we can anticipate the effect of each of the parameters, we should consider the parameters as tunable. This may be considered good or bad depending on the

situation. Ideally, a parameterization should not have any tunable coefficients; all values should be globally valid. In reality, this is almost never the case. We have no doubts that in some cases the parameterization will produce convection which is too strong or too weak. Then, the tunable parameters are welcomed.

For now, we recommend users use a value of α close to 10^8. As we test the parameterization over a wider variety of cases and become more familiar with its behavior, we may find more specific or appropriate values. Specifying the value of $\mathcal{A}$ will not be necessary in the operational version. Instead, it will be diagnosed from the bulk Richardson Number as previously discussed. We do not really intend for the user to alter the filter function. However, since it is basically an unknown which we have used intuition to specify, we thought it would be worthwhile to investigate its influence.

3.6 Cloud Resolving Simulation in Three Dimensions

The three-dimensional, cloud resolving simulation (E3DA) is similar in many ways to its two-dimensional counterpart (E2DA), but there are some significant differences. Many of the differences may be attributable to the slightly different configurations. The 3-D simulation has a narrower strip of land (120 km compared to 200 km in 2-D). Also, there is less water on either side of the land (only 30 km). The strip of land is 90 km long and cyclic boundary conditions at the North-South boundaries make the land semi-infinite. The smaller domain was necessary to allow the simulation to fit on the 128 megabyte workstation.

The most fundamental difference in the results of E3DA and E2DA is that the steady-state mode of convection seen in 2-D was not present in the the three-dimensional simulation. While this may be due to the narrower land mass, it is probably more a result of the extra degree of freedom. Although it is not at all a focus of this research, the difference does point out the potential pitfalls of reducing an

inherently 3-D phenomena to two dimensions. Besides the lack of a quasi-steady convective mode, the sea-breezes in E3DA collided earlier than in E2DA. This is a direct result of the narrower land mass. Finally, convection is triggered a little earlier in the 3-D configuration and convection is active on both coasts simultaneously throughout the simulation.

We decided not to produce any averaged fields from E3DA. The decision was motivated by the arbitrariness of the averaging techniques. We believe the reader can do a better job of visualizing a "blurry" picture than we can do creating it numerically. We will examine two times from the explicit simulation and corresponding parameterized simulations. The first time is 1800 UTC, about an hour and one-half after convection becomes active. The second time is 2115 UTC which is about one-half hour after the sea-breezes have collided.

3.7 Parameterization at Twenty, Twelve and Six Kilometers in Three Dimensions

The width of the land mass in all the simulations is fixed at 120 km, but the amount of water and length of the land mass in the twenty (P3DA), twelve (P3DB) and six (P3DC) kilometer simulations is variable. In P3DA, the land is 340 km long with 100 km of water on each side. P3DB and P3DC have land which is 204 km long with 120 km of water on each side. Once again, the configurations were dictated by computer memory constraints. The length of the land in each of the parameterized simulations is much longer than the cyclic frequency of the CRM so that they are, for all practical purposes, infinite strips of land. The variable amounts of water was necessary to allow several model grid points to extend over the water at the larger grid spacing while keeping the width of the land the same in each simulation. We did not apply cyclic boundary conditions in any of the parameterized runs (thus the variable length of the land strips). Also, the parameterized simulations all use $\alpha = 10^8$, $\sqrt{\mathcal{A}}$=120 km, and the filter function as given by Eq. 2.29. In the following

figures of P3DA, P3DB and P3DC we have cropped the east-west (water) domain so that the land/sea boundaries approximately line-up with the boundaries in E3DA. These boundaries are at model points 6 and 12 in P3DA, 9 and 19 in P3DB and 20 and 40 in P3DC. In the cloud resolving simulation, the land/sea boundaries are at model grid points 20 and 100. This should aid in the interpretation of the results. We will display the north-south domains in their entirety.

Shown in Fig. 3.20 are vertical velocity, total water mixing ratio and condensate mixing ratio for the cloud resolving simulation (E3DA) and the corresponding parameterized runs P3DA, P3DB and P3DC at 1800 UTC and approximately 2 km AGL. At this time the east coast sea-breeze has propagated approximately half way across the land mass in all the simulations. The decrease in propagation speed with increasing grid spacing is apparent although not significant. In contrast to the two-dimensional simulation, convection is simultaneously present on the east and west coast. The west coast convection appears less organized while the east coast convection is organized into a line. All the parameterized simulations reflect the convective characteristics and place the convection in the correct places. In P3DA, the isolated convection along and ahead of the west coast sea-breeze is present although its signature is masked by the more intense east coast convection.

To investigate the vertical structure of the convection, we show along-line cross sections of the east coast sea-breeze for each of the simulations in Fig. 3.21. Cloud top heights inferred from the condensate fields of the parameterized simulations compare very well with cloud resolving simulation. The Peak vertical velocity is 21 ms^{-1} in E3DA, 20 ms^{-1} in P3DC, 10 ms^{-1} in P3DB and 3.5 ms^{-1} in P3DA. These are approximately what we expect.

A significant difference between the two and three dimensional parameterized simulations is that the transport of water in 3-D is not as excessive as was seen in 2-D. This was a persistent problem in all of the two-dimensional parameterized simulations. Also, we do not see the extensive and over-developed anvils which

plagued the 2-D simulations. The parameterized convection still appears to be a little too strong when compared to E3DA, but it is well within reason.

We now focus on the simulations at 2115 UTC which is after the sea-breezes have collided. The cloud resolving simulation exhibits multicellular convective clusters along the collision boundary with weaker convective regions between and to the west (Fig. 3.22). The six kilometer parameterized simulation (P3DC) clearly shows similar clustering of convection, but the twelve (P3DB) and twenty (P3DA) kilometer simulations are not as obvious (Fig. 3.22). Interestingly, the location of the convection is reproduced best by P3DB. Convection in P3DA is about 20 km too far east (a one Δ_x error) and about 20 km too far west in P3DC. The reason for this is unknown.

Along line cross sections (Fig. 3.23) show that the vertical structure of the convection in the cloud resolving simulation is well captured in the parameterized experiments. Magnitudes of vertical velocity, total water and condensate all appear well within reason and expectations. As in all the previous cases, the parameterized convection is probably a bit too active, but appears less of a problem than in two-dimensions.

As a final comparison between E3DA and the parameterized simulations, we present the surface precipitation record at 0000 UTC (Fig. 3.24). Most of the convection had died down by this time. Except for P3DC, the parameterized simulations did not do as well as we would have liked. The magnitudes of the precipitation are only a little higher than expected in P3DC, but much too high in P3DA and P3DB. This once again suggests that the parameterized convection was too strong especially at the larger grid spacings. Some of the excess precipitation could be corrected by reducing the precipitation efficiency of the updraft. However, a large fraction comes from resolved microphysics. Therefore, the best fix may be to decrease $\mathcal{A}$ or modify $\mathcal{F}$.

Another obvious feature present in all the parameterized simulations was the bimodal precipitation pattern. Apparently, the convection was focused too strongly

along the sea-breezes. Examination of earlier precipitation records (not shown) shows that the west coast convection produced too much rain and created the western most precipitation maximum. Differences in the propagation and location of the sea-breeze collisions are also partially responsible. The precipitation field is probably the most disappointing and worst handled aspect of the 3-D simulations.

As a side note, there are indications that there is a bug in the RAMS precipitation sedimentation code which causes inaccuracies in the amount of precipitation which reaches the ground. At this point, the exact cause has not been isolated, but the code is being re-worked. Unfortunately, the bug was not suspected until after all the simulations were completed, and a working version of the code has not yet been introduced. We suspect some of the precipitation errors seen in the parameterized simulations may be partially accounted for by the sedimentation bug, although even with the code working properly, we are almost certain we would still see the same general pattern. To a large extent, the errors caused by the bug should be systematic since both the cloud resolving and parameterized simulations were run with the same RAMS code.

3.7.1 Summary of the Three-Dimensional Simulations

All things considered, the 3-D experiments were successful. Convection was triggered at approximately the right locations and at the correct times. Vertical velocity and water substance were within expected values and captured the basic structure and characteristics of the convection simulated in the cloud resolving simulations. Surface precipitation was not handled well, although values were still within 50% or so of those produced in E3DA. While most of the precipitation errors are likely attributable to the parameterization itself, there is some question about errors in the host model code which could be reducing the amount of precipitation in E3DA.

No attempt was made to tune the parameterization for optimal results. Simulations P3DA, P3DB and P3DC were first-try experiments. It is quite likely that we

could have generated data which would have had much better agreement with E3DA. However, one of the expected implementations of this parameterization is in the real-time forecast model. In a forecast model you do not have the luxury of repeatedly running simulations to optimize the results. In retrospect, we believe that we should probably alter the filter function to decrease the tendencies. In other words, the model seems to resolve convection better than we anticipated and we are seeing the effects of double counting.

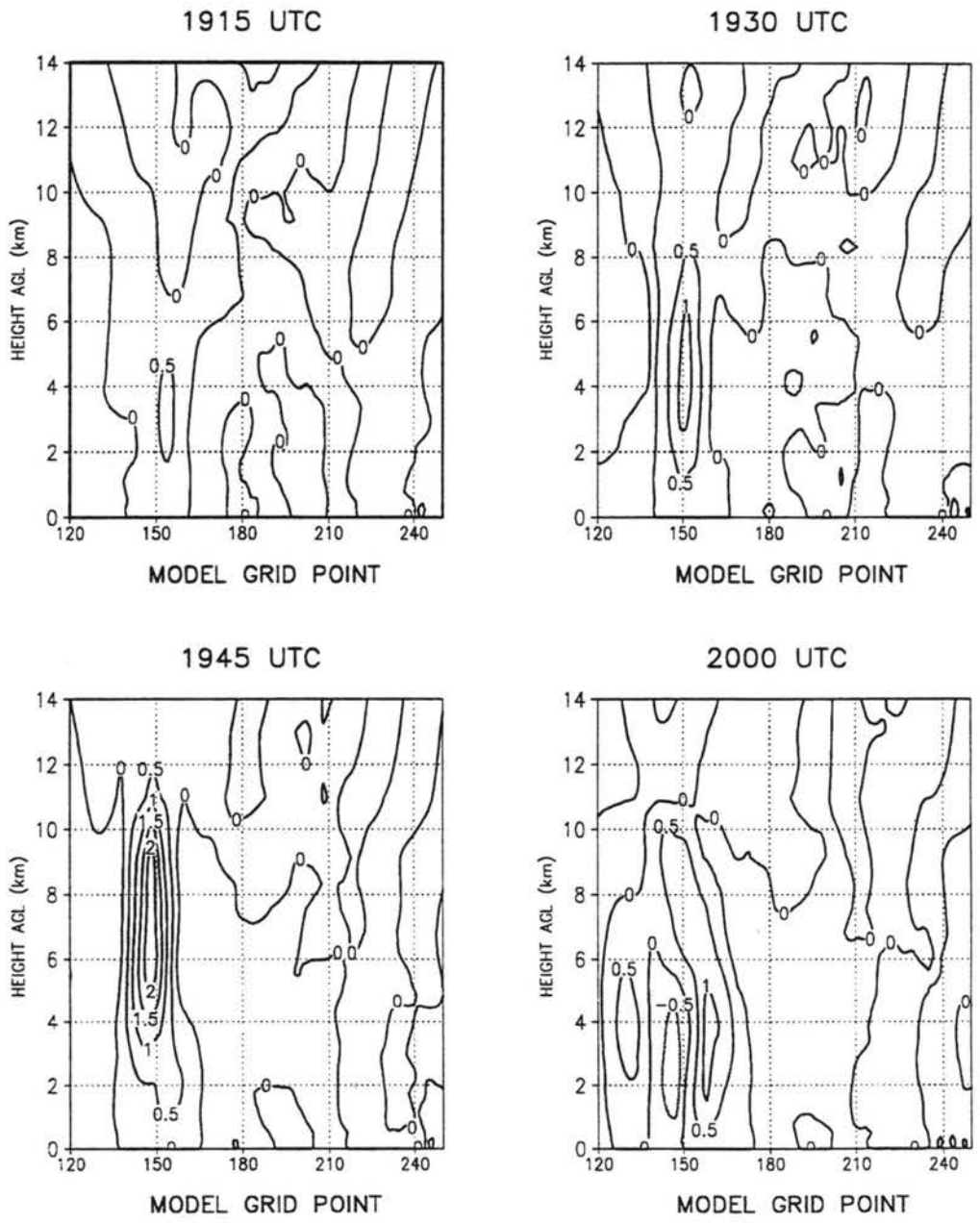

Figure 3.2a: Snapshots in time at fifteen minute intervals from Experiment E2DA averaged to 20 km: vertical velocity (ms^{-1}) from 1915-2000 UTC. Land/sea boundaries are at model grid points 133 and 267.

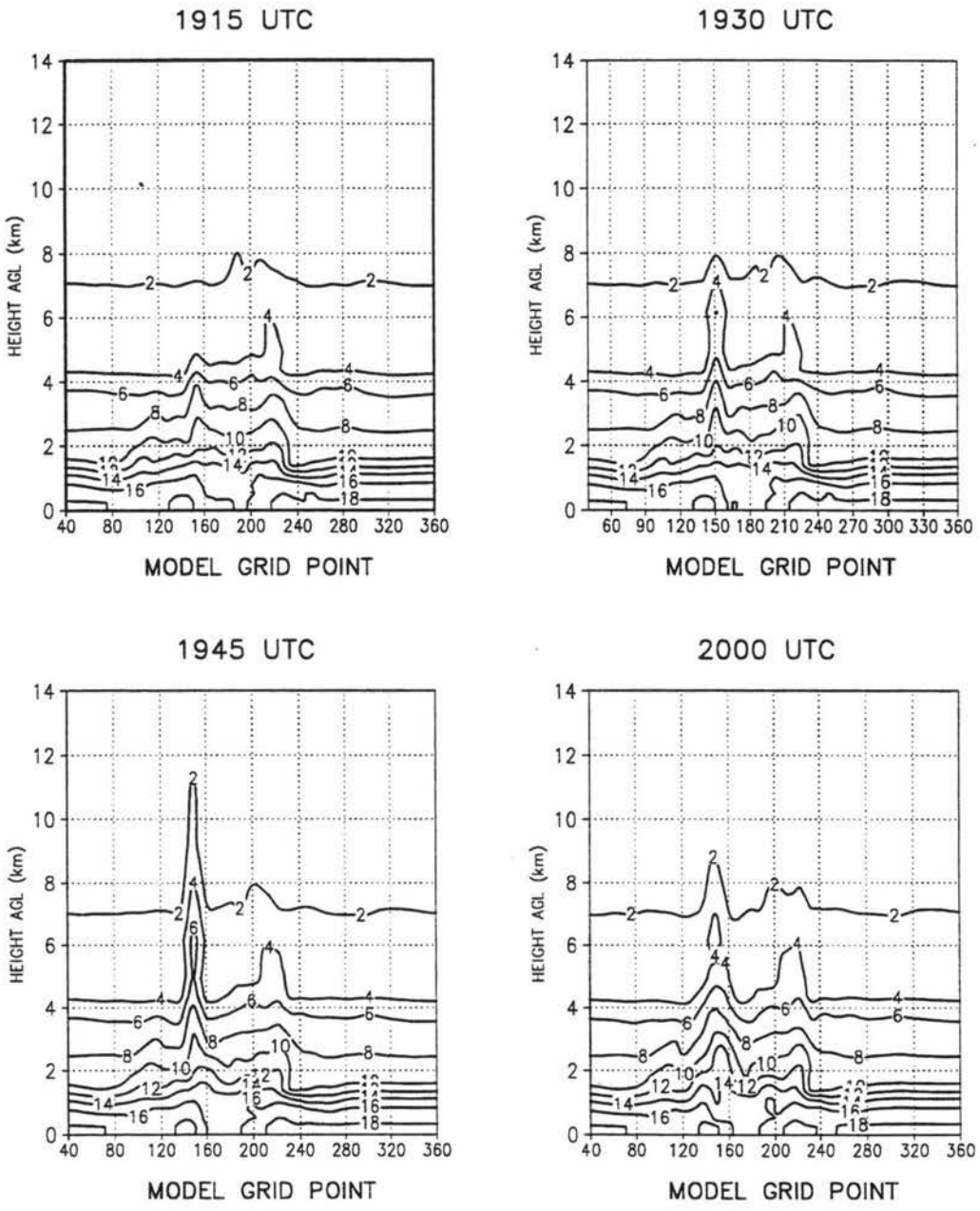

Figure 3.2b: Snapshots in time at fifteen minute intervals from Experiment E2DA averaged to 20 km: total water mixing ratio ($g\ kg^{-1}$) from 1915-2000 UTC. Land/sea boundaries are at model grid points 133 and 267.

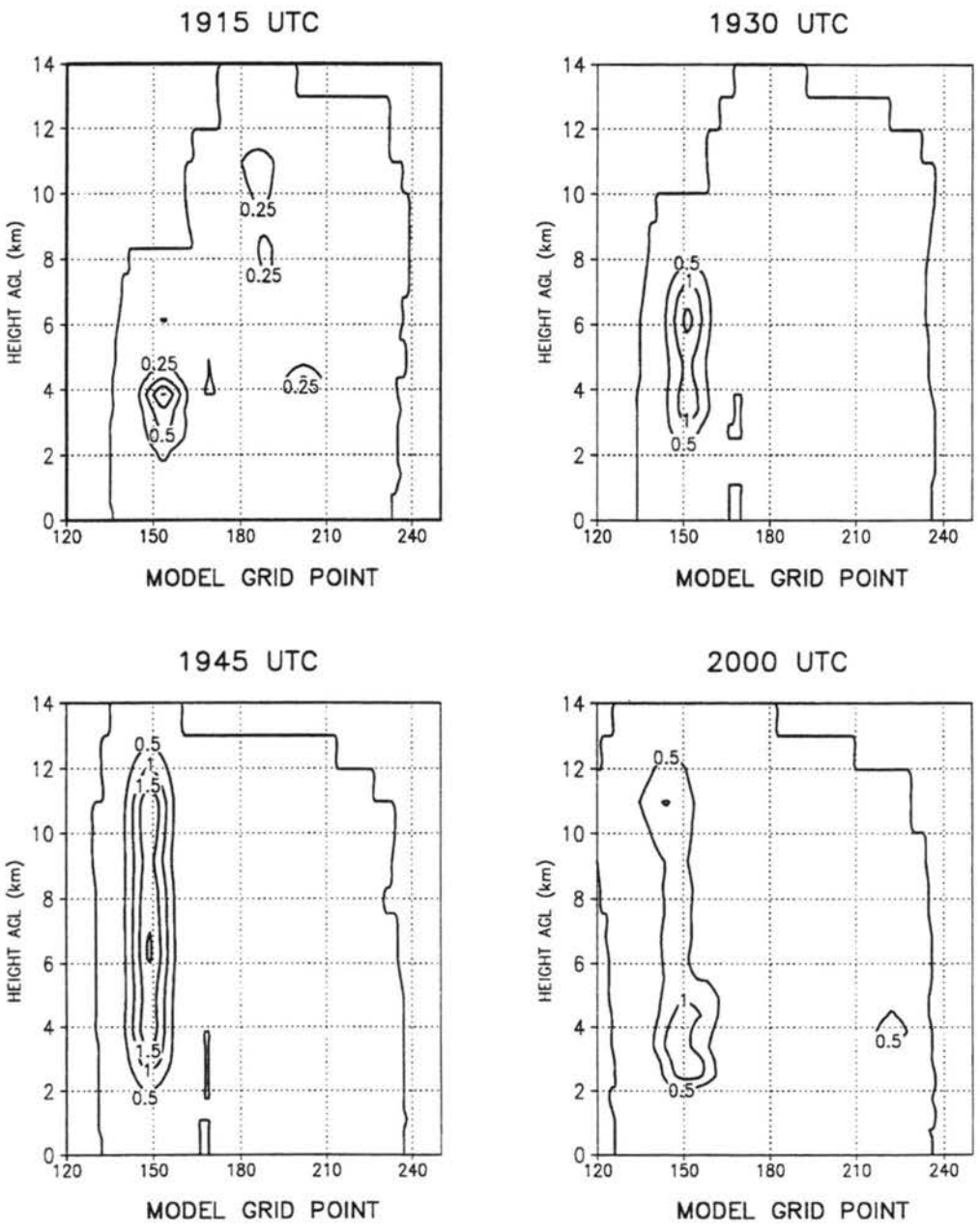

Figure 3.2c: Snapshots in time at fifteen minute intervals from Experiment E2DA averaged to 20 km: condensate mixing ratio ($g\ kg^{-1}$) from 1915-2000 UTC. Land/sea boundaries are at model grid points 133 and 267.

EXPERIMENT P2DB

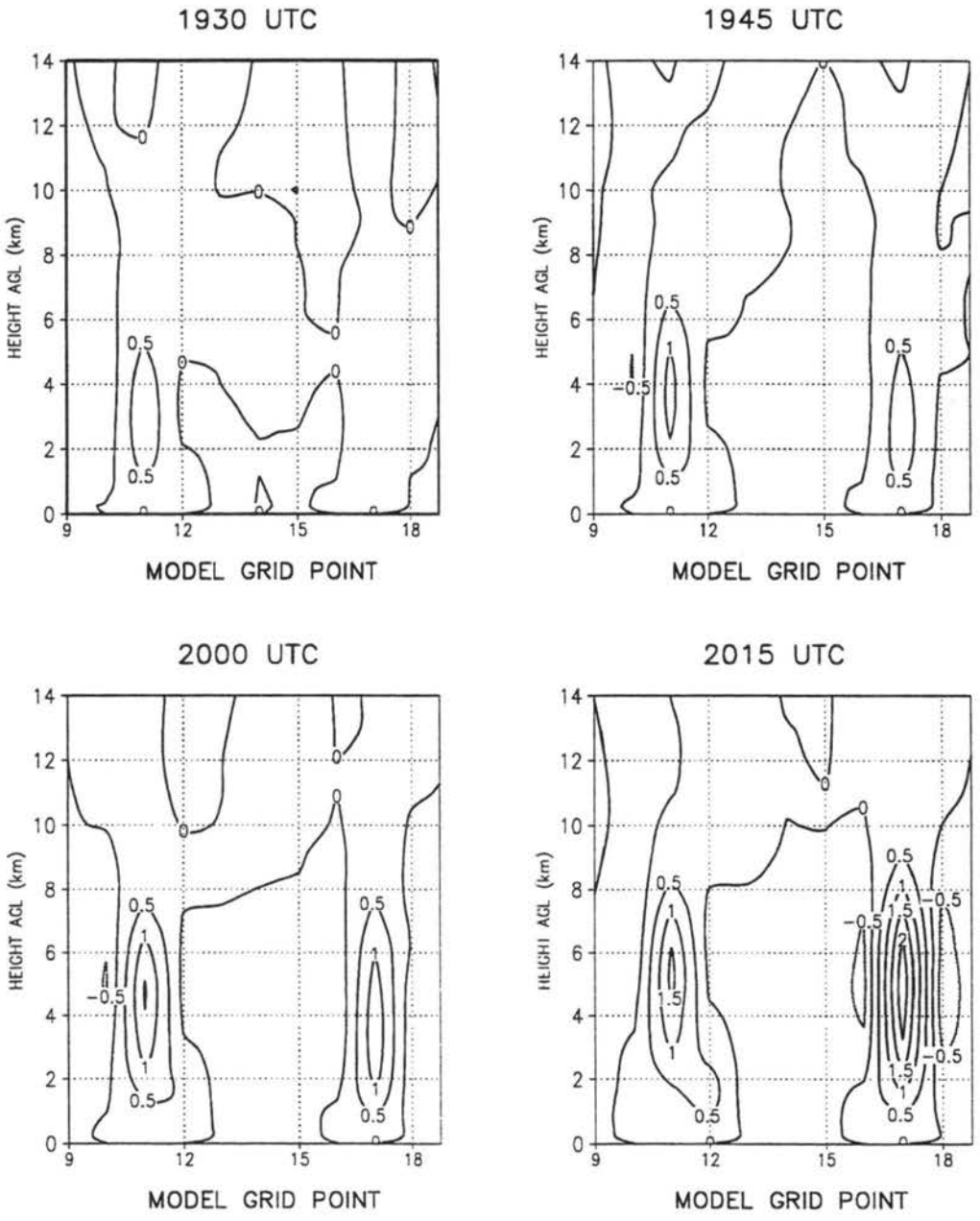

Figure 3.3a: Snapshots in time at fifteen minute intervals from Experiment P2DB: vertical velocity (ms^{-1}) from 1930-2015 UTC. Land/sea boundaries are at model grid points 10 and 20.

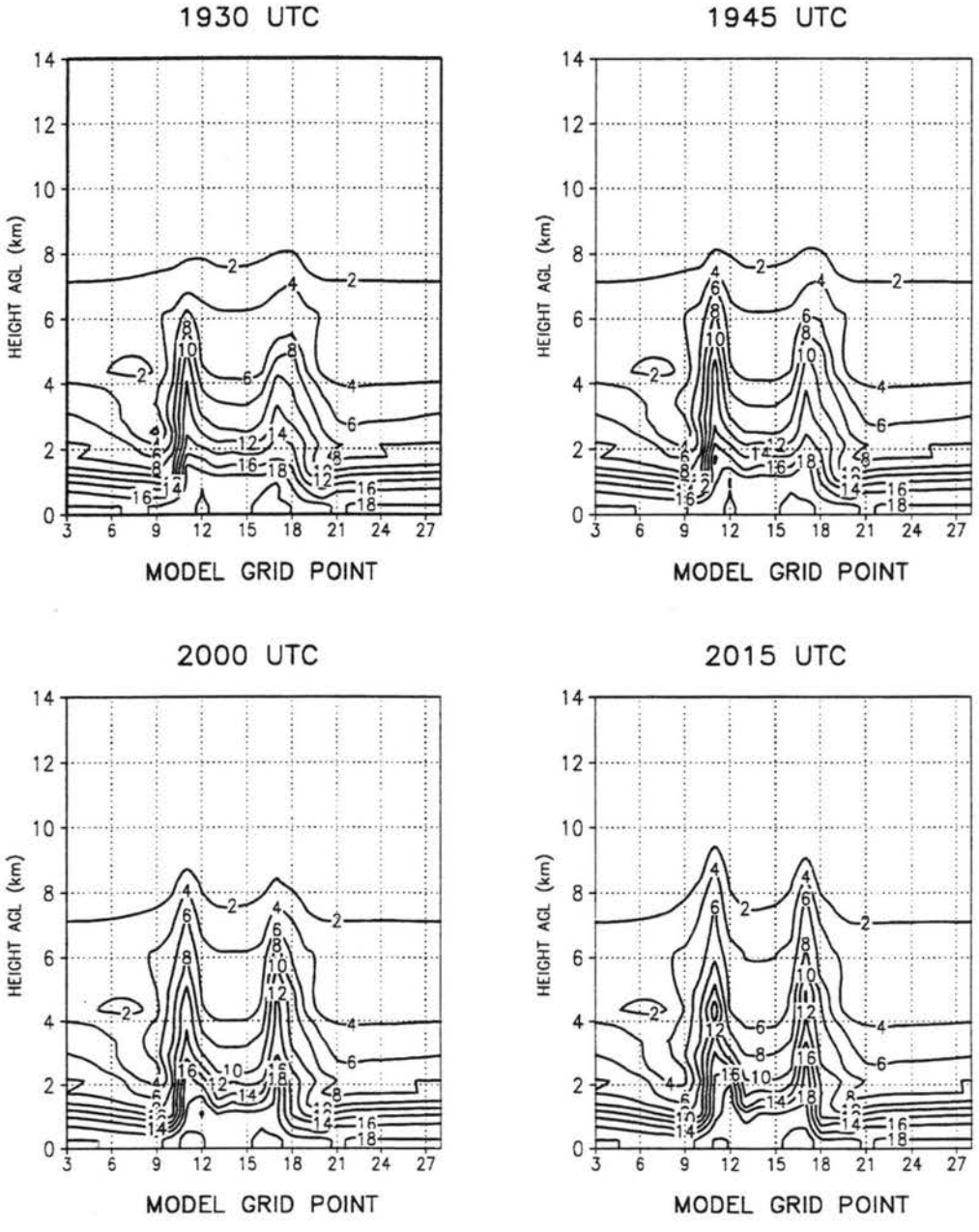

Figure 3.3b: Snapshots in time at fifteen minute intervals from Experiment P2DB: total water mixing ratio ($g\ kg^{-1}$) from 1930-2015 UTC. Land/sea boundaries are at model grid points 10 and 20.

EXPERIMENT P2DB

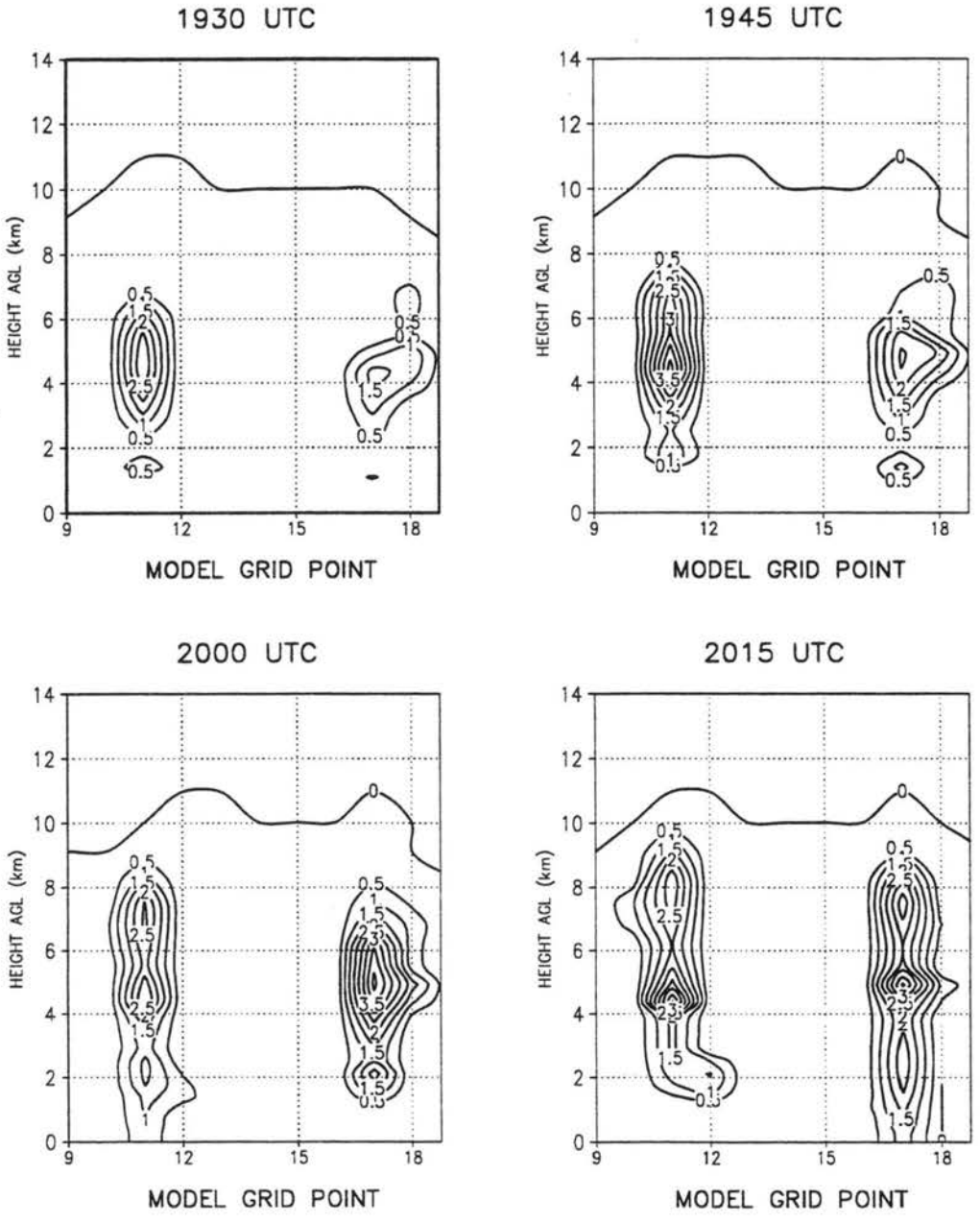

Figure 3.3c: Snapshots in time at fifteen minute intervals from Experiment P2DB: condensate mixing ratio ($g\ kg^{-1}$) from 1930-2015 UTC. Land/sea boundaries are at model grid points 10 and 20.

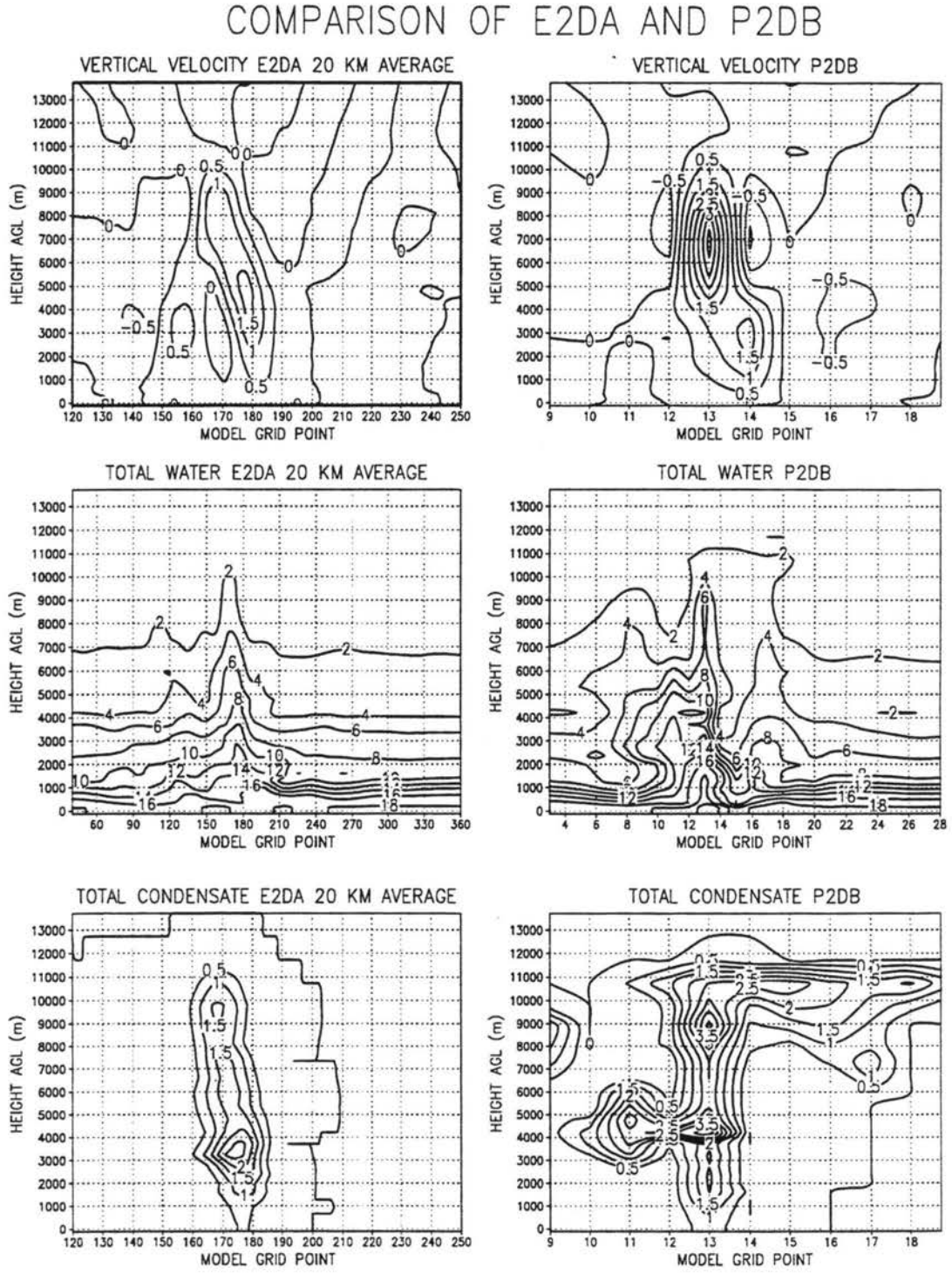

Figure 3.4: Vertical velocity (ms^{-1}), total water ($g\ kg^{-1}$), and total condensate ($g\ kg^{-1}$) at 2230 UTC for E2DA and P2DB

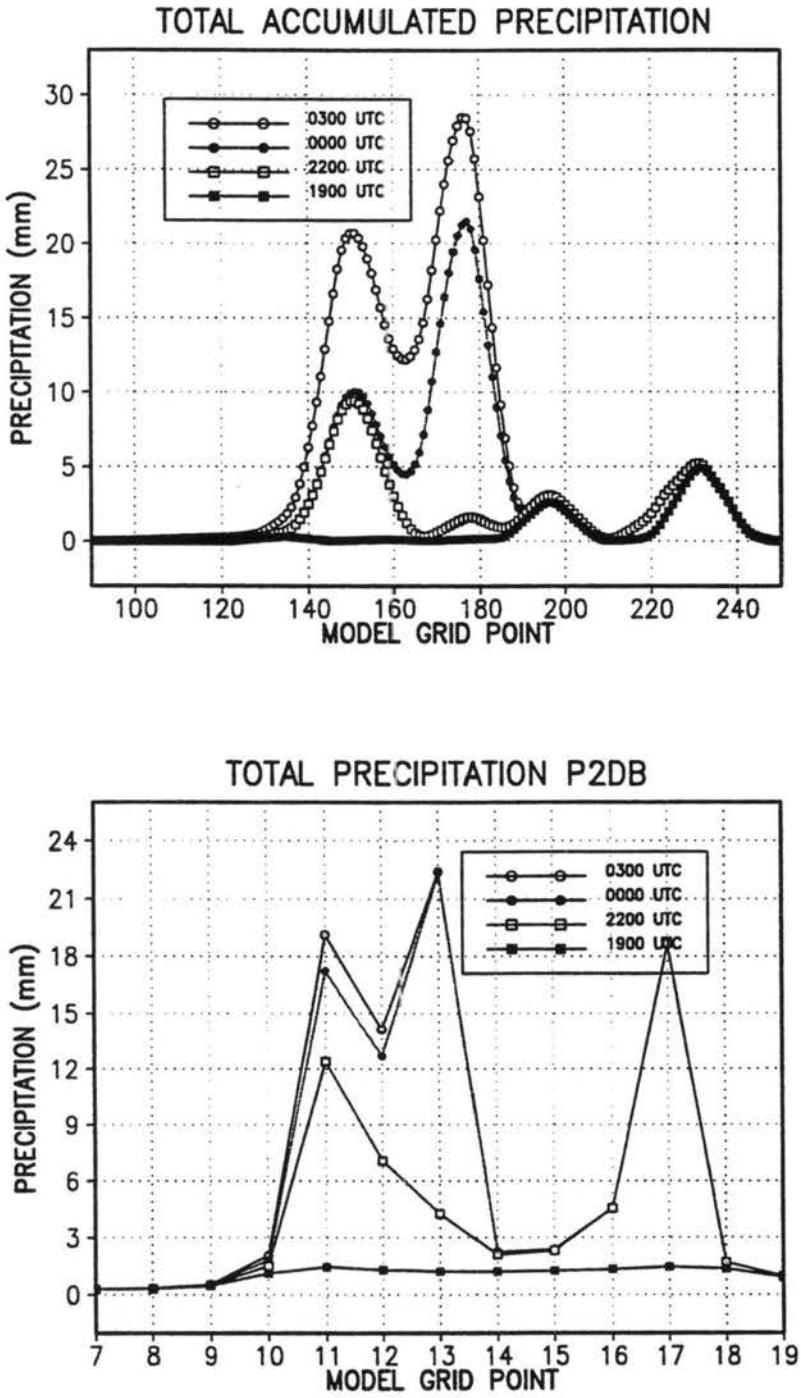

Figure 3.5: The surface precipitation record for E2DA averaged to 20 km and P2DB.

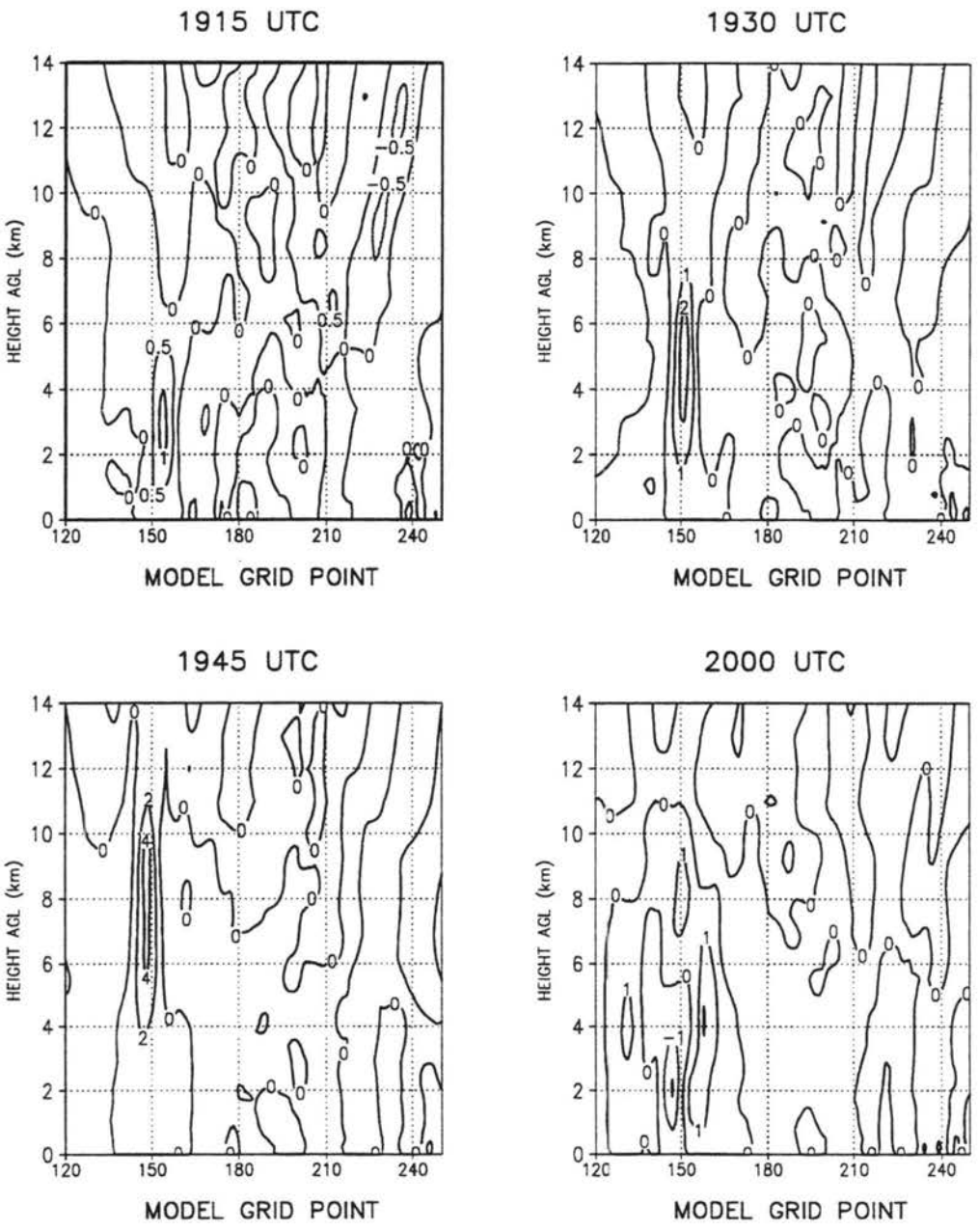

Figure 3.6a: Snapshots in time at fifteen minute intervals from Experiment E2DA averaged to 12 km: vertical velocity (ms^{-1}) from 1915-2000 UTC. Land/sea boundaries are at model grid points 133 and 267.

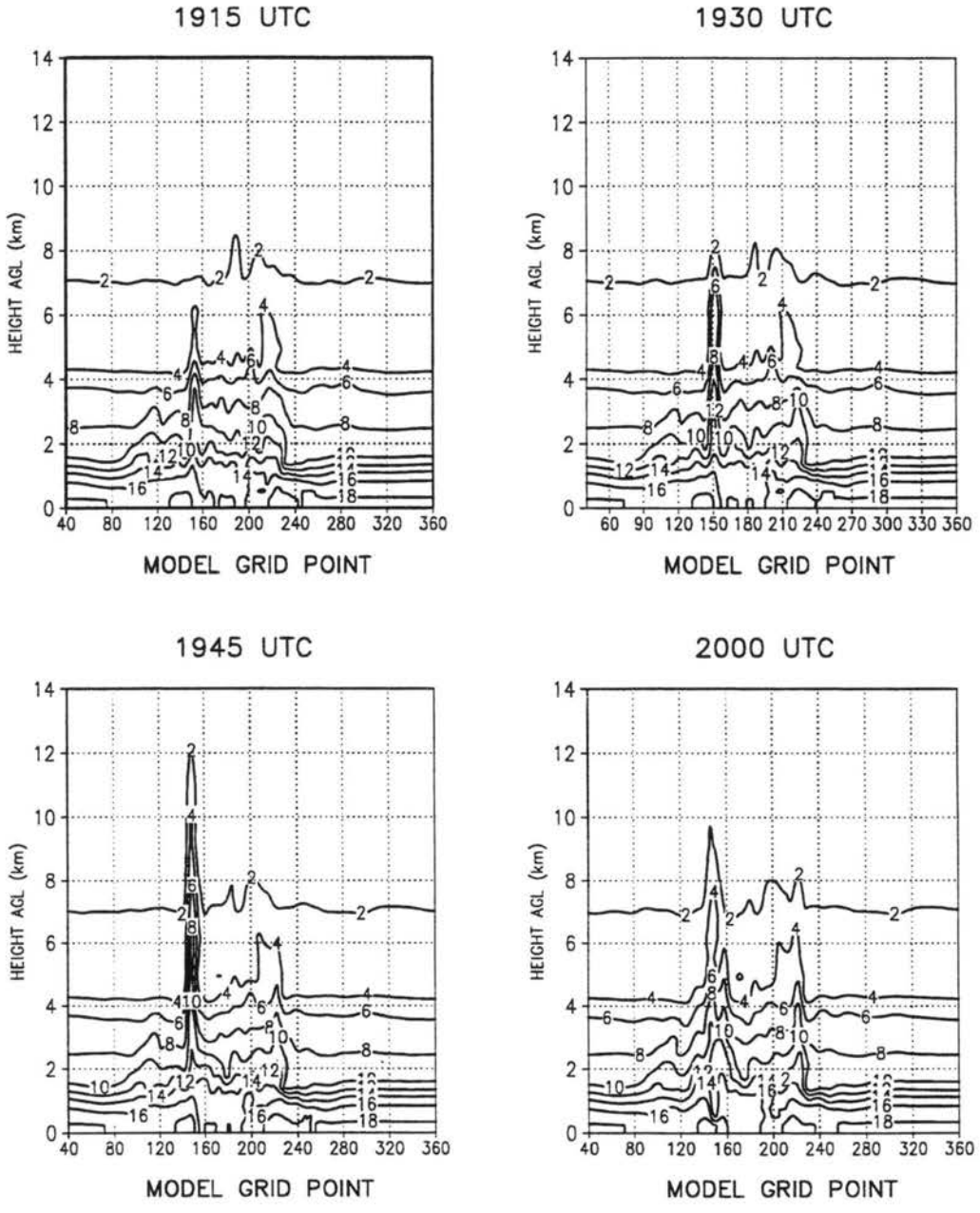

Figure 3.6b: Snapshots in time at fifteen minute intervals from Experiment E2DA averaged to 12 km: total water mixing ratio ($g\ kg^{-1}$) from 1915-2000 UTC. Land/sea boundaries are at model grid points 133 and 267.

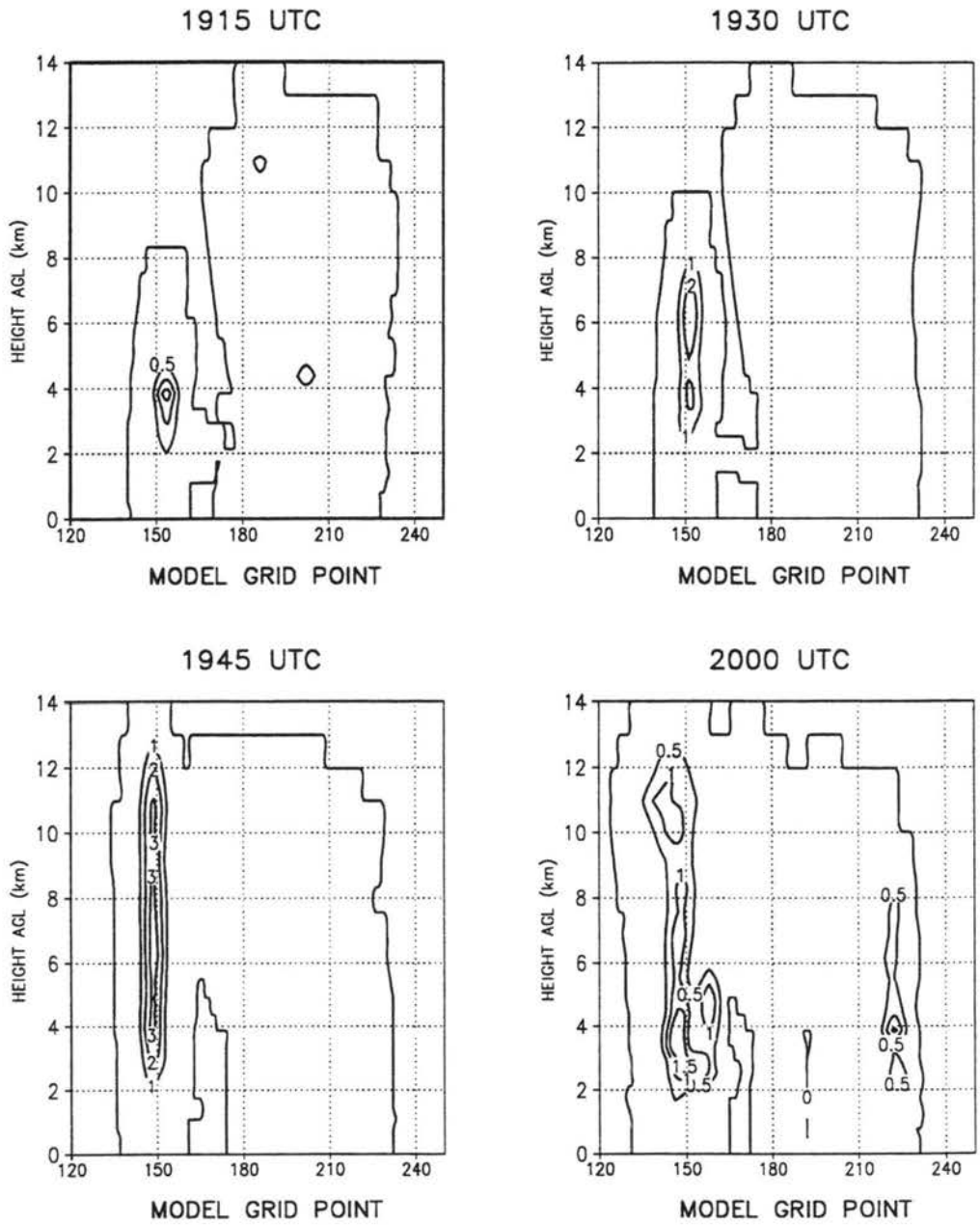

Figure 3.6c: Snapshots in time at fifteen minute intervals from Experiment E2DA averaged to 12 km: condensate mixing ratio ($g\ kg^{-1}$) from 1915-2000 UTC. Land/sea boundaries are at model grid points 133 and 267.

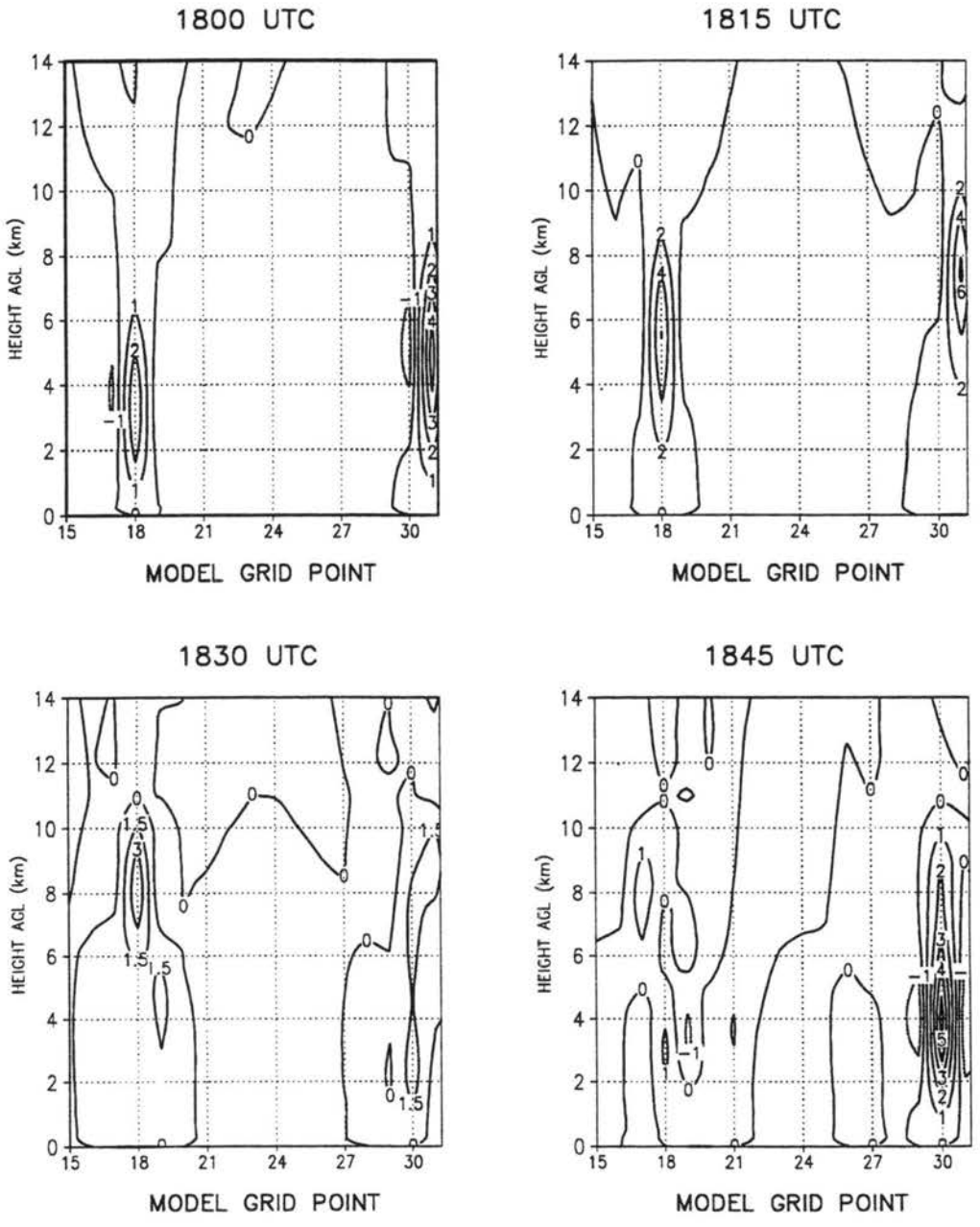

Figure 3.7a: Snapshots in time at fifteen minute intervals from Experiment P2DD: vertical velocity (ms^{-1}) from 1800-1845 UTC. Land/sea boundaries are at model grid points 17 and 33.

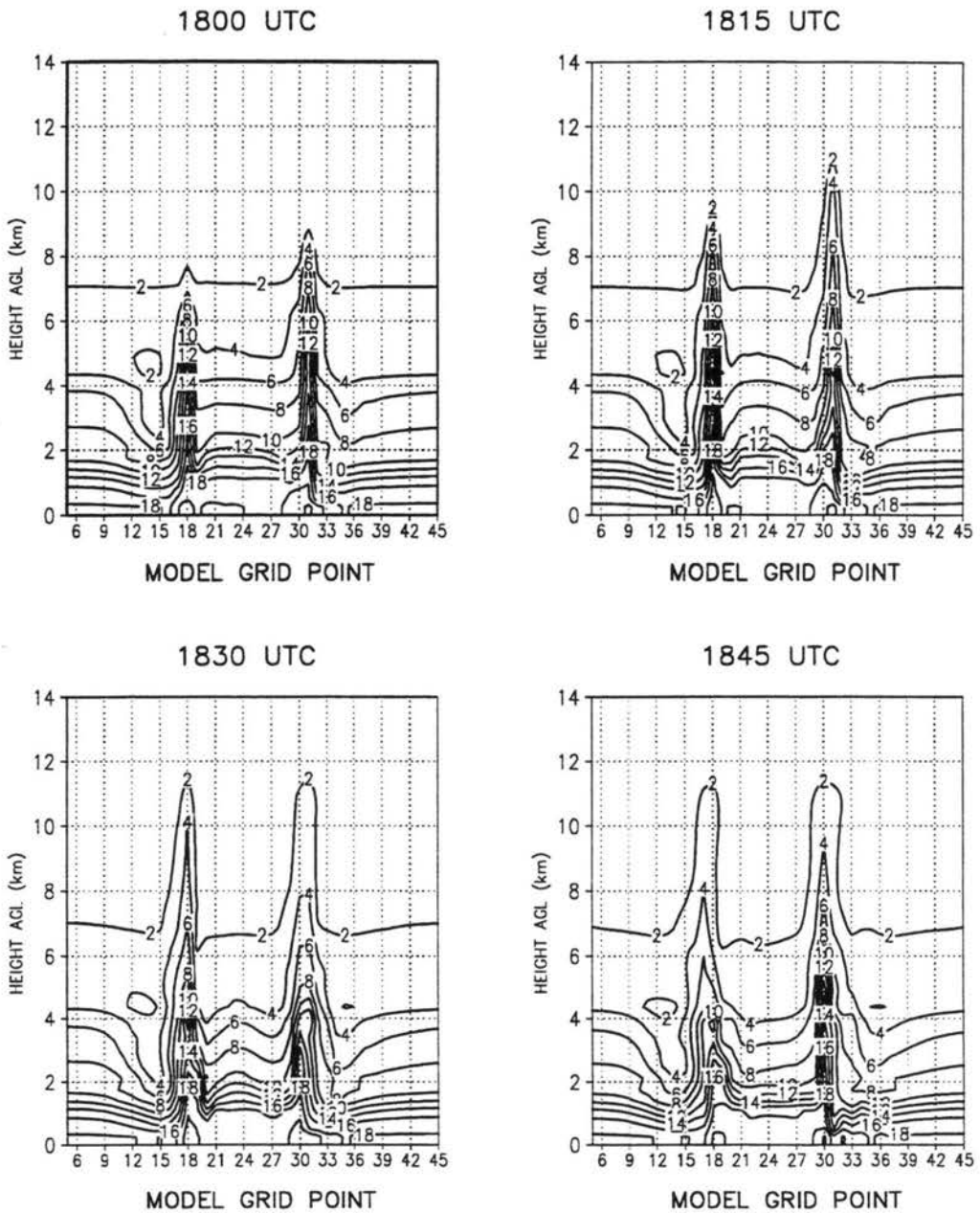

Figure 3.7b: Snapshots in time at fifteen minute intervals from Experiment P2DD: total water mixing ratio ($g\ kg^{-1}$) from 1800-1845 UTC. Land/sea boundaries are at model grid points 17 and 33.

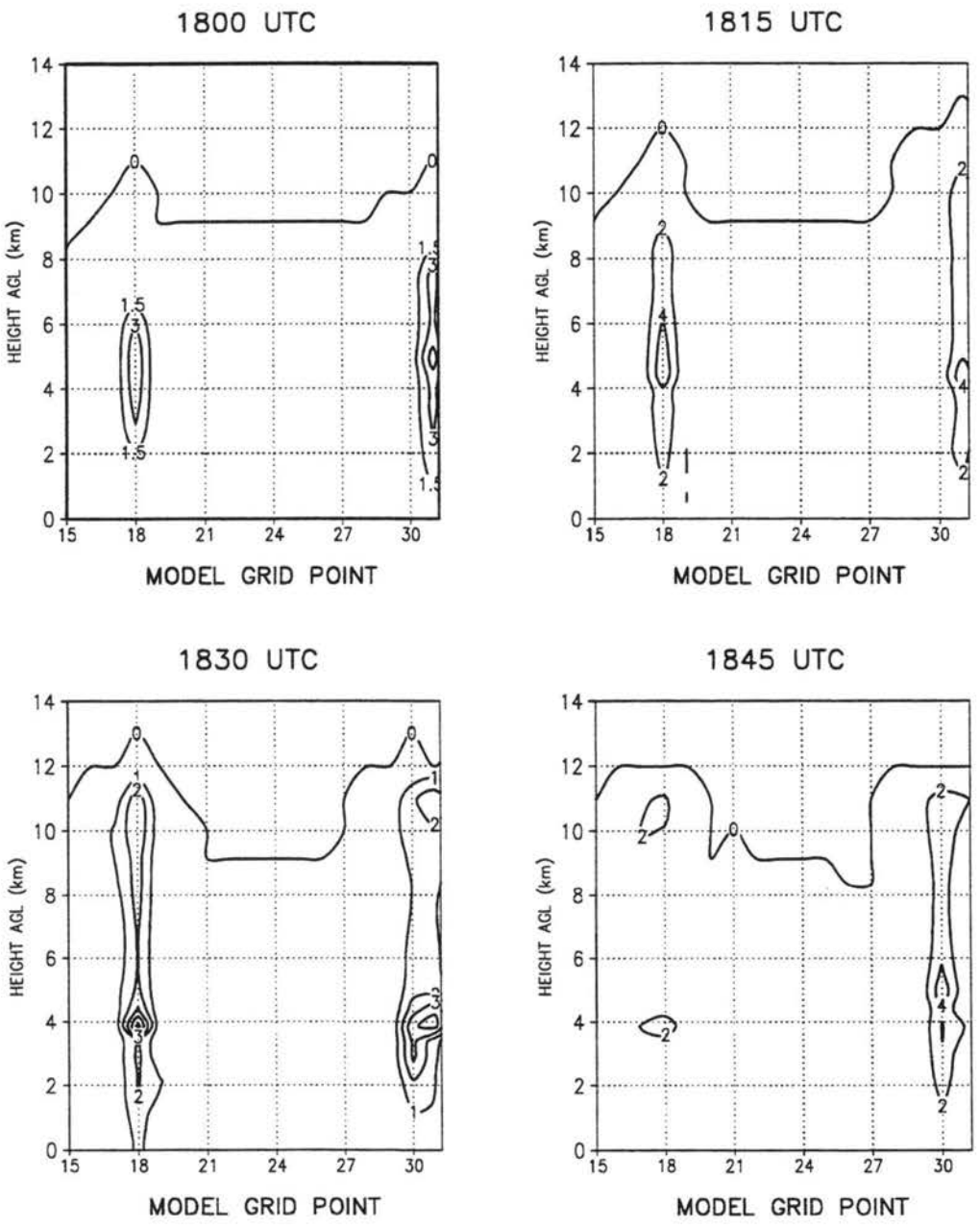

Figure 3.7c: Snapshots in time at fifteen minute intervals from Experiment P2DD: condensate mixing ratio ($g\ kg^{-1}$) from 1800-1845 UTC. Land/sea boundaries are at model grid points 17 and 33.

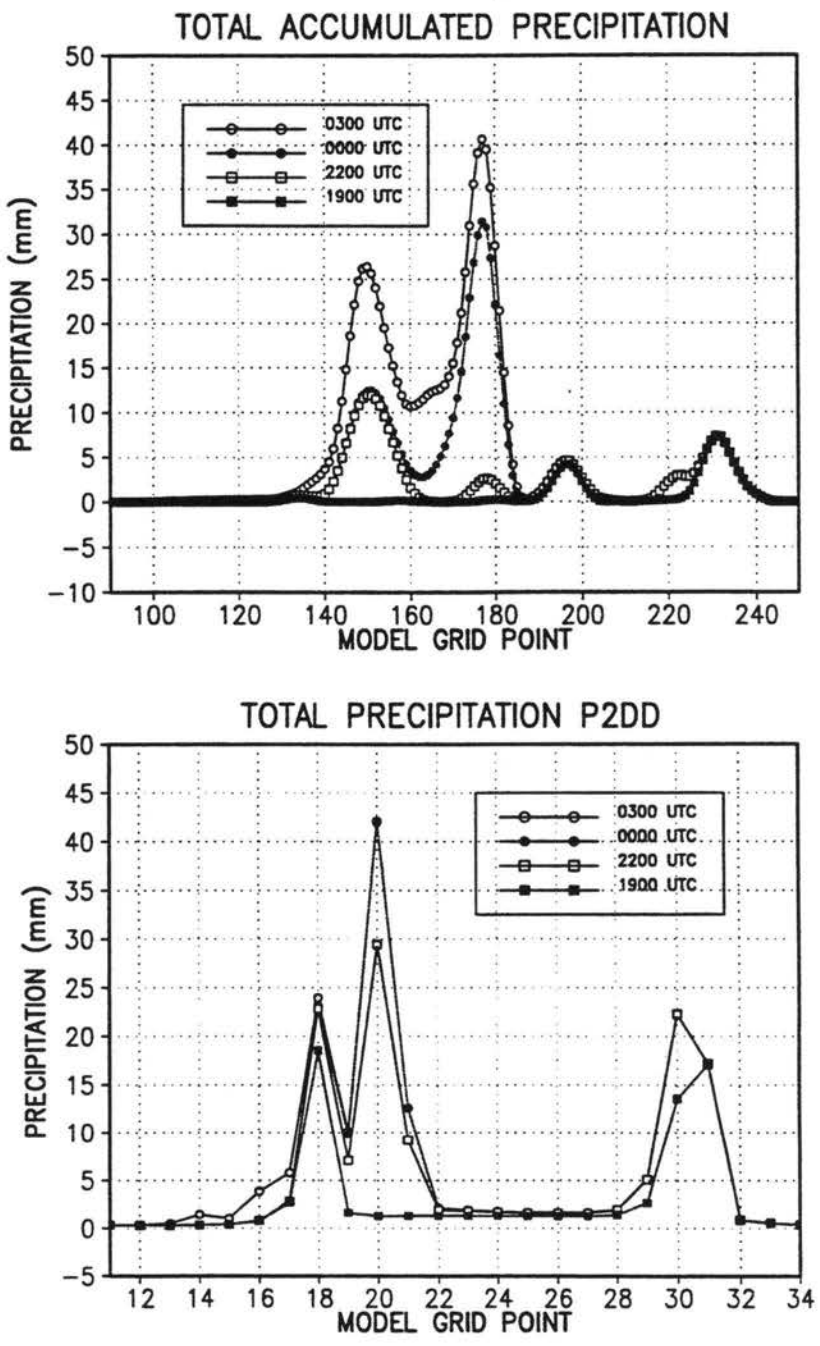

Figure 3.8: The surface precipitation record for E2DA averaged to 12 km and the parameterized run P2DD.

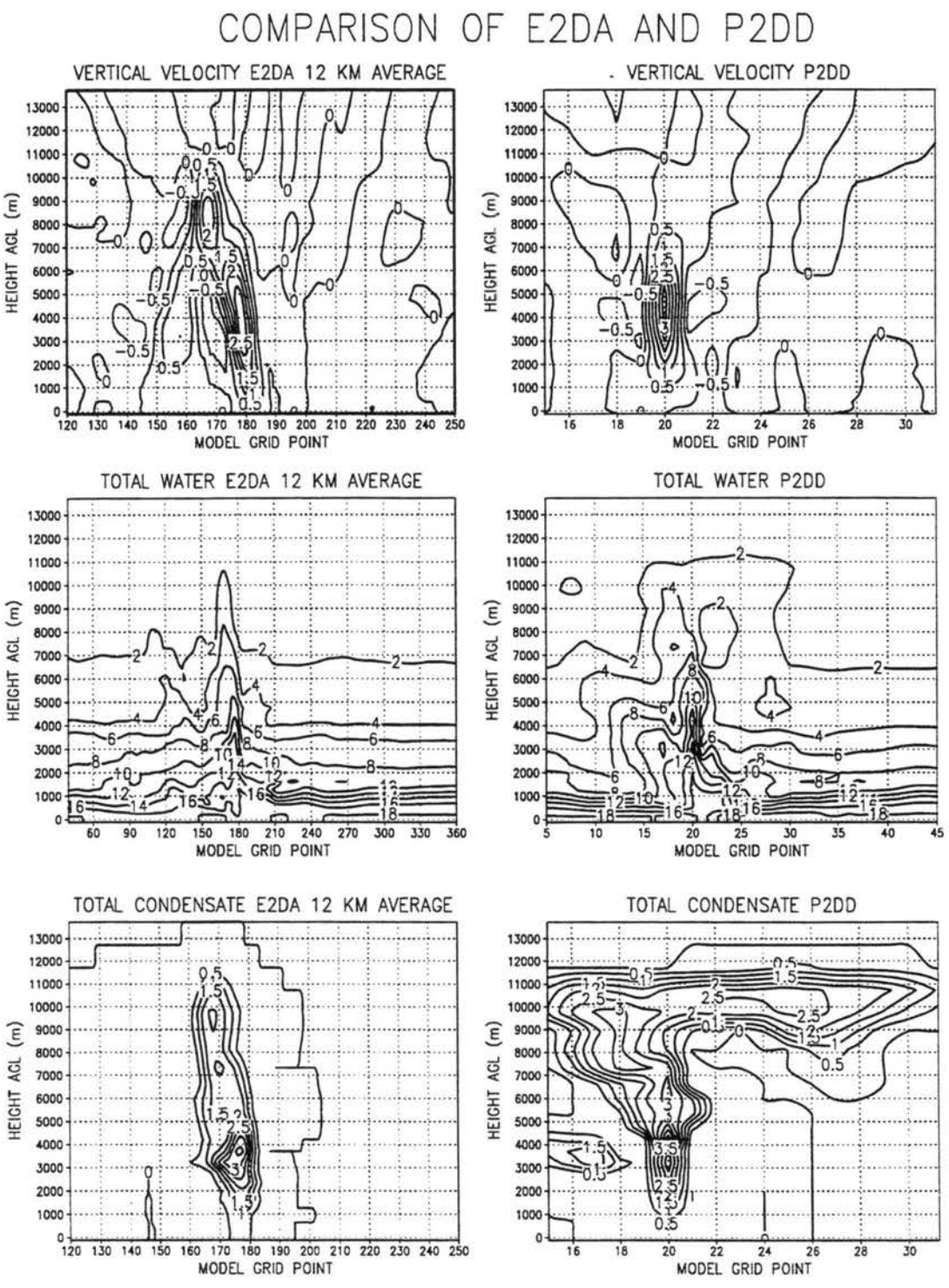

Figure 3.9: Vertical velocity (ms^{-1}), total water ($g\ kg^{-1}$), and total condensate ($g\ kg^{-1}$) at 2230 UTC for E2DA and P2DB

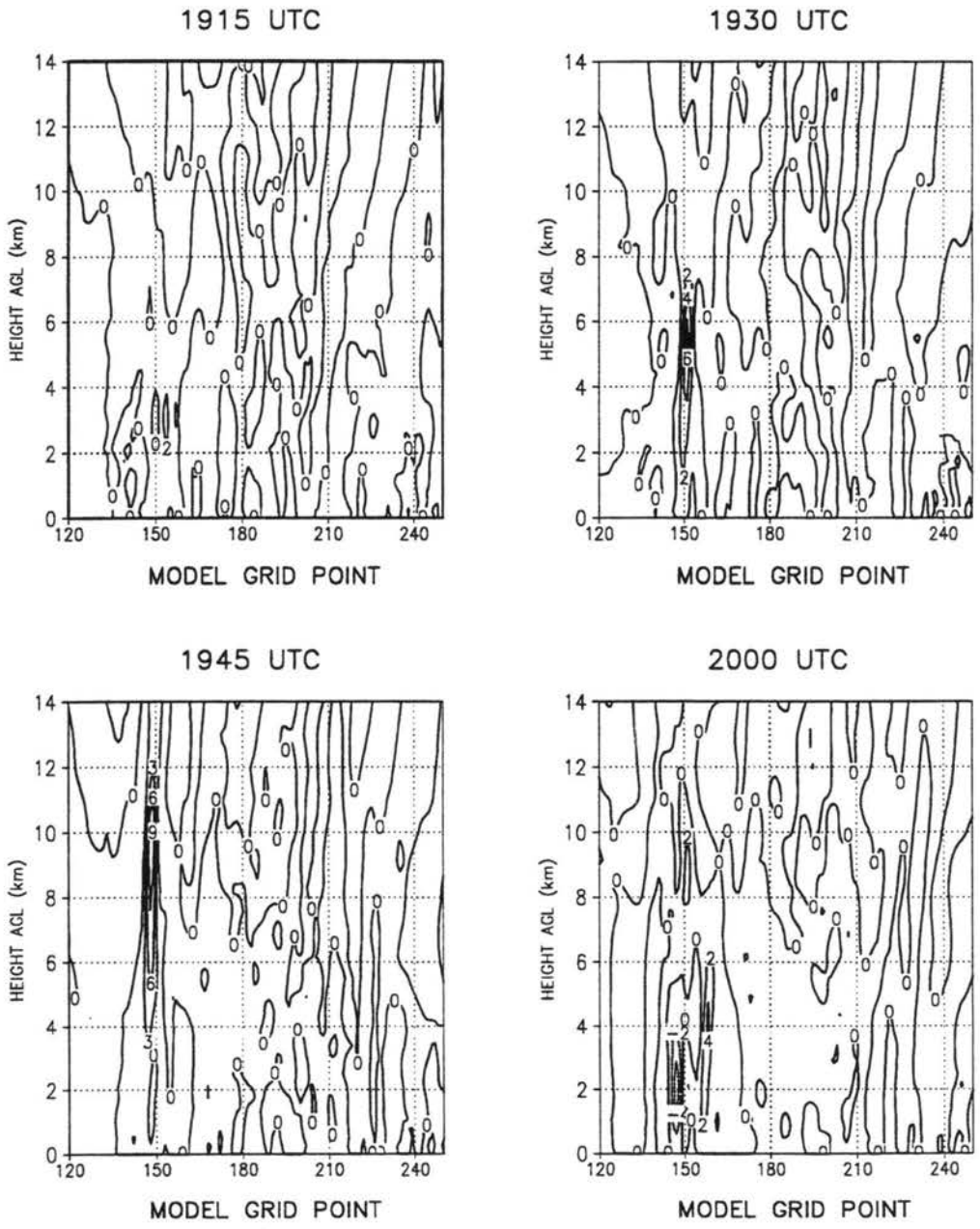

Figure 3.10a: Snapshots in time at fifteen minute intervals from Experiment E2DA averaged to 6 km: vertical velocity (ms^{-1}) from 1915-2000 UTC. Land/sea boundaries are at model grid points 133 and 267.

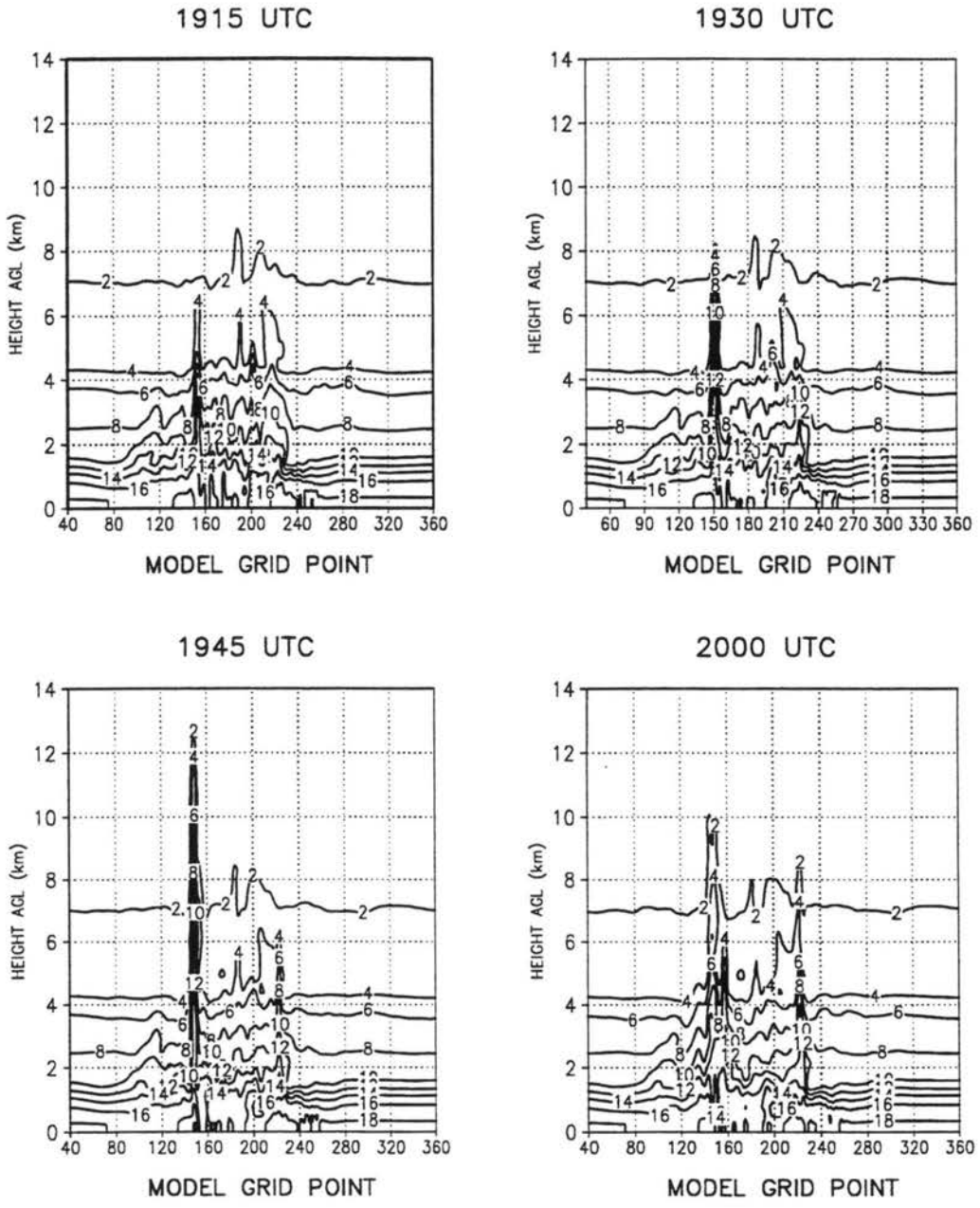

Figure 3.10b: Snapshots in time at fifteen minute intervals from Experiment E2DA averaged to 6 km: total water mixing ratio ($g\ kg^{-1}$) from 1915-2015 UTC. Land/sea boundaries are at model grid points 133 and 267.

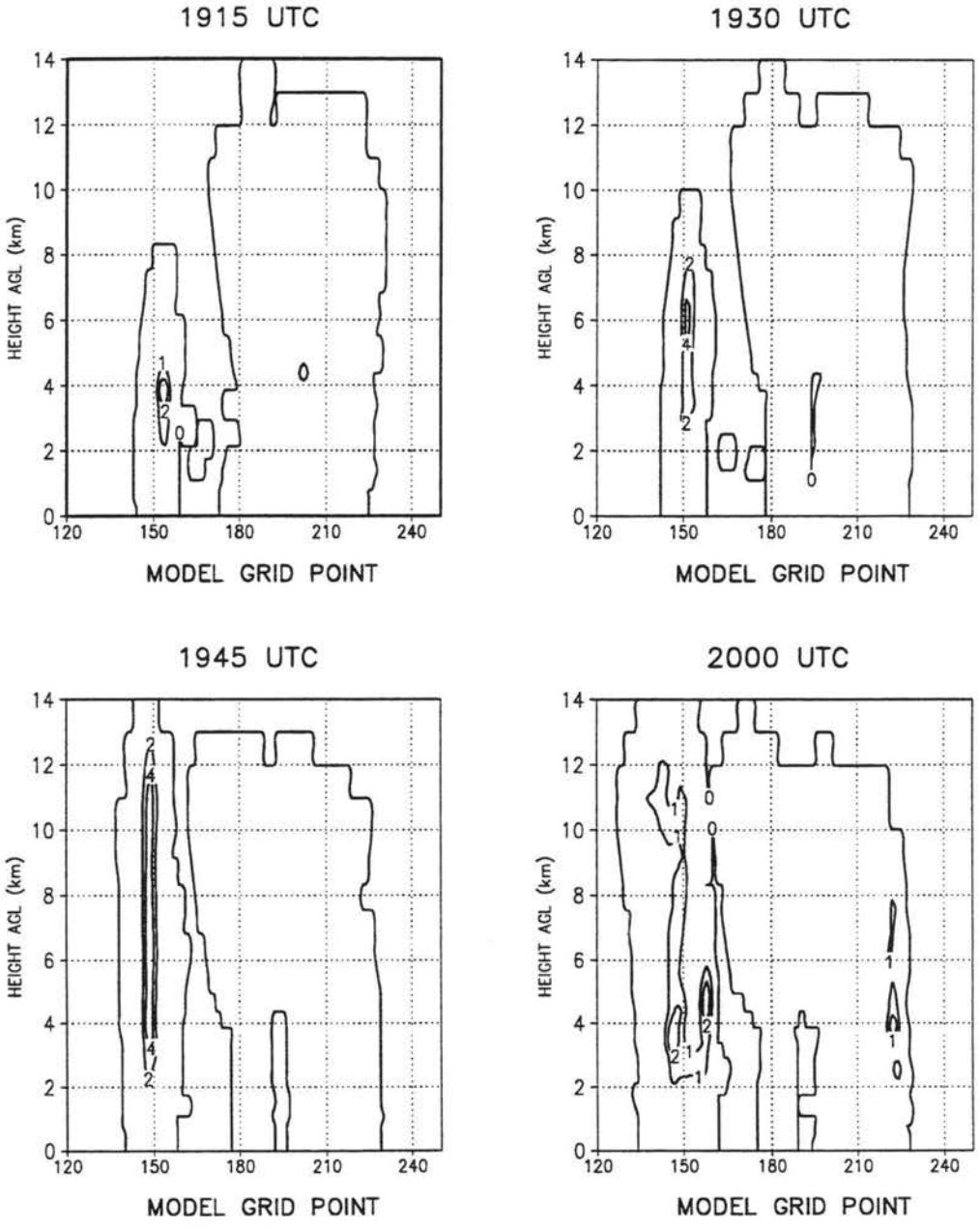

Figure 3.10c: Snapshots in time at fifteen minute intervals from Experiment E2DA averaged to 6 km: condensate mixing ratio ($g\ kg^{-1}$) from 1915-2015 UTC. Land/sea boundaries are at model grid points 133 and 267.

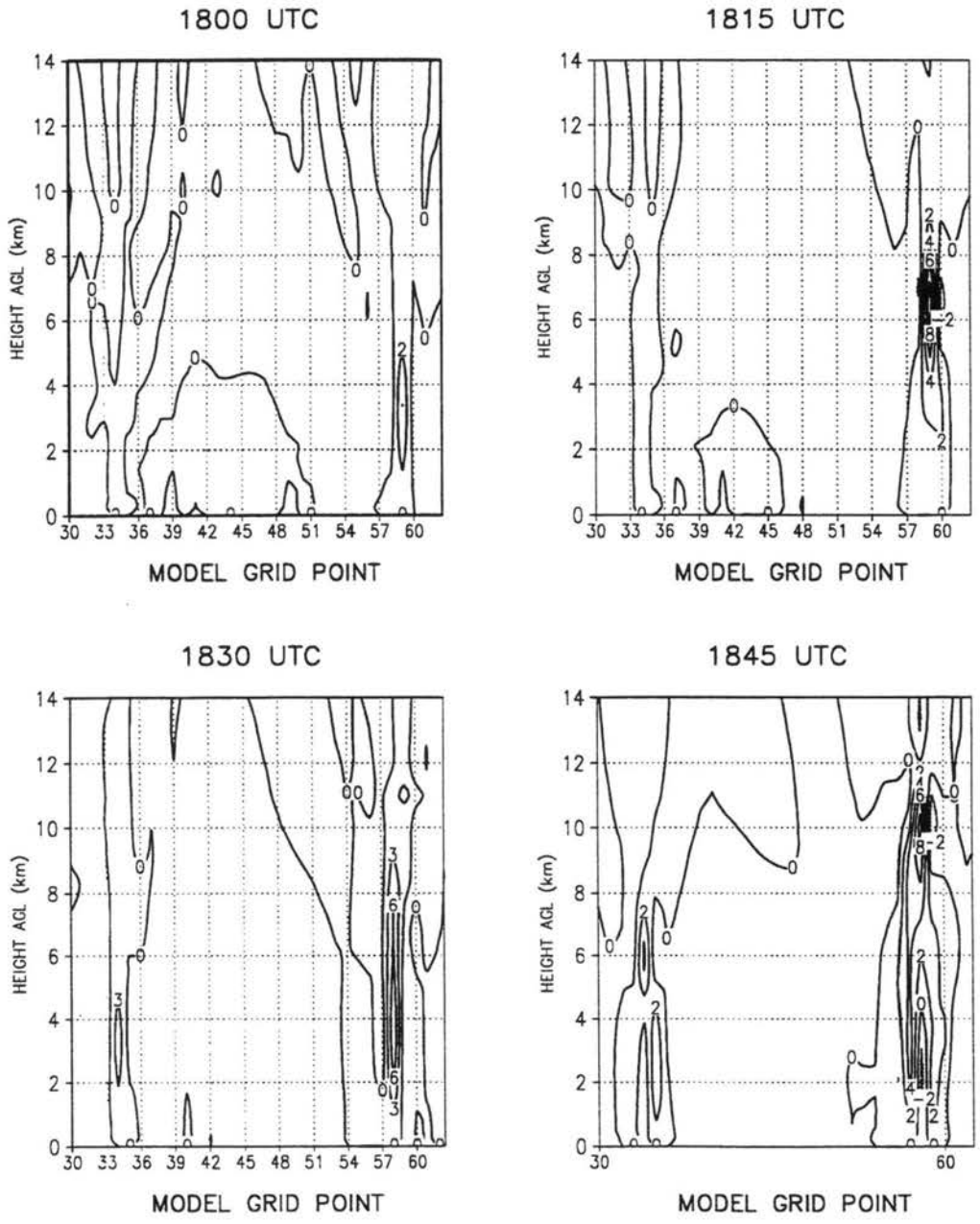

Figure 3.11a: Snapshots in time at fifteen minute intervals from Experiment P2DI: vertical velocity (ms^{-1}) from 1800-1845 UTC. Land/sea boundaries are at model grid points 33 and 67.

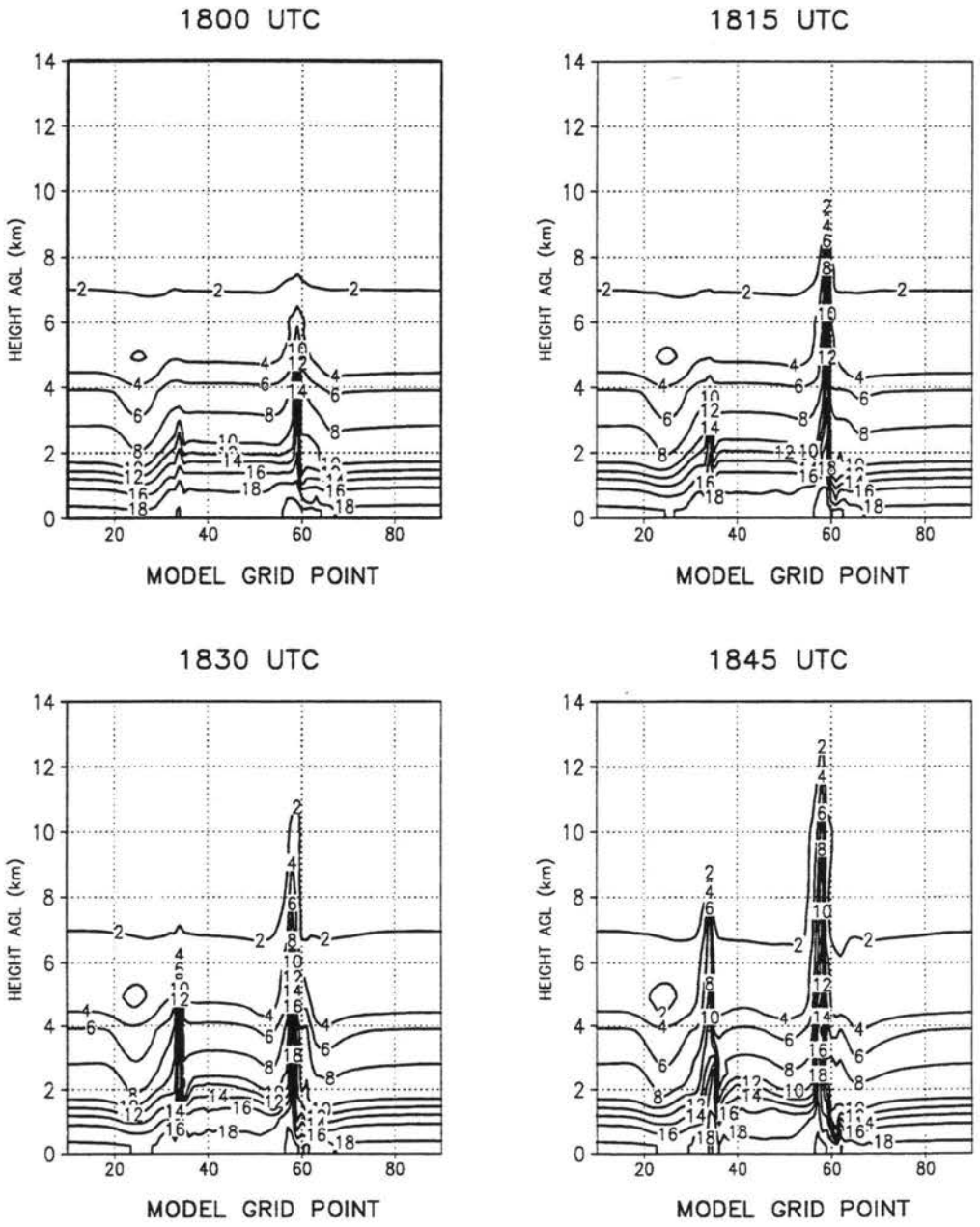

Figure 3.11b: Snapshots in time at fifteen minute intervals from Experiment P2DI: total water mixing ratio ($g\ kg^{-1}$) from 1800-1845 UTC. Land/sea boundaries are at model grid points 33 and 67.

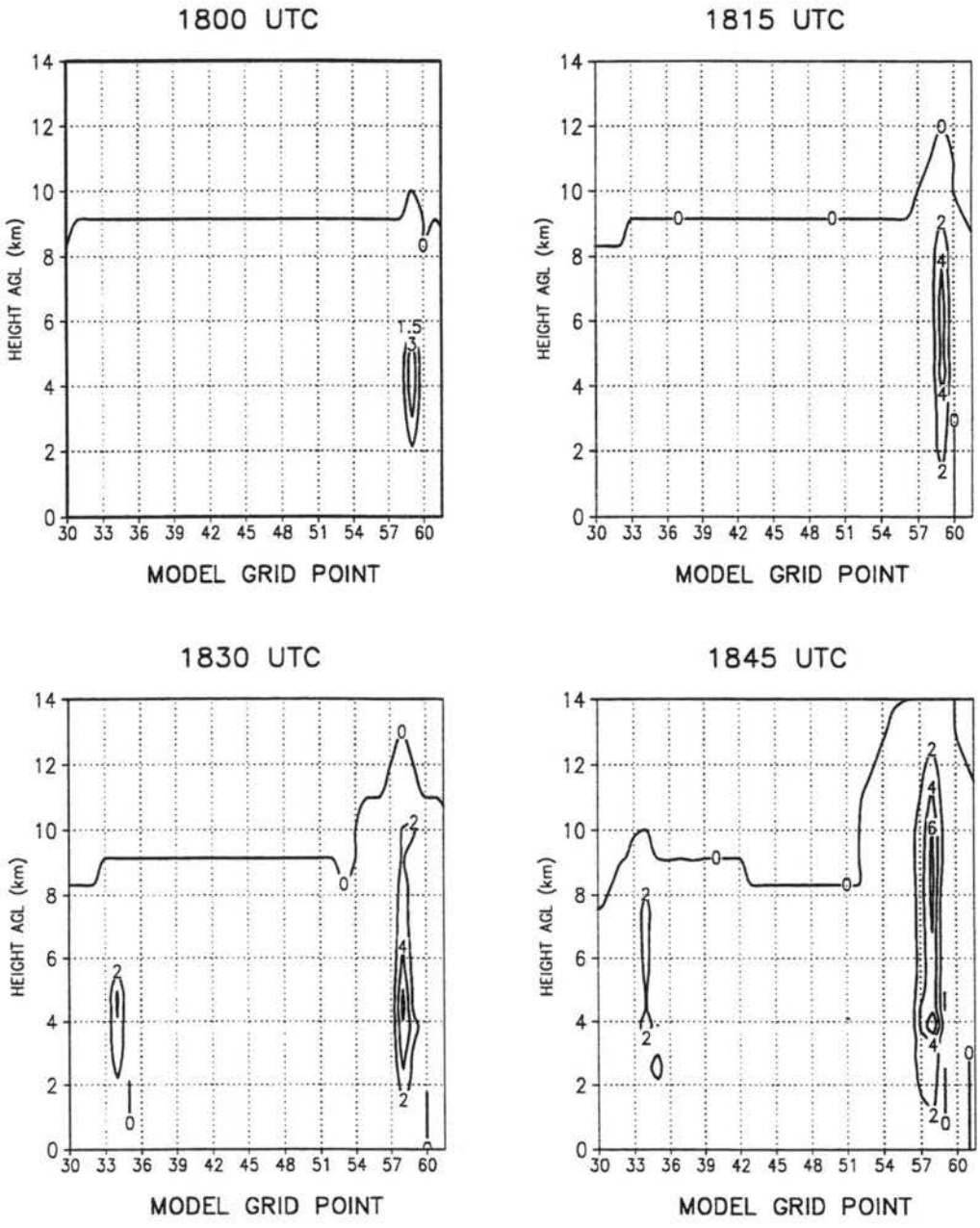

Figure 3.11c: Snapshots in time at fifteen minute intervals from Experiment P2DI: condensate mixing ratio ($g\ kg^{-1}$) from 1800-1845 UTC. Land/sea boundaries are at model grid points 33 and 67.

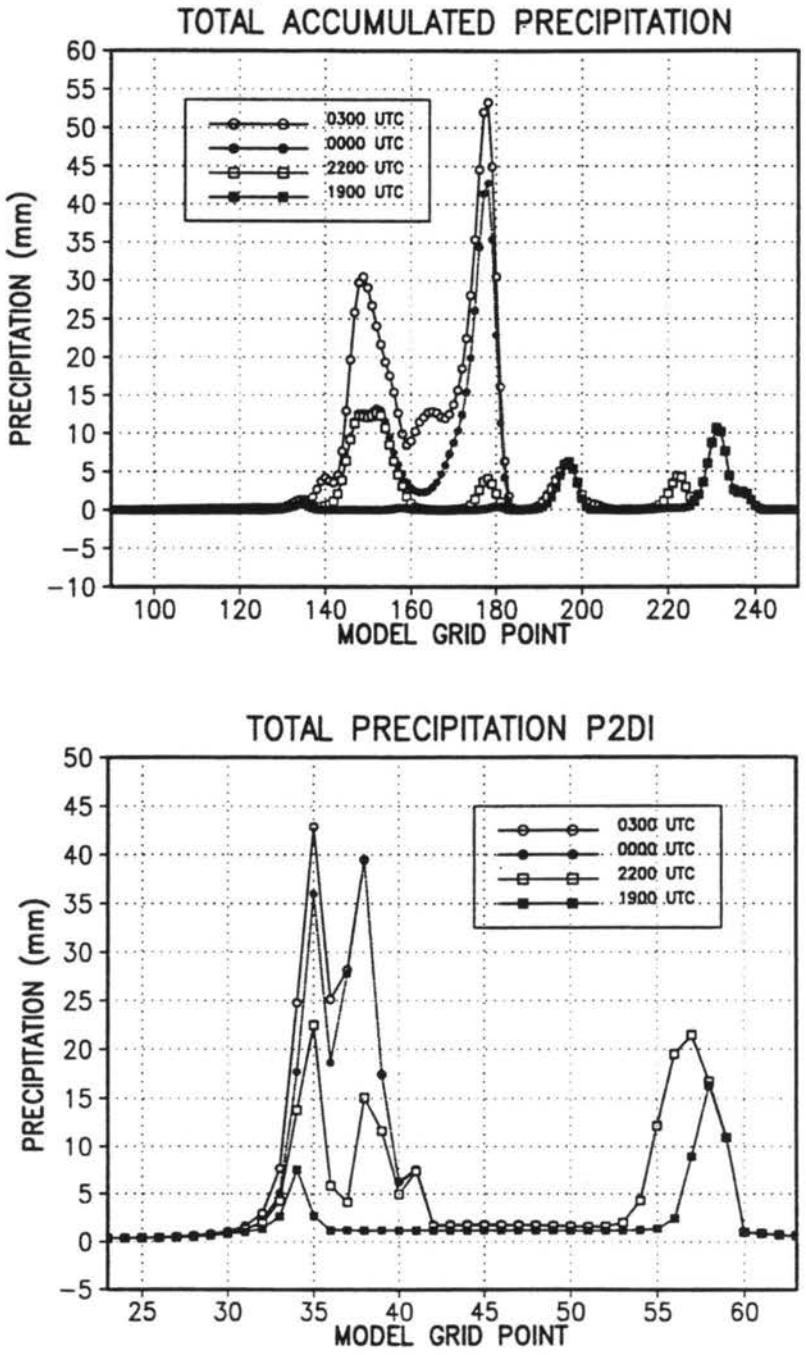

Figure 3.12: The surface precipitation record for E2DA averaged to 6 km and the parameterized run P2DI.

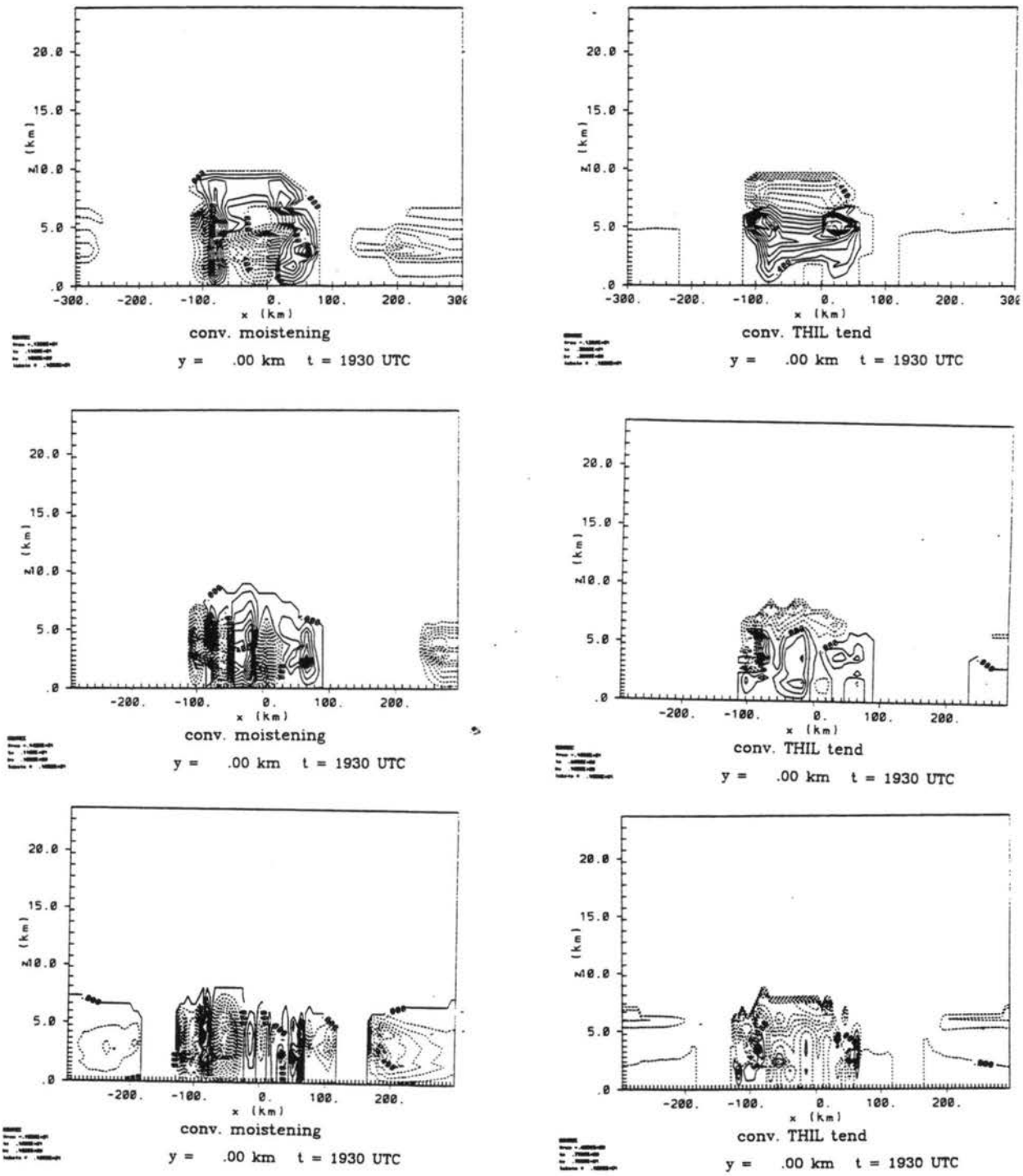

Figure 3.13: Total water and Θ_{il} tendency at 1930 UTC for P2DB, P2DD and P2DI.

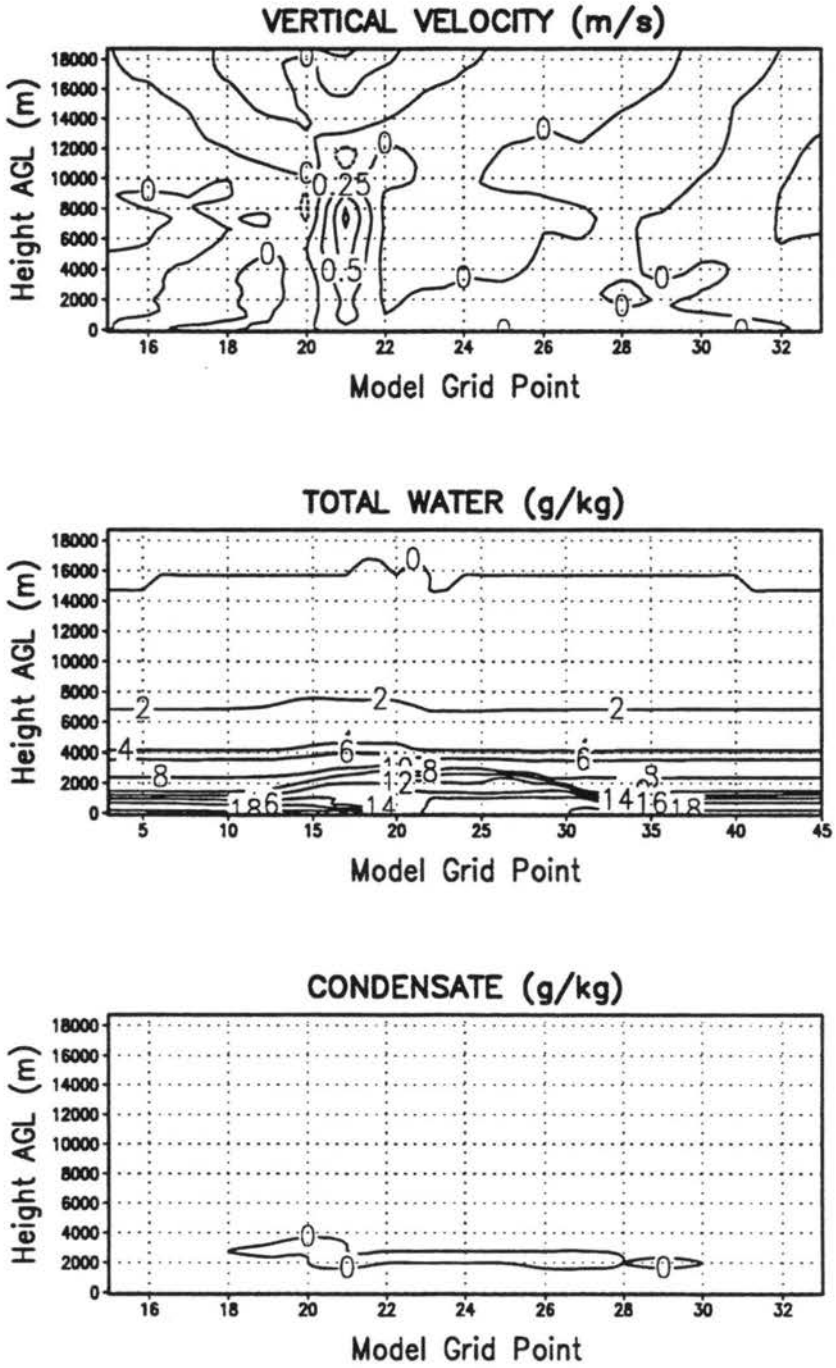

Figure 3.14: Results at 2000 UTC from Kuo simulation P2DO

P2DO (KUO) AT 2300 UTC
12 KM GRID SPACING

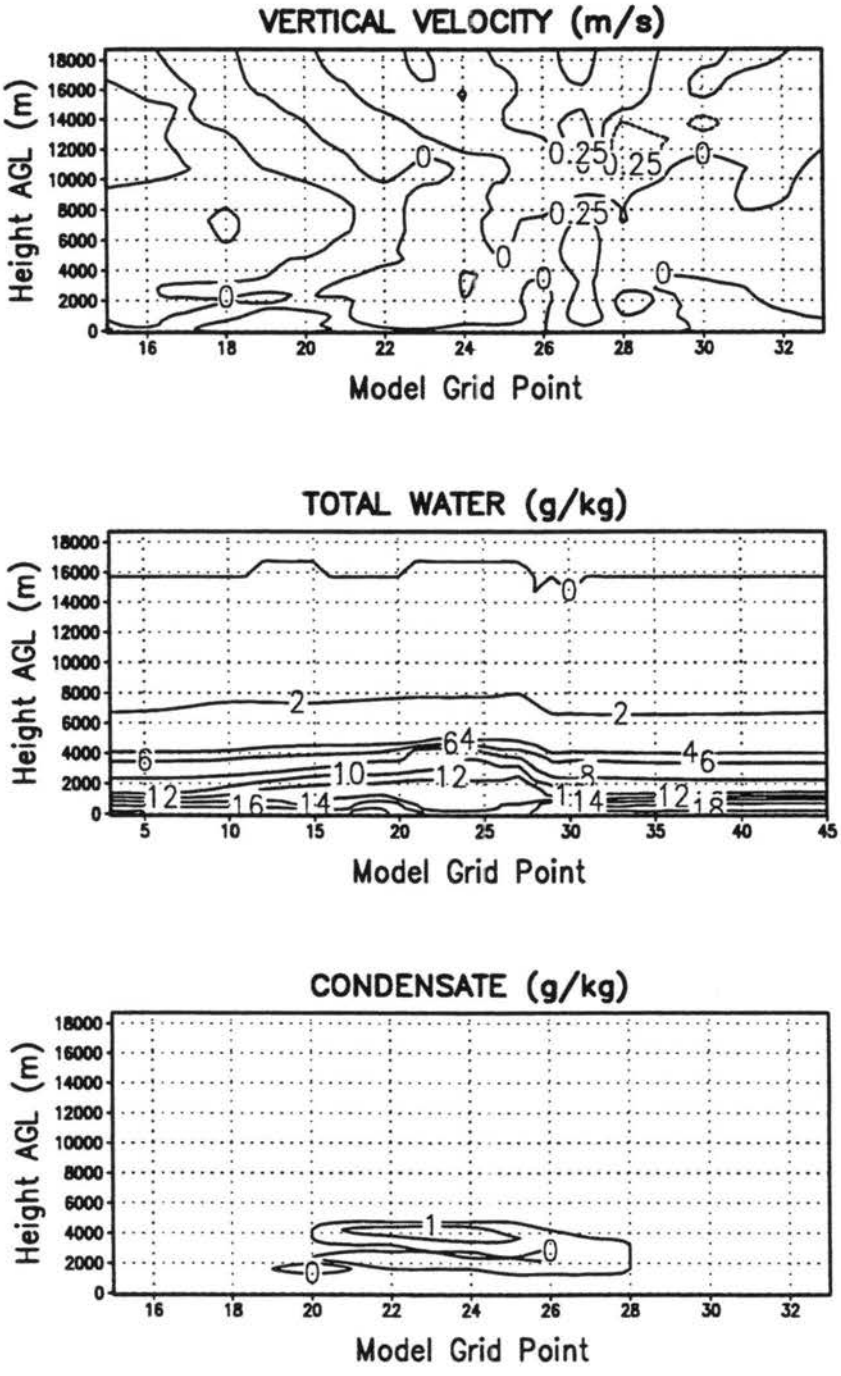

Figure 3.15: Results at 2300 UTC from Kuo simulation P2DO

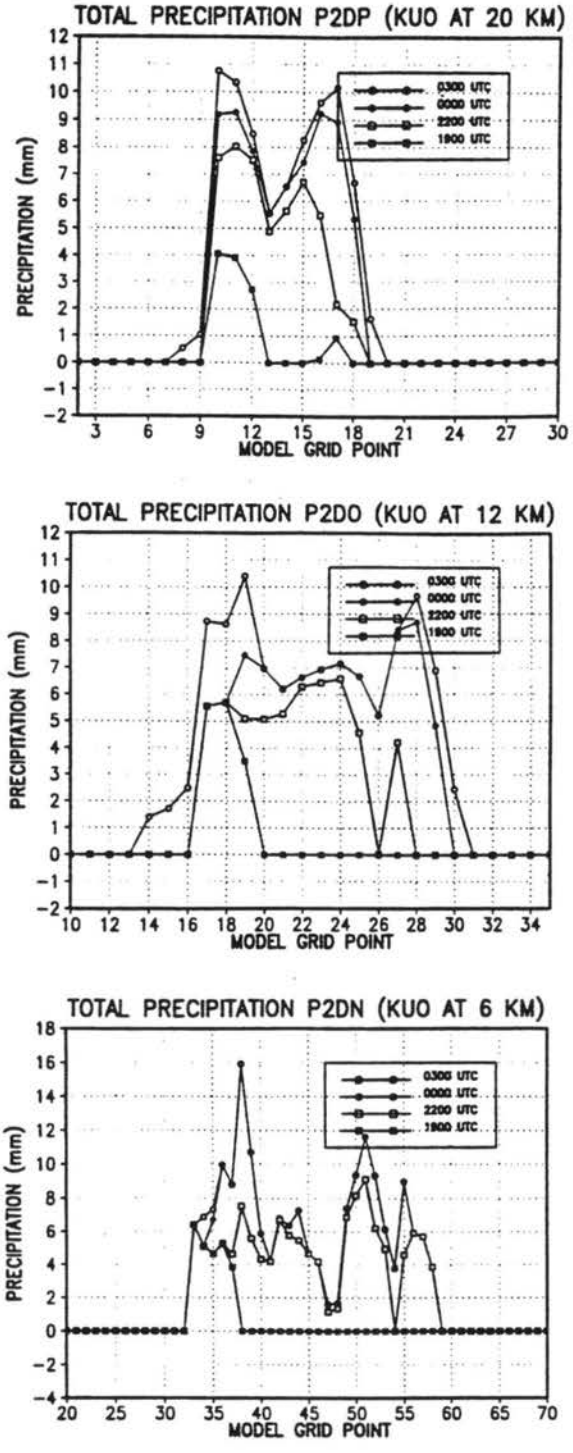

Figure 3.16: Precipitation record from simulations using the Kuo convective parameterization at grid resolutions of 20 km, 12 km and 6 km.

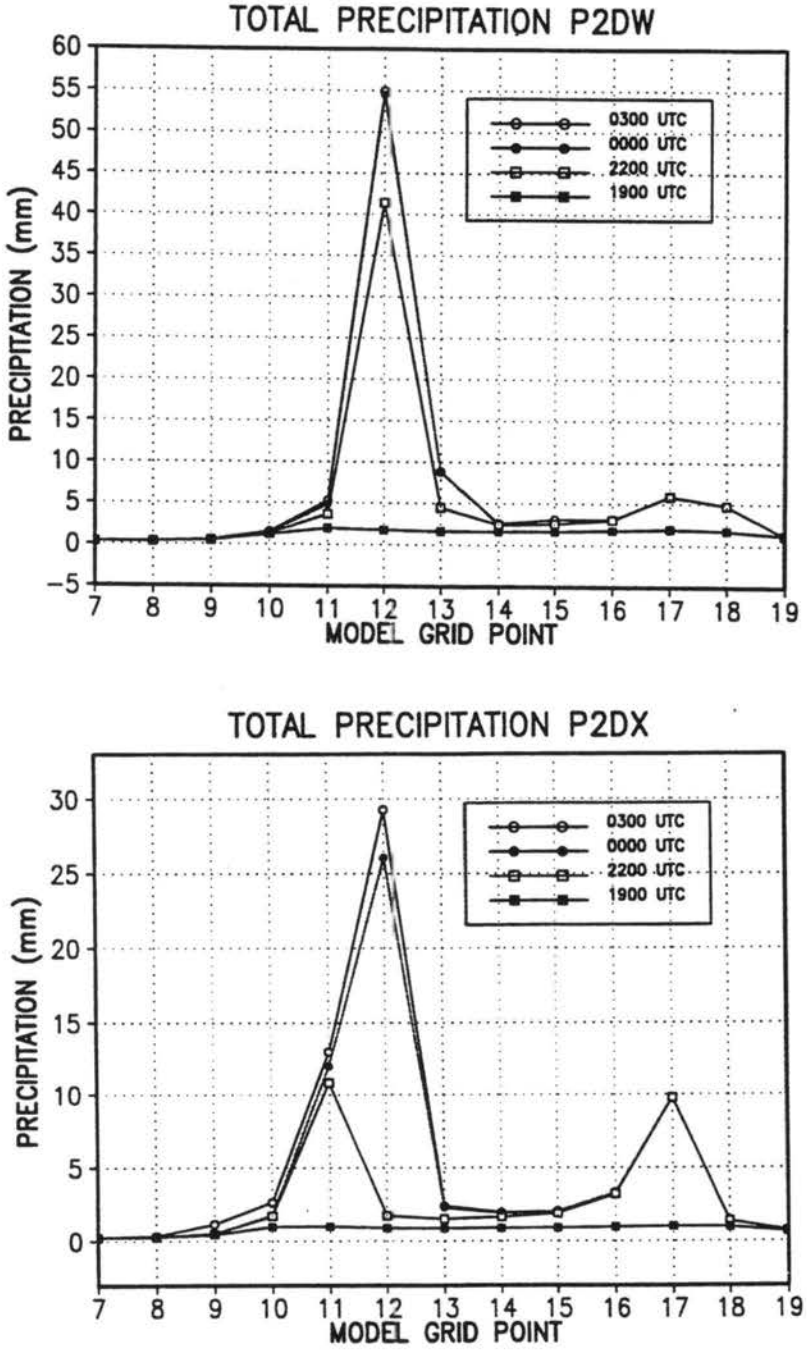

Figure 3.17: The precipitation record from the α sensitivity studies: P2DW and P2DX

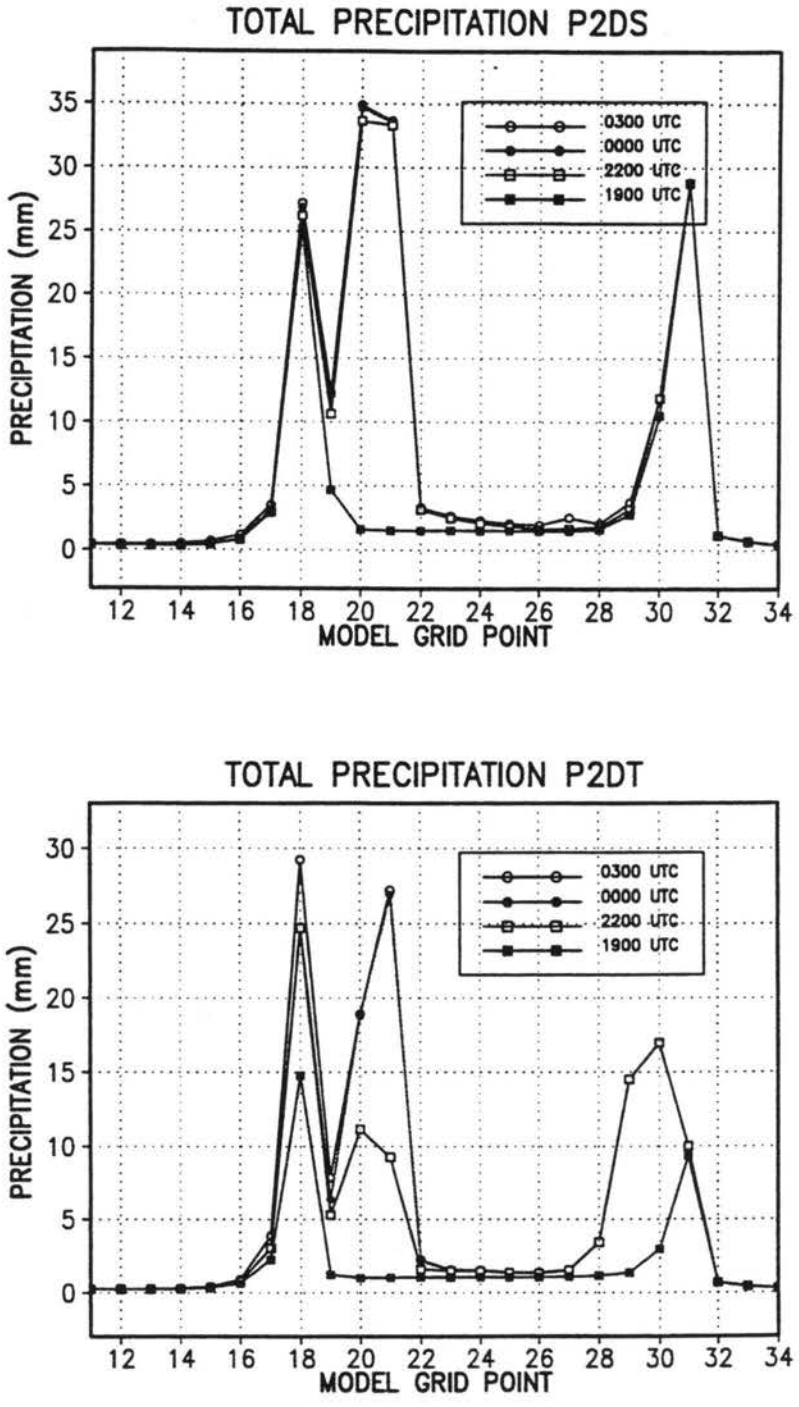

Figure 3.17: continued: P2DS and P2DT

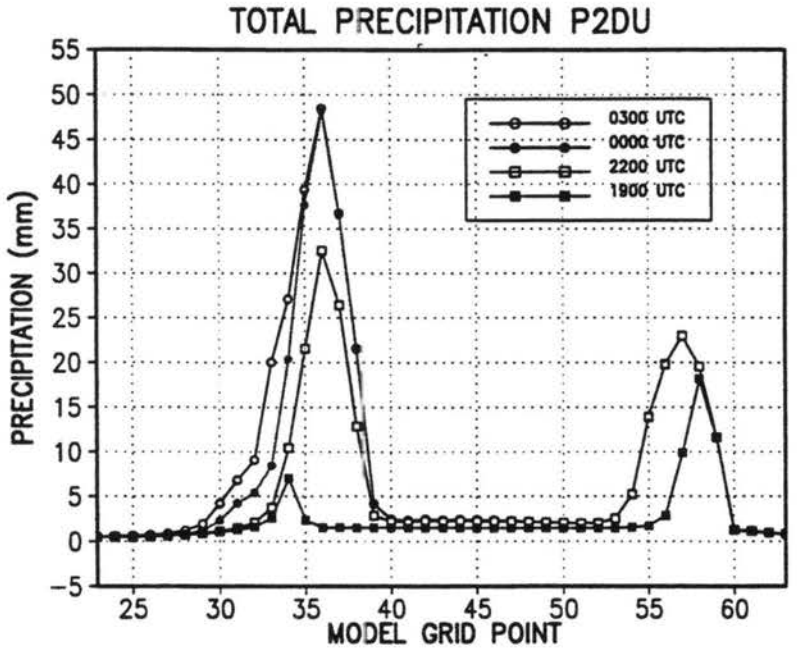

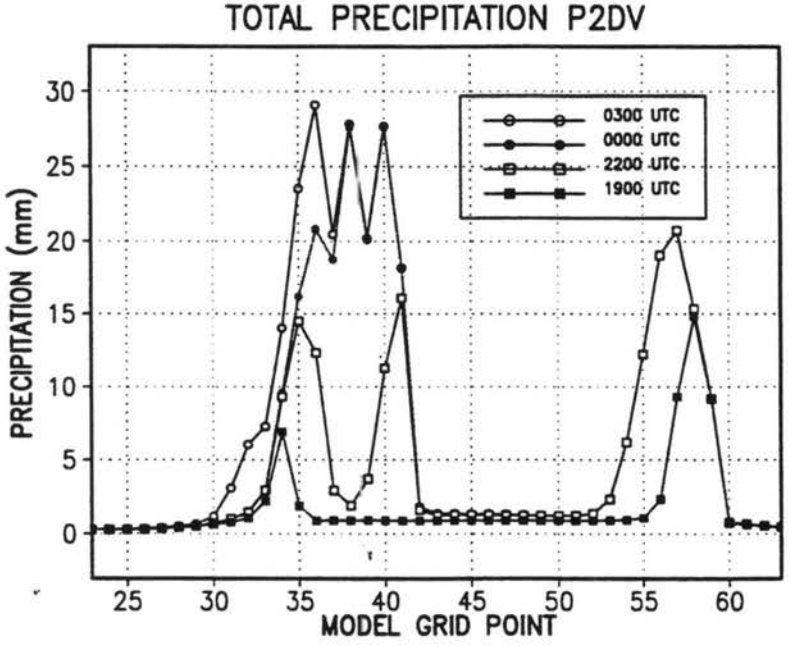

Figure 3.17: continued: P2DU and P2DV

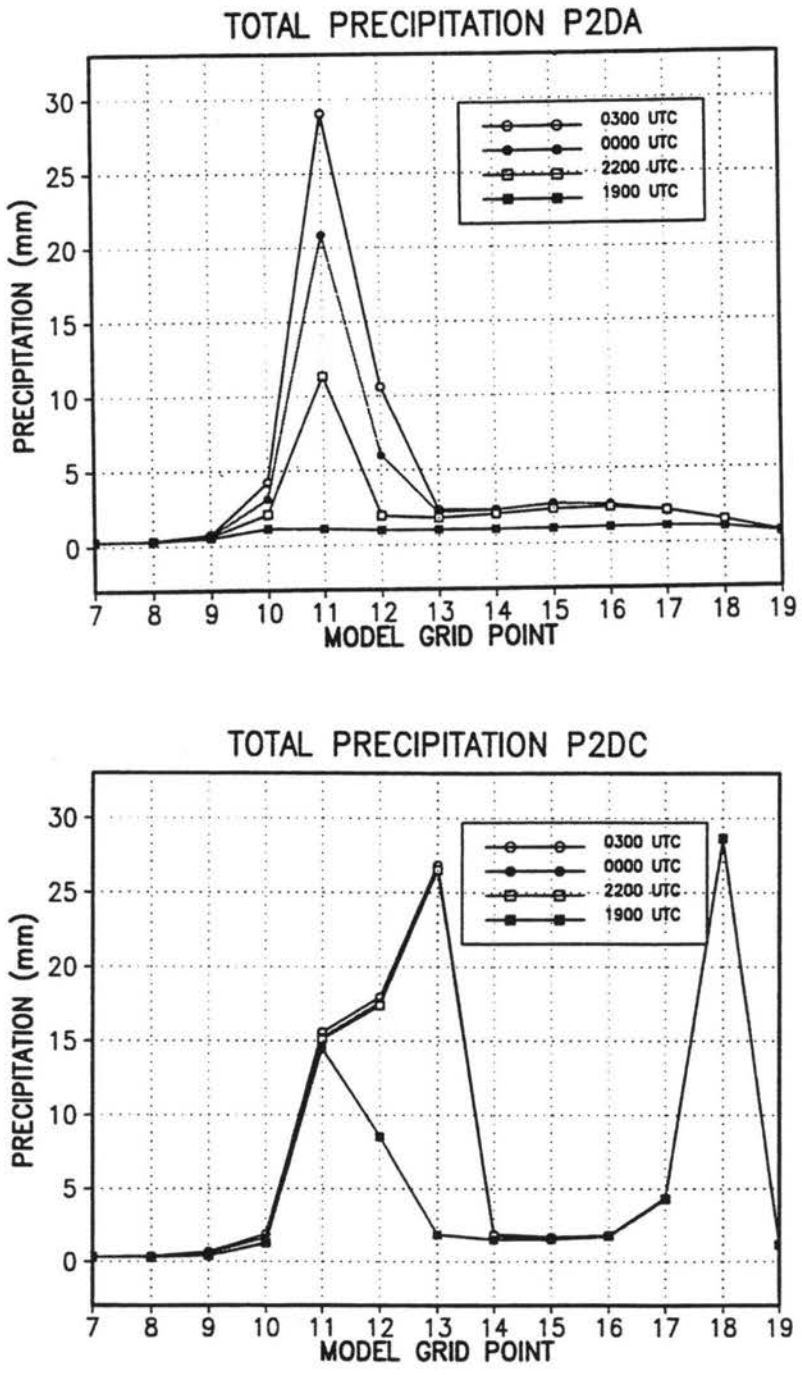

Figure 3.18: The precipitation record from the $\mathcal{A}$ sensitivity studies: P2DA and P2DC

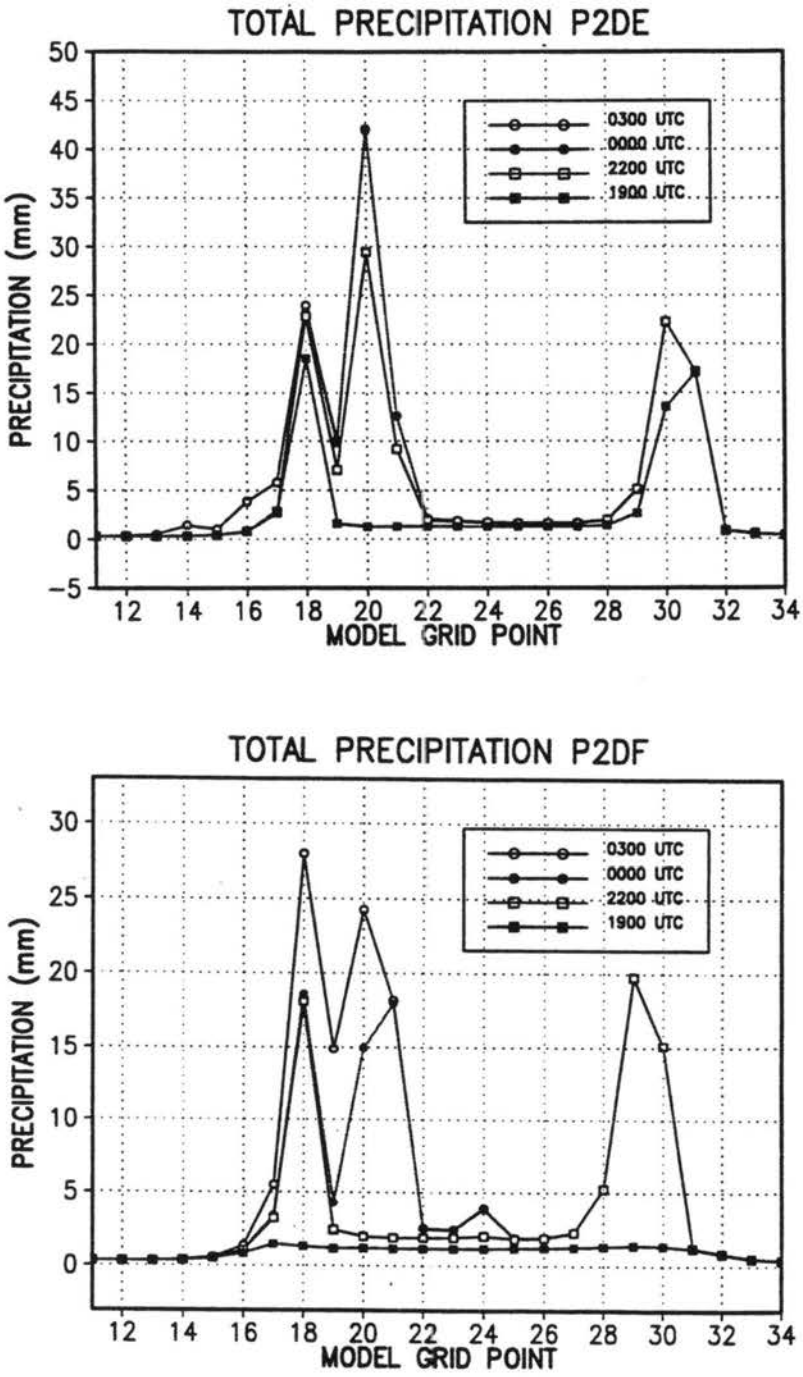

Figure 3.18: continued: P2DE and P2DF

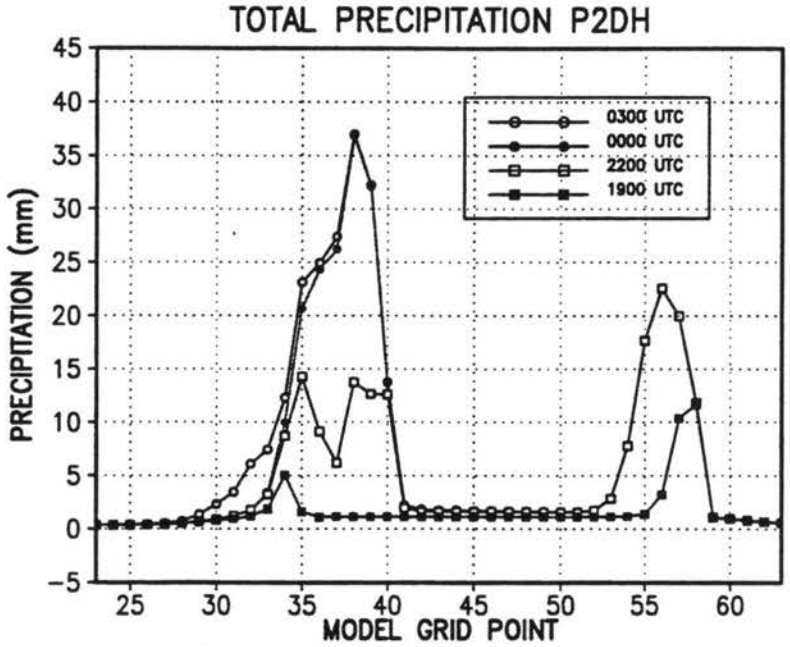

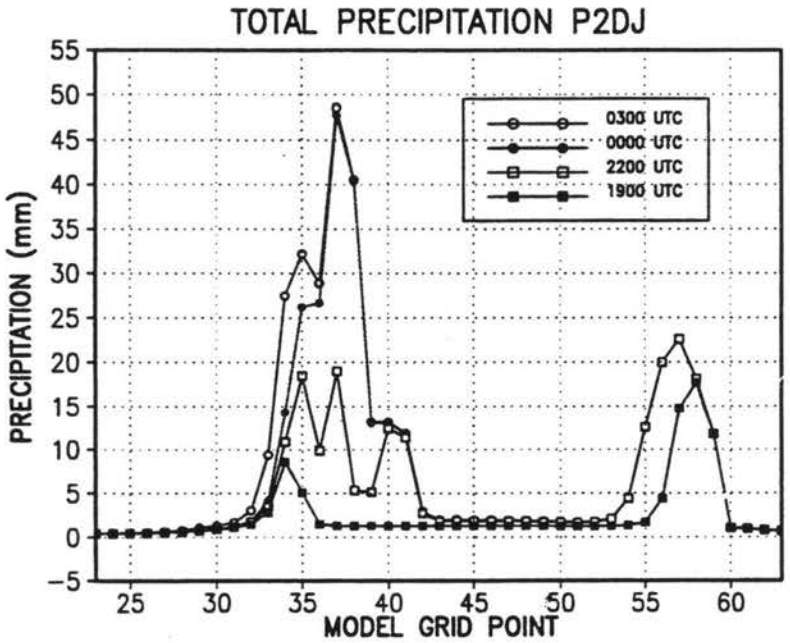

Figure 3.18: continued: P2DH and P2DJ

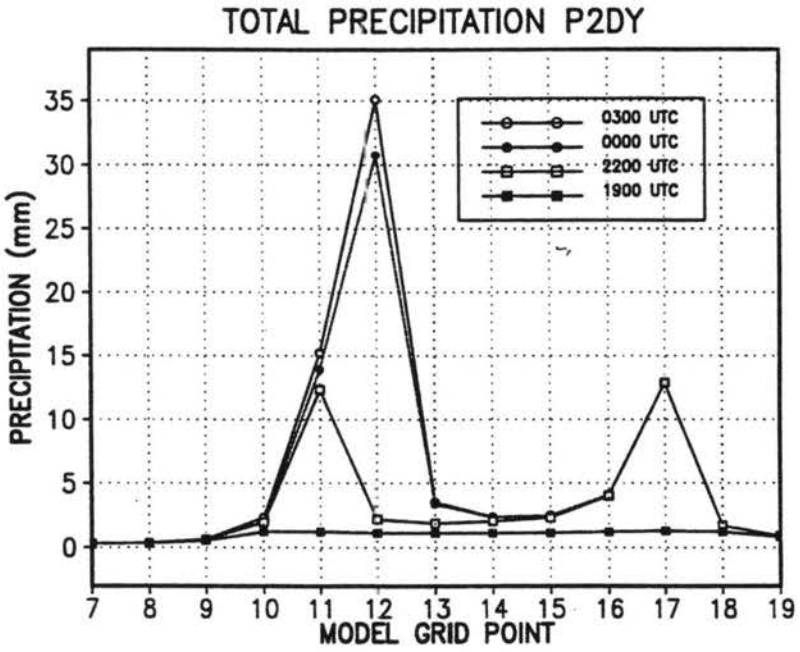

Figure 3.19: The precipitation record from the $\mathcal{A}$ sensitivity studies: P2DY

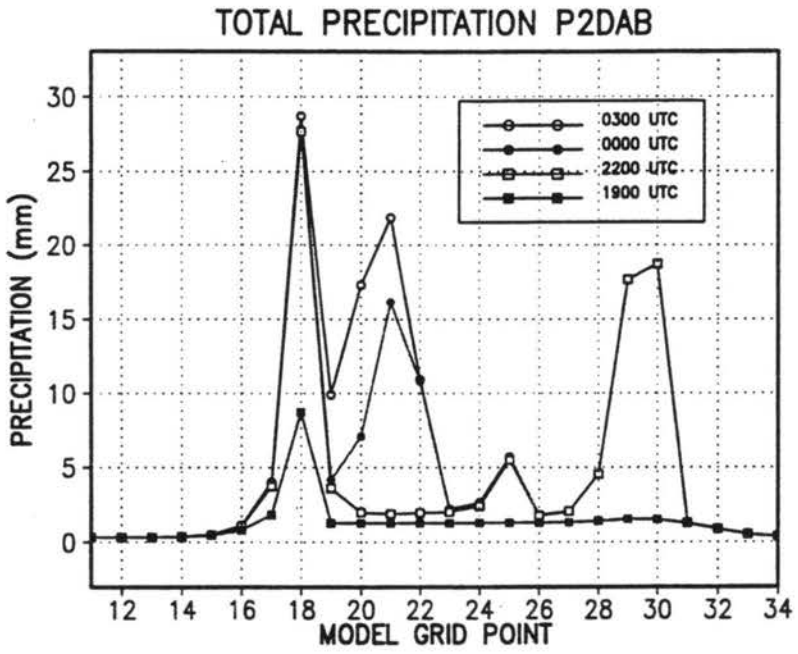

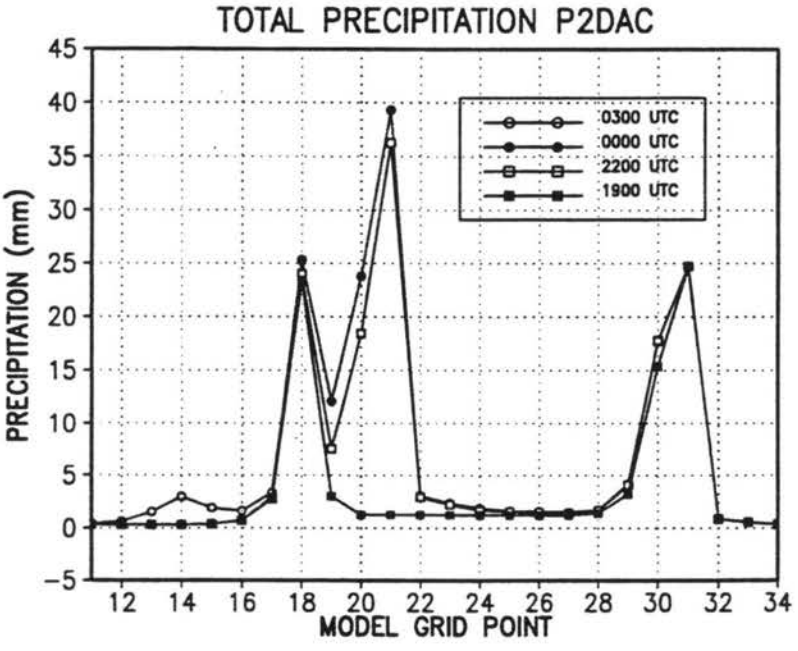

Figure 3.19: continued: P2DAB and P2DAC

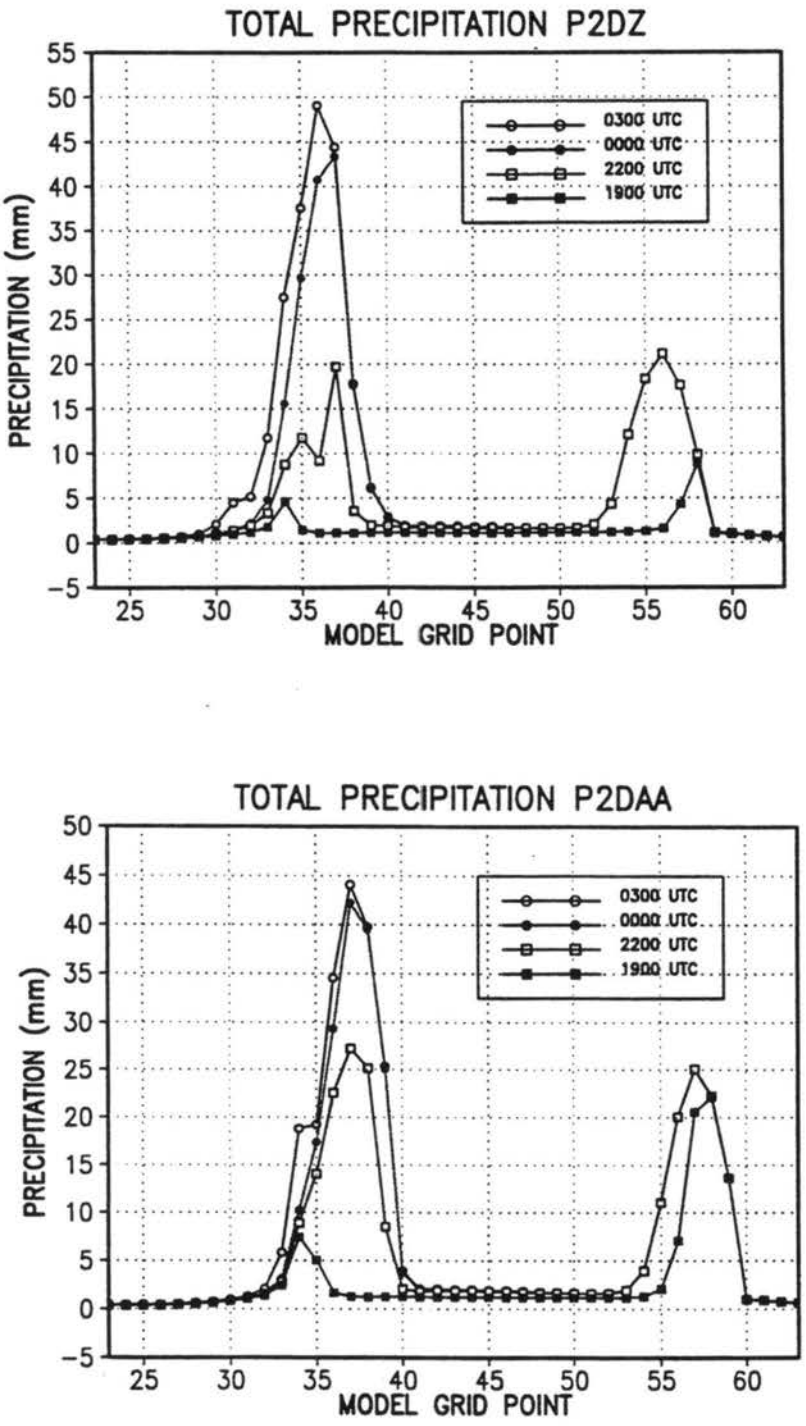

Figure 3.19: continued: P2DZ and P2DAA

3-D AT 1800 UTC

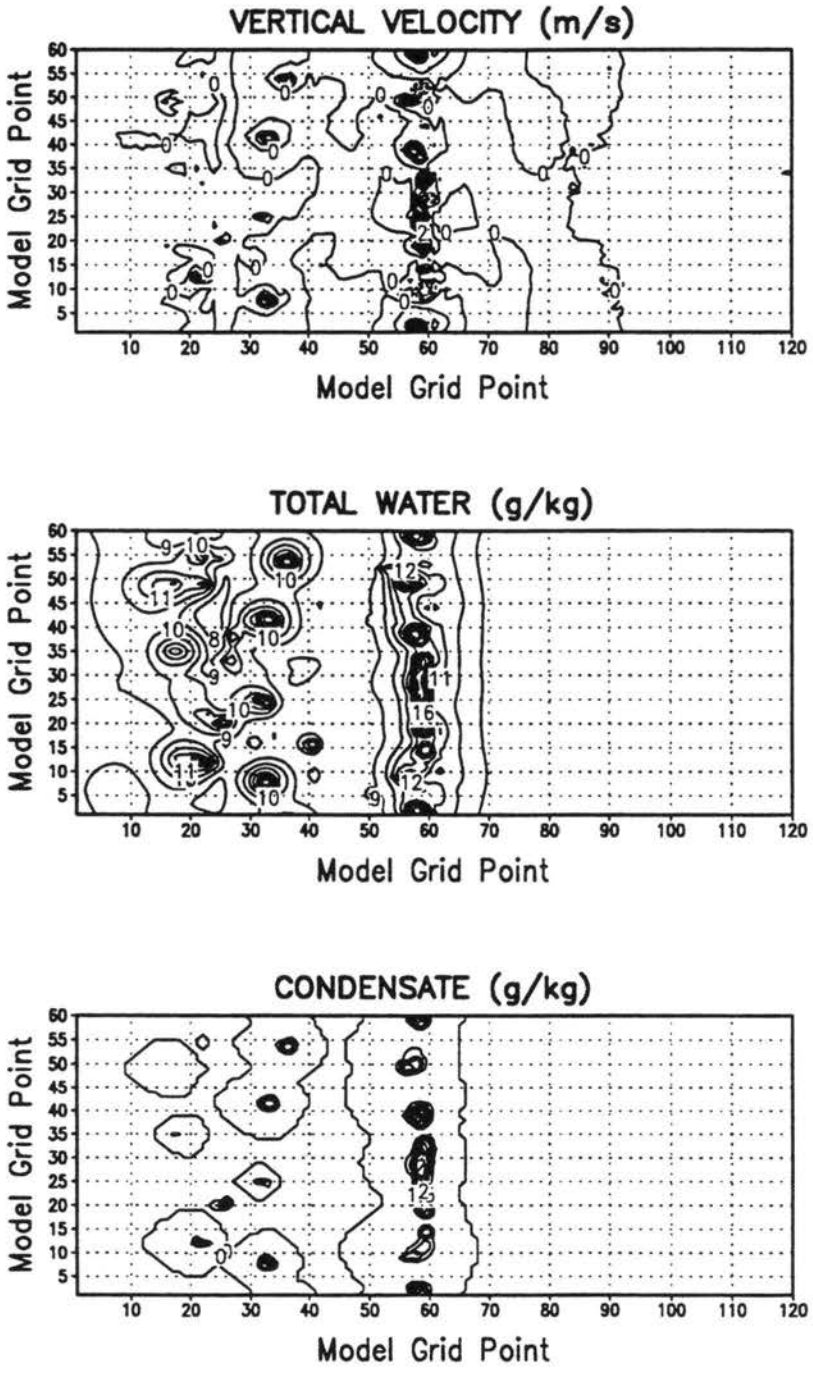

Figure 3.20: Vertical velocity (ms^{-1}), total water mixing ratio ($g\ kg^{-1}$) and condensate mixing ratio ($g\ kg^{-1}$) at 1800 UTC and 2 km AGL: E3DA

3–D AT 1800 UTC
20 KM GRID SPACING

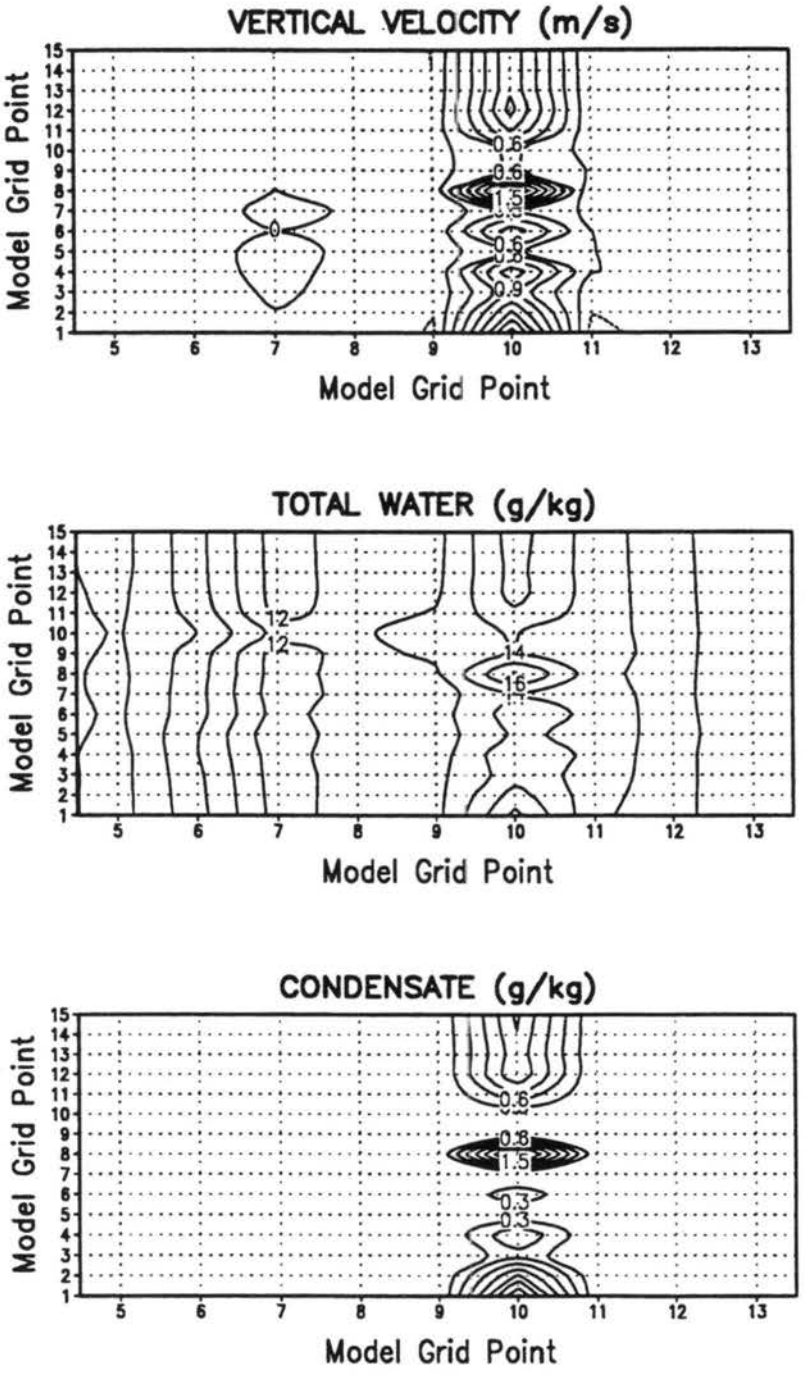

Figure 3.20: continued: P3DA

3-D AT 1800 UTC
12 KM GRID SPACING

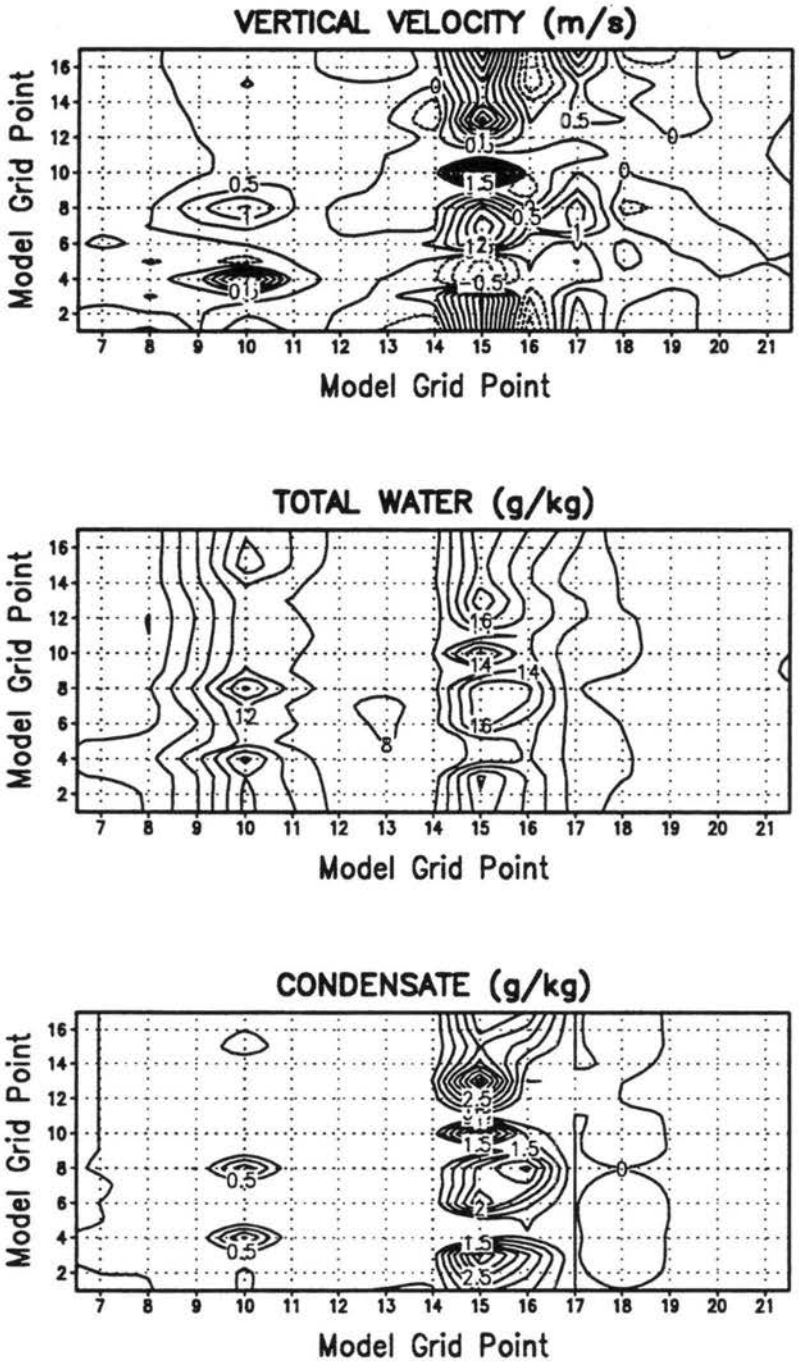

Figure 3.20: continued: P3DB

3-D AT 1800 UTC
6 KM GRID SPACING

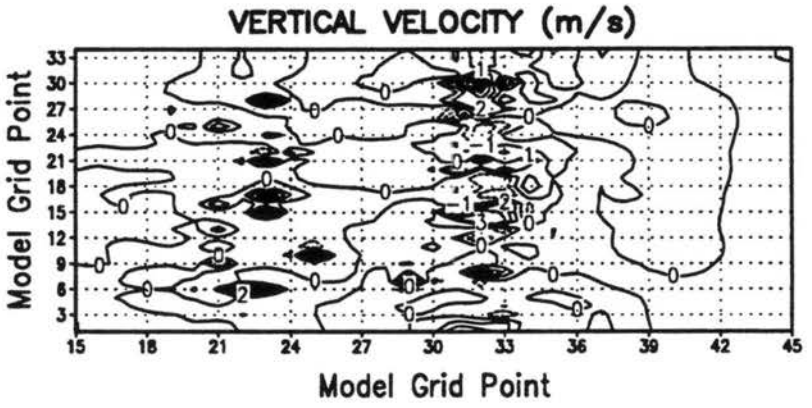

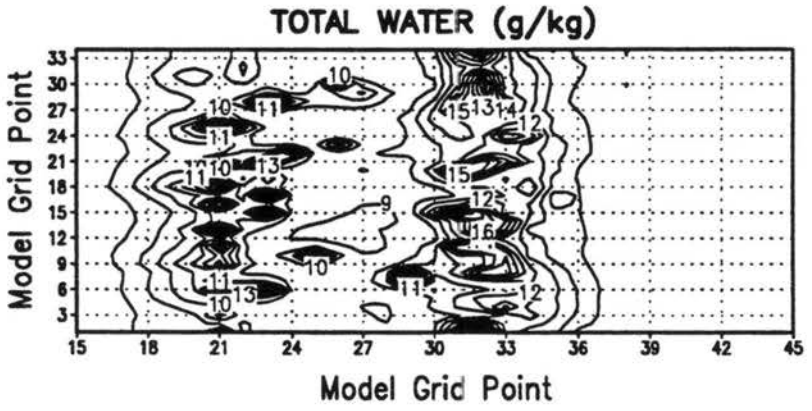

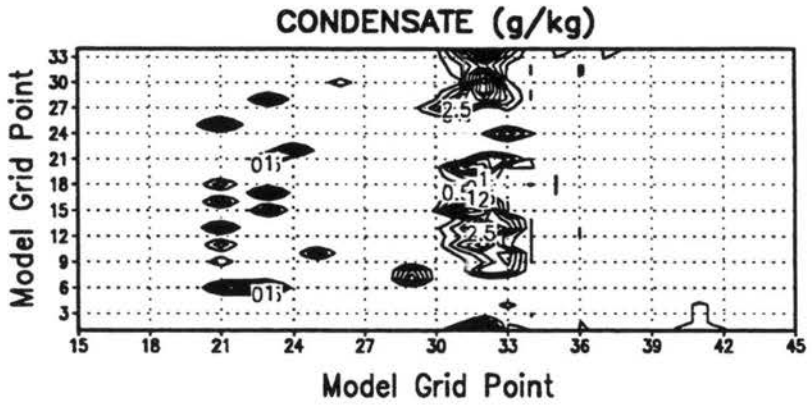

Figure 3.20: continued: P3DC

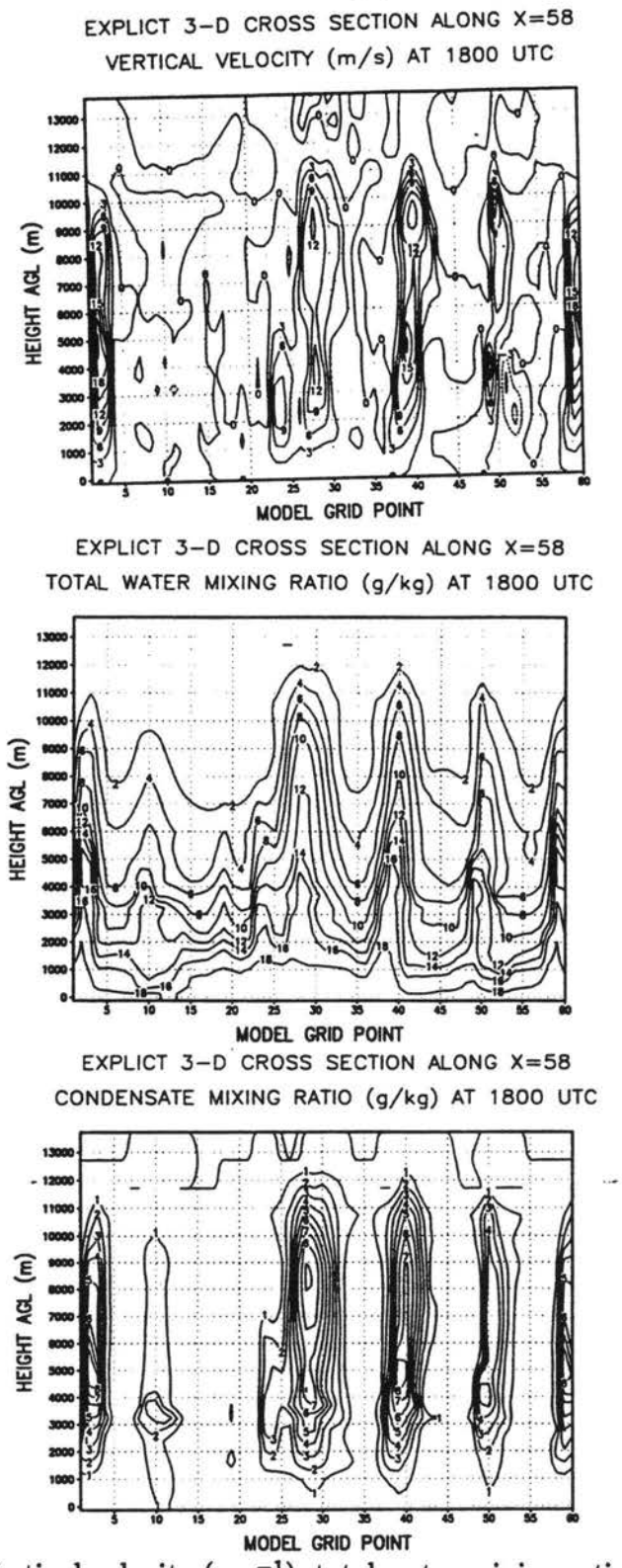

Figure 3.21: Vertical velocity (ms^{-1}), total water mixing ratio ($g\ kg^{-1}$) and condensate mixing ratio ($g\ kg^{-1}$) at 1800 UTC: E3DA

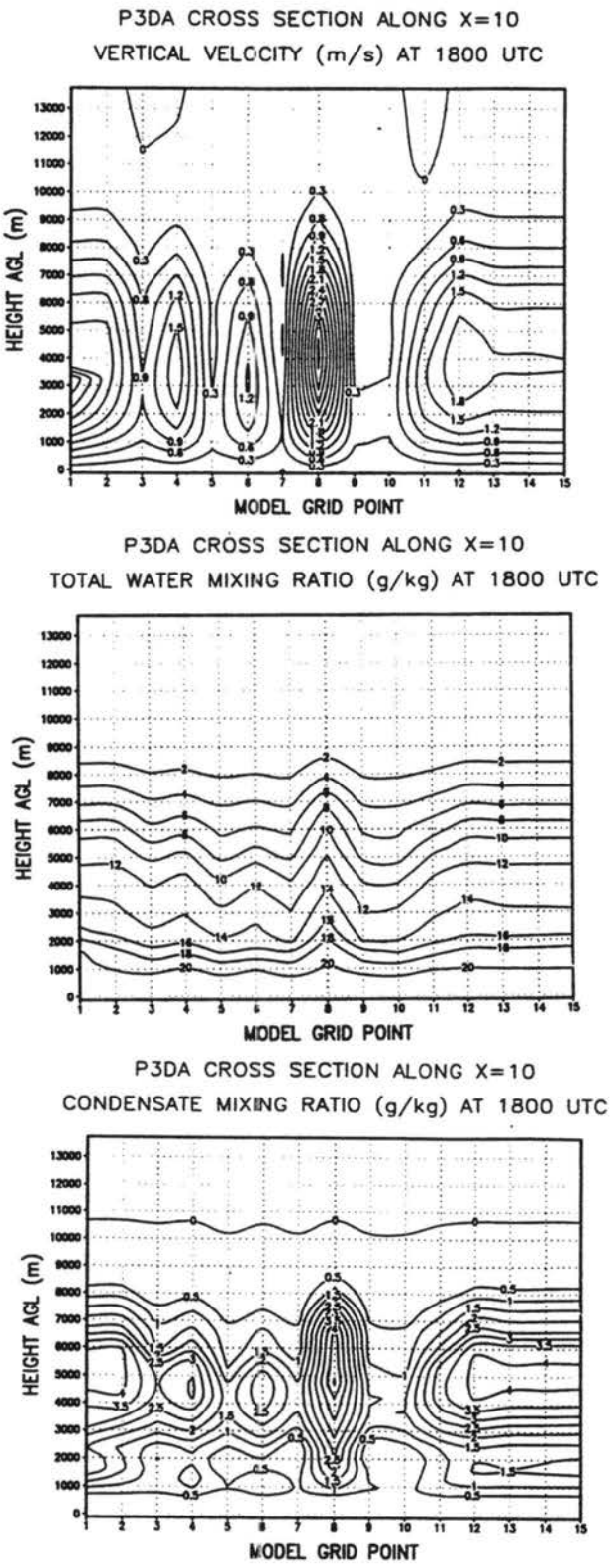

Figure 3.21: continued: P3DA

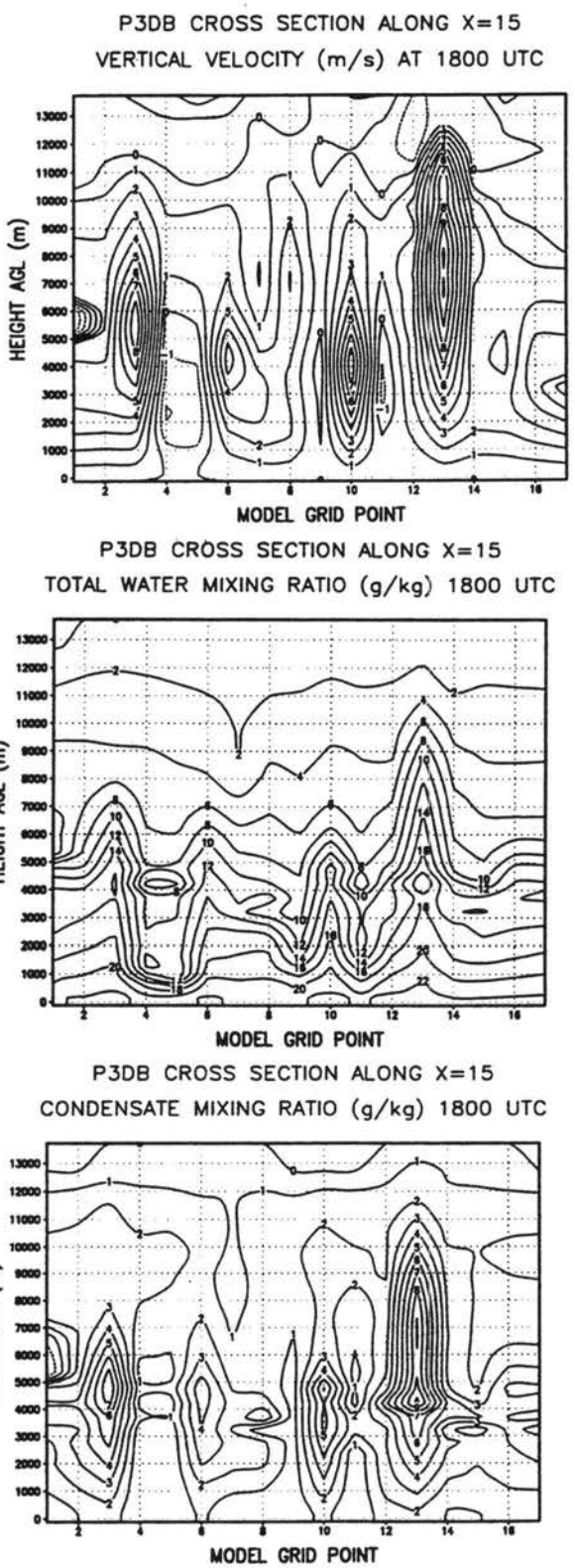

Figure 3.21: continued: P3DB

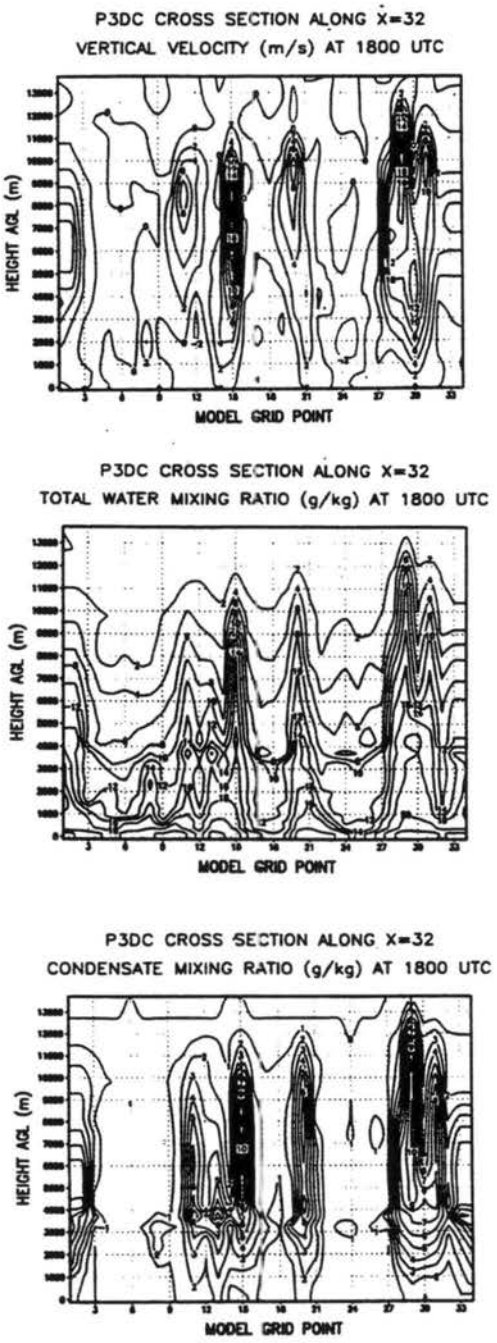

Figure 3.21: continued: P3DC

3–D AT 2115 UTC

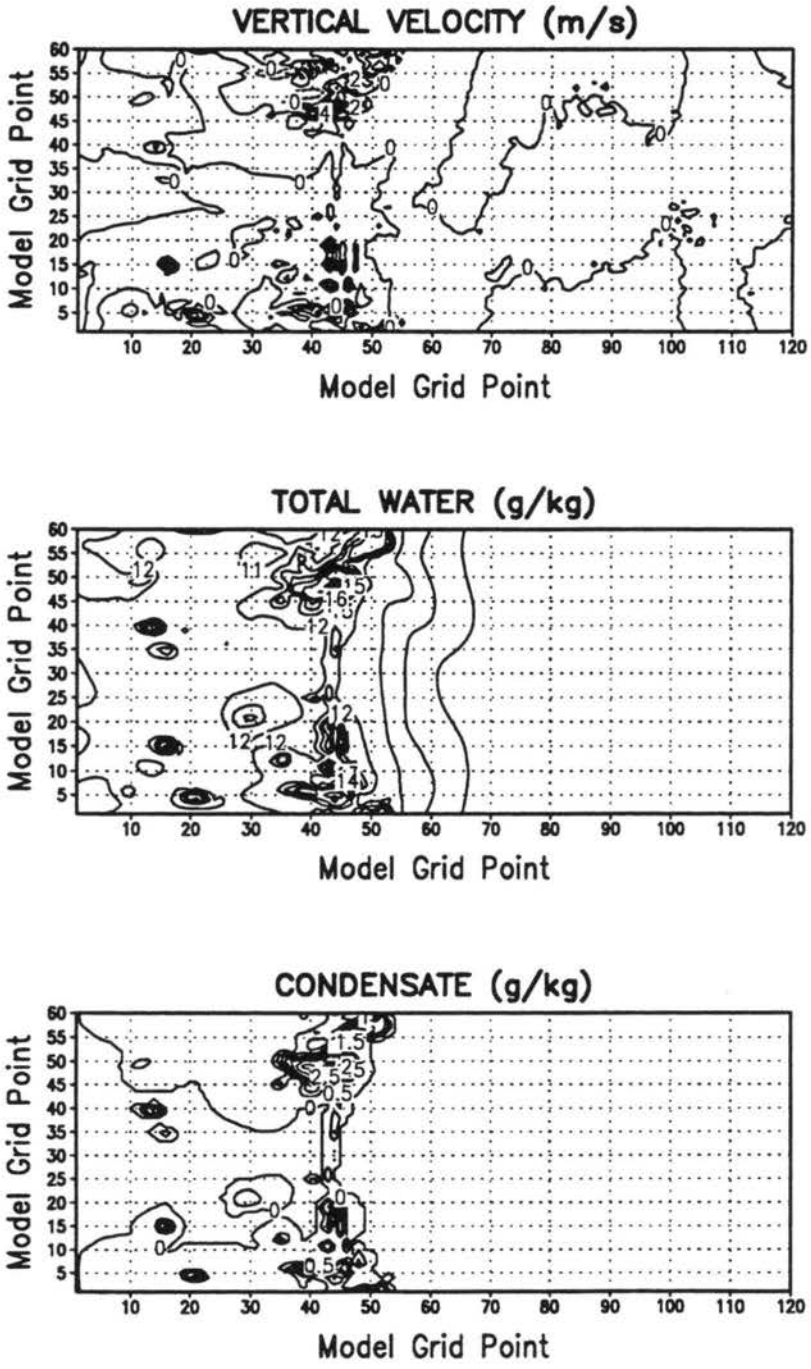

Figure 3.22: Vertical velocity (ms^{-1}), total water mixing ratio ($g\ kg^{-1}$) and condensate mixing ratio ($g\ kg^{-1}$) at 2115 UTC and 2 km AGL: E3DA

3-D AT 2115 UTC
20 KM GRID SPACING

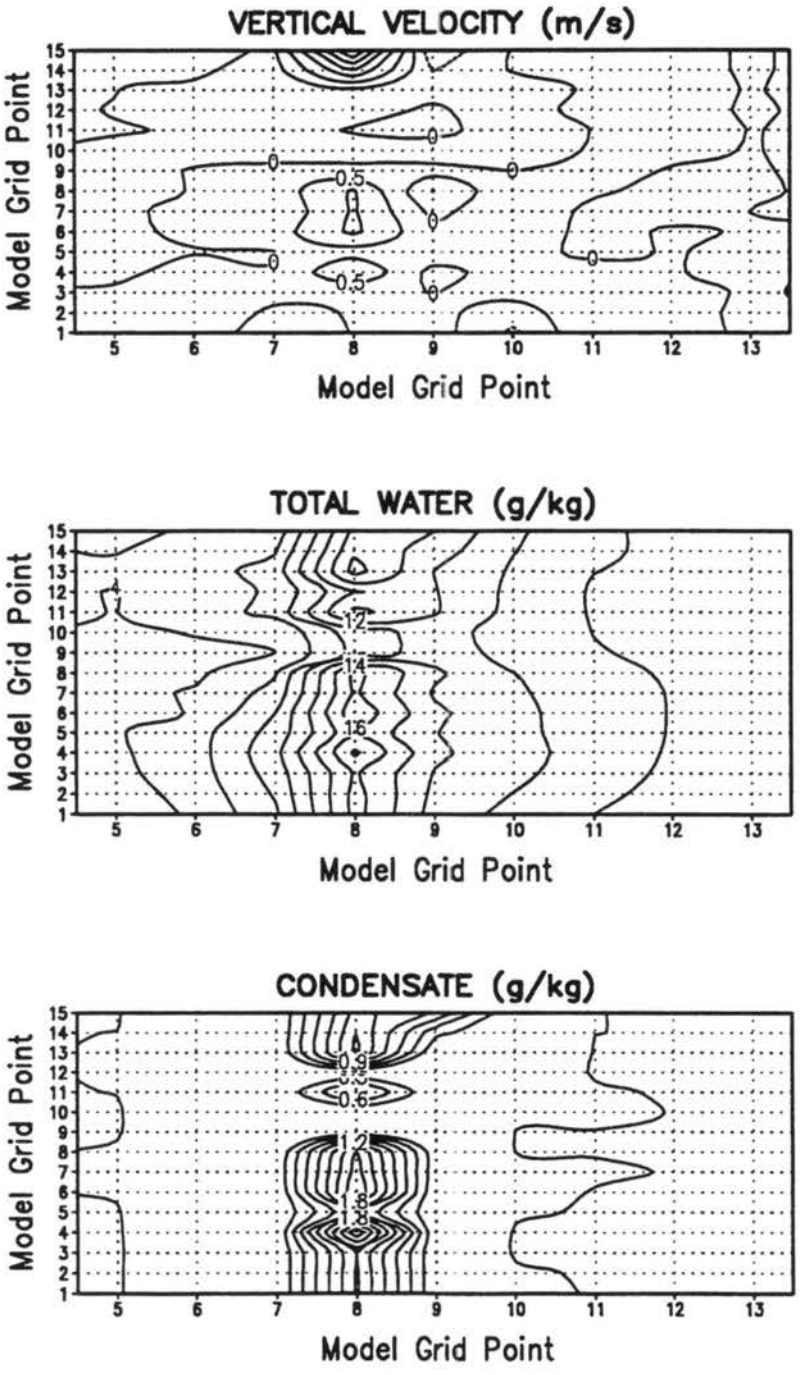

Figure 3.22: continued: P3DA

3–D AT 2115 UTC
12 KM GRID SPACING

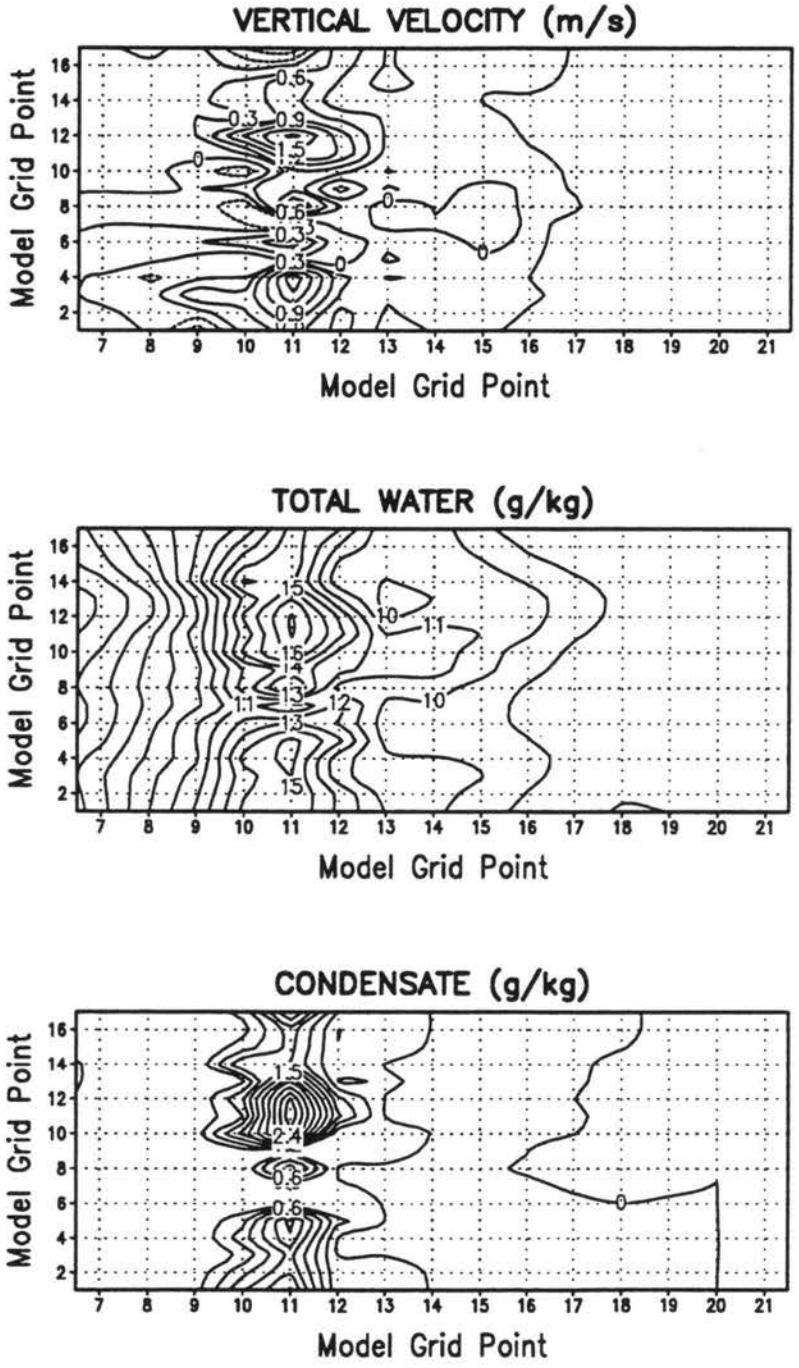

Figure 3.22: continued: P3DB

3-D AT 2115 UTC

6 KM GRID SPACING

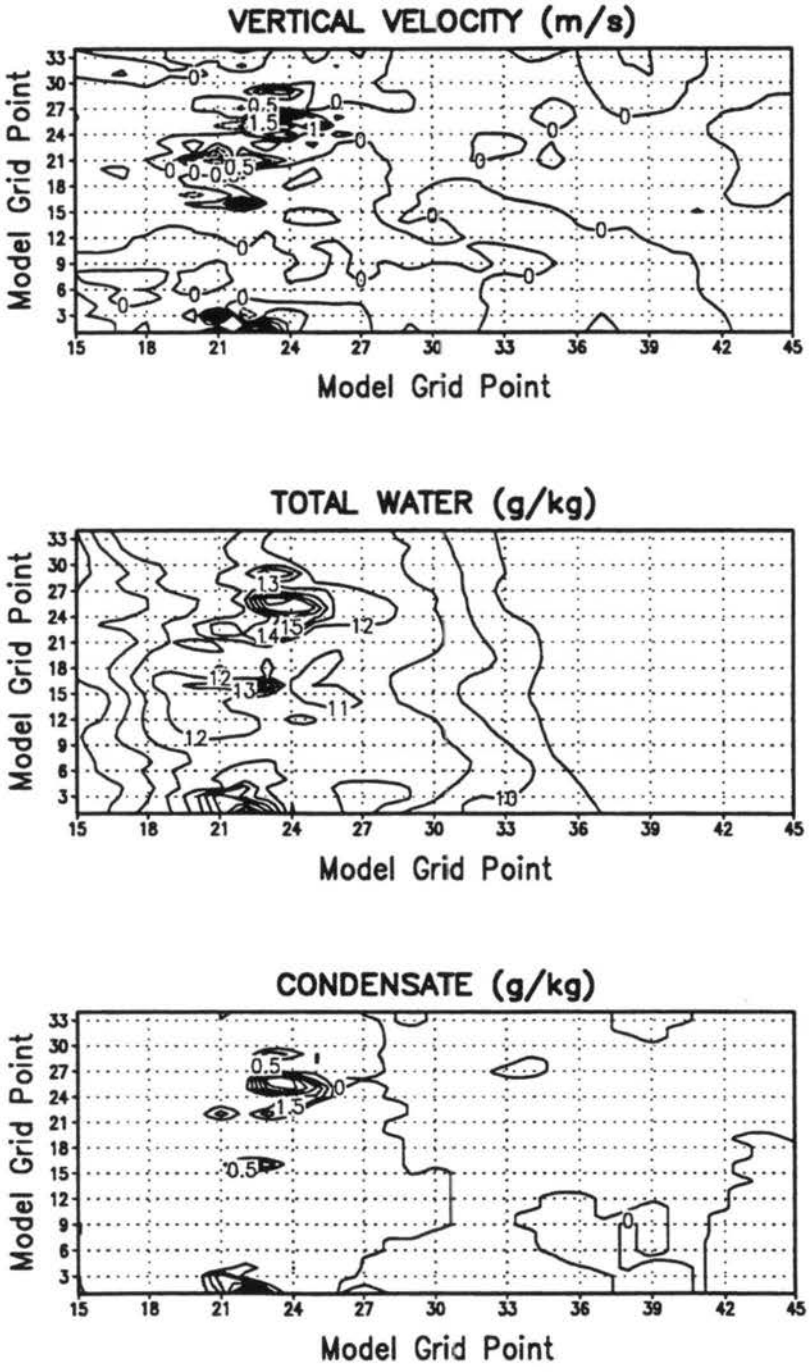

Figure 3.22: continued: P3DC

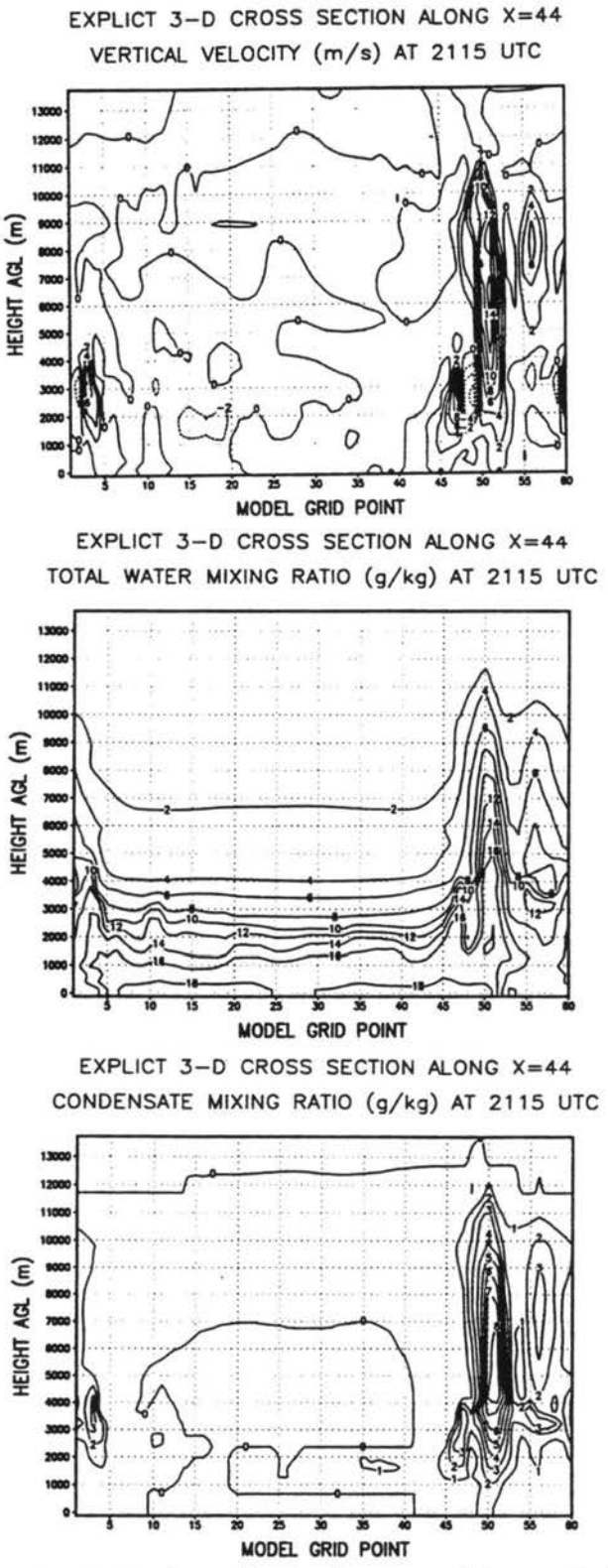

Figure 3.23: Vertical velocity (ms^{-1}), total water mixing ratio ($g\ kg^{-1}$) and condensate mixing ratio ($g\ kg^{-1}$) at 1800 UTC: E3DA

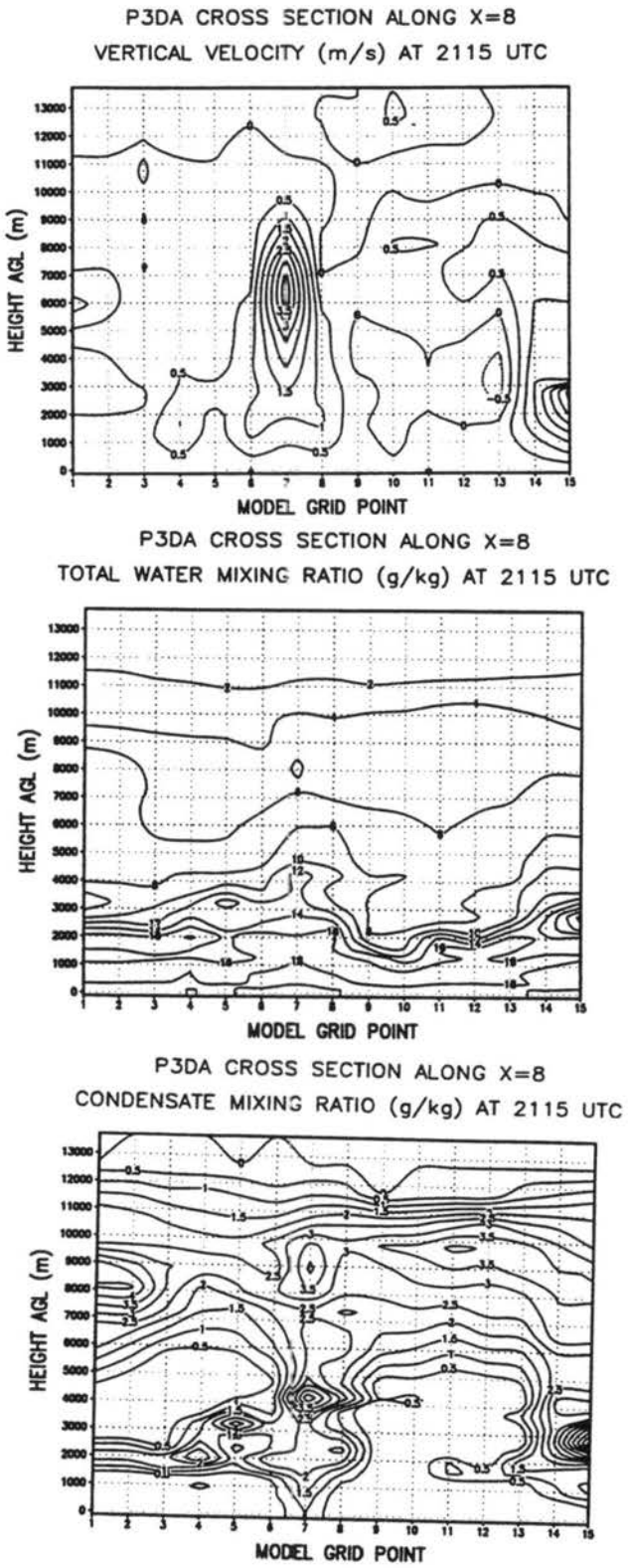

Figure 3.23: continued: P3DA

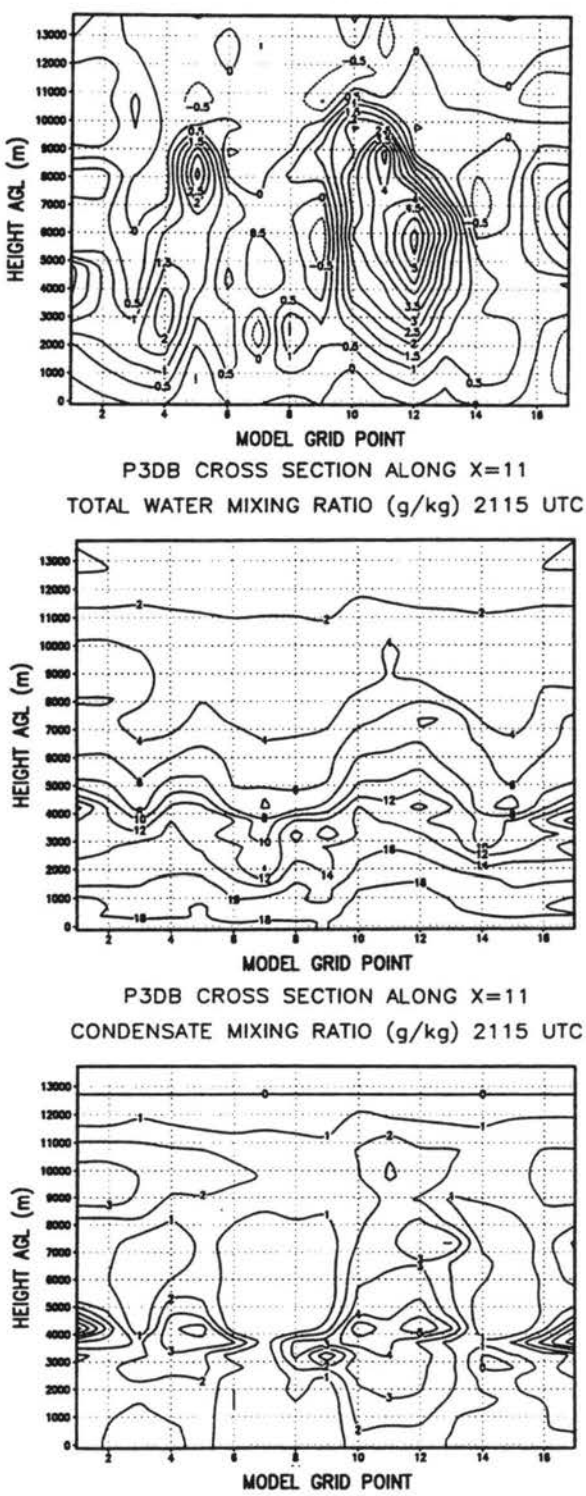

Figure 3.23: continued: P3DB

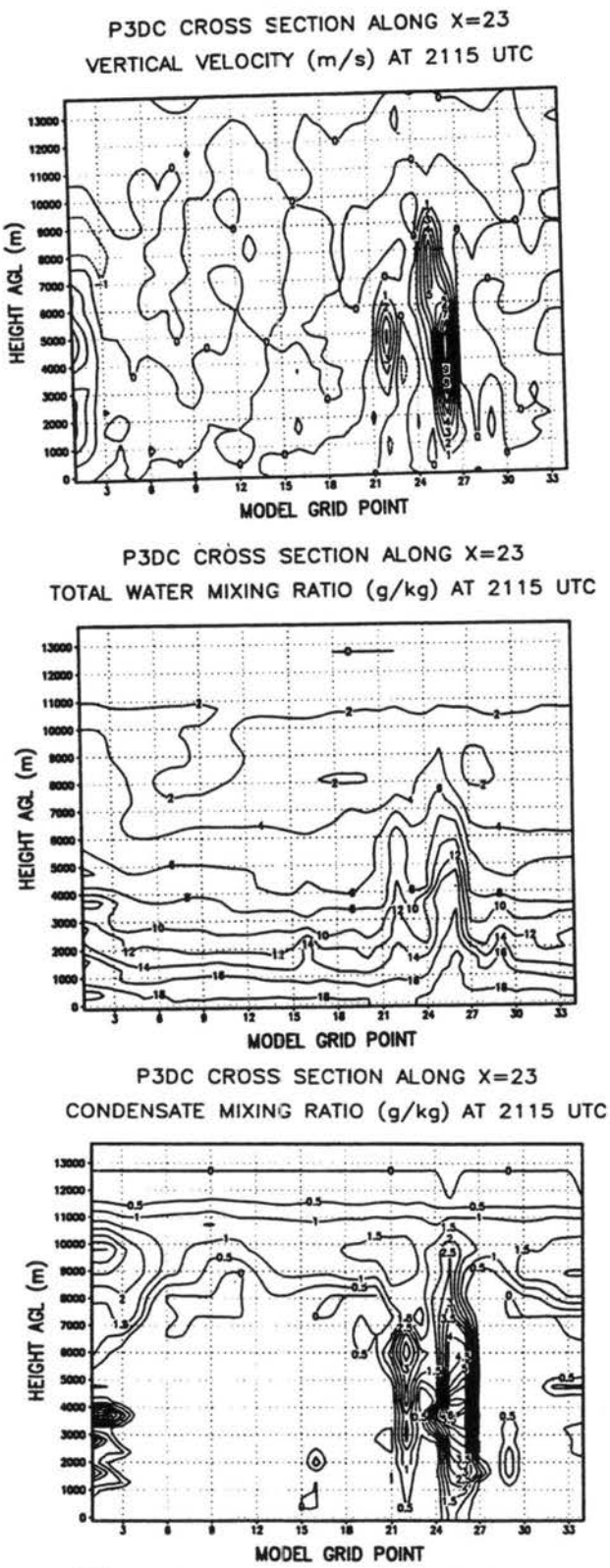

Figure 3.23: continued: P3DC

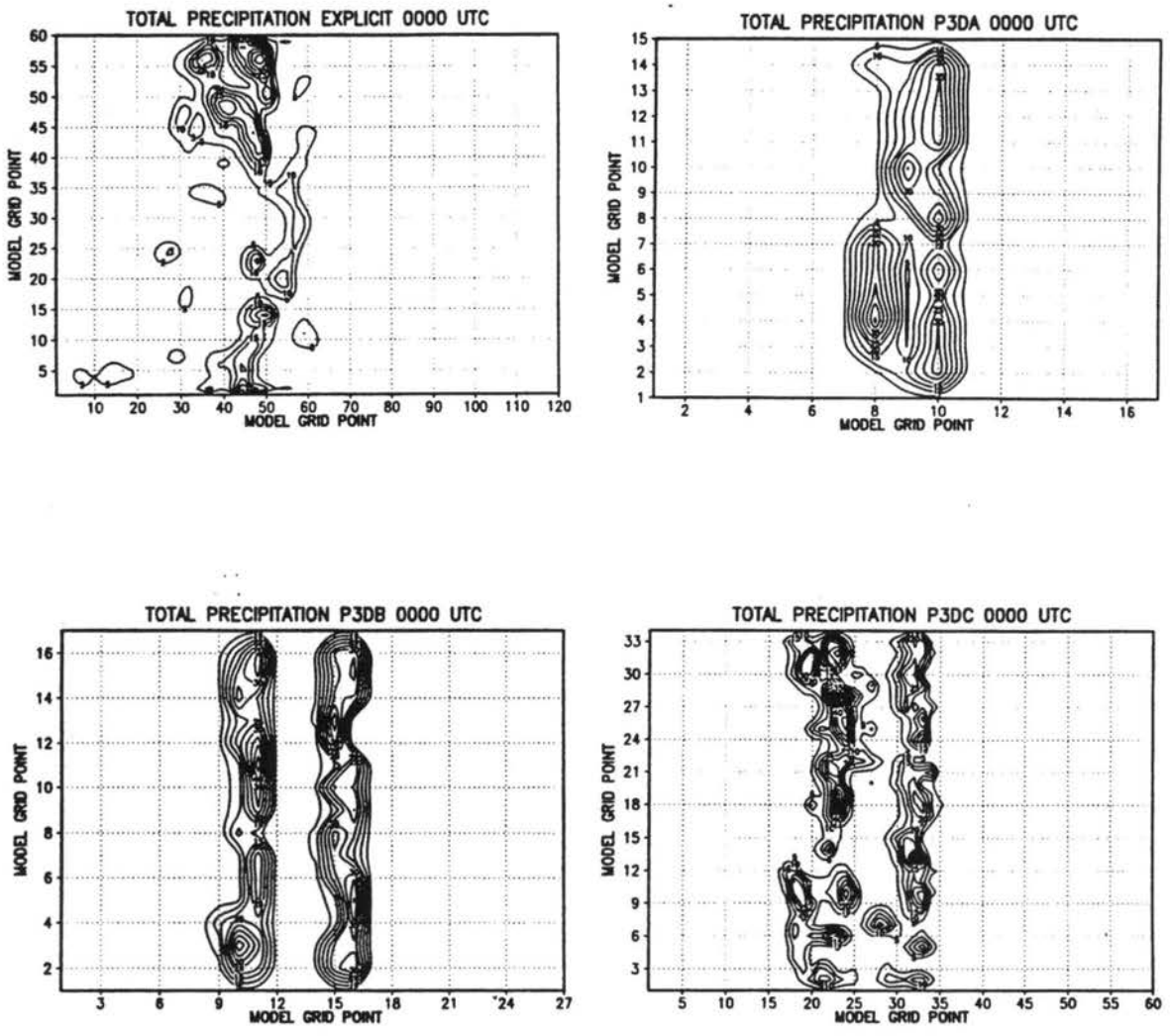

Figure 3.24: Surface precipitation (mm) at 0000 UTC for E3DA, P3DA, P3DB and P3DC.

Chapter 4

SUMMARY AND CONCLUSIONS

A new cumulus parameterization scheme designed for use over a wide range of model grid spacings has been presented. The effects of unresolved cumulus activity is modelled using a combination of a subsident mass flux term and a convective adjustment term. The subsident term is an extension of the Arakawa-Schubert parameterization and uses a prognostic cumulus kinetic energy closure to obtain the large-scale, cloud-base mass flux. The adjustment term is a function of the area growth rate of convective subensembles. The parameterization differs from many others in that there is no explicit trigger function. Also, the adjustment term can nudge the grid value toward or away from the cloud property depending on the whether the sub-ensemble area is expanding or contracting.

In addition to the new scheme, a new philosophical approach has been developed, the basis of which is the idea of the cloud probability density function. The new methodology provides a philosophical continuum for parameterization from the cloud resolving scale to the large-scale and eliminates the need for different parameterizations when the model grid spacing changes. This is an important feature for nested grid models such as RAMS which often have GCM-like grid spacing on the coarsest grid and meso-γ or smaller grid spacing on the finest grid.

The parameterization was tested on a large number of two- and three-dimensional idealized sea-breeze simulations and compared to corresponding cloud resolving simulations. Overall the parameterized fields compared quite well with the fields in the cloud resolving simulation. Sensitivity studies in two-dimensions indicated that the

parameterization was most sensitive to the parameter α and less sensitive to $\mathcal{F}$ and $\mathcal{A}$. This was somewhat expected since α should have an exponential influence while $\mathcal{F}$ and $\mathcal{A}$ are linear parameters.

Because α can be set to a value large enough to effectively shut the parameterization down, there may be a tendency to label it as a trigger function. However, this is not the case. Even with a large α, convection is active. All that α does is control the growth rate of the cloud base mass flux. It does not control whether there is a mass flux associated with convection.

The major strengths of the parameterization are its ability to reproduce the effects of transient, steady-state and multicellular convection. In addition, the need for specifying a trigger function which is globally valid is eliminated. Since the parameterization is valid over a wide range of grid spacing, there is no need to make an arbitrary decision of when to use a different parameterization, and it can be implemented in nested grid models on all the grids. The parameterization also performs significantly better than the Kuo convective parameterization which is the only scheme currently implemented into RAMS. Finally, since there was no guarantee that the parameterization would work at all, we consider the overall success to be a major strength. Additional research and development has the potential to make the parameterization a more attractive alternative to what is currently available to the mesoscale modeller.

The major weakness of the parameterization is the tendency to transport too much water substance into the upper troposphere. The result was most pronounced in the two-dimensional simulations where excessive anvil cloudiness developed. The over abundance of upper level water might be partially remediated with a more properly chosen filter function, by allowing a larger fraction of the cloud condensate to be placed into heavier hydrometeors which will not remain aloft, or by increasing the convective precipitation efficiency factor. The surface precipitation of the two-dimensional simulations compared favorably with the cloud resolving simulation, but

agreement deteriorated in three dimensions. This may be partially due to the sedimentation bug. The final significant, but temporary weakness of the parameterization is that it runs too slow. Because the parameterization was a new development effort, our first priority was simply to get it to run—numerical efficiency took a back seat. We are however, confident that the scheme will be able to be run in the real-time forecast model in the near future. This belief is based on an earlier, prototype version of the scheme which was modified for numerical efficiency and which produced an acceptable level of computing cost. We estimate a clean version of the parameterization will add approximately 5% to 25% additional computing overhead depending on the amount of convective activity.

4.1 Future Research

The first task to be completed in the near future will be to implement the parameterization into the current RAMS code. Hopefully, by this time, the model developers will have fixed the sedimentation bug. Implementation will require modifying the dynamic memory allocation routines to allow for multiple, nested grids and adding the ability to do history restarts with the parameterization activated. Once this is accomplished the next step will be to create a more efficient code and implement the parameterization into the real-time forecast version of RAMS. Additional modifications will include introducing a diagnostic equation for $\mathcal{A}$ which is a function of the Richardson Number, and perhaps a variable precipitation efficiency parameter which is a function of the sub-ensemble (Hack et al. 1989).

Once the parameterization has been incorporated into the standard and forecast version of RAMS, we will be able to test the scheme under realistic atmospheric conditions rather than just idealized sea-breezes. However, we will re-run all the idealized simulations with the properly working version of RAMS. Clearly, the "anvil problem" will have to be addressed. We suspect that a large part of the problem is a result of our ignorance: we just don't have enough experience using the parameterization

to set the constants appropriately. Hopefully, the fix will be rather straight forward. Additional cloud resolving simulations would aid in this effort.

The last major problem that will need to be addressed is the issue of the advection term. Inclusion of this term will generally require the parameterization to be column non-local. Therefore, parameterized convection in one model grid column will directly effect other columns. Besides the closure problems this creates—problems to which we have not found a satisfactory answer—a non-local parameterization will create enormous problems for the forecast model which is run on parallel processors. Until the advection term is properly accounted for, we will keep track of the error we introduce through neglect of the term.

Ideally, we would like to introduce a diagnostic method which will allow for a variable α in time and for each sub-ensemble. This is not a priority and will have to wait until the more serious problems are tackled. Research is also currently underway to connect this parameterization to a Mesoscale Convective System parameterization for use in GCM-scale models (Alexander 1995; Alexander and Cotton 1996a,b; Jiang 1996).

REFERENCES

Alexander, G. David and W. R. and Cotton, 1995: A cumulus parameterization including mass fluxes, vertical momentum dynamics and mesoscale effects. *J. Atmos. Sci.*, **50**, 889-906.

_____, and William R. Cotton, 1996a: The use of cloud-resolving simulations of mesoscale convective systems to build a convective parameterization scheme. I: Simulations. Submitted *J. Atmos. Sci.*

_____, and William R. Cotton, 1996b: The use of cloud-resolving simulations of mesoscale convective systems to build a convective parameterization scheme. II: The parameterization scheme. Submitted *J. Atmos. Sci.*

_____, 1996:

Arakawa, A. and W. H. Schubert, 1974: Interaction of a cumulus cloud ensemble with the large-scale environment, Part I. *J. Atmos. Sci.*, **31**, 674–701.

Arakawa, A. and K. -M. Xu, 1990: The macroscopic behavior of simulated cumulus convection and semiprognostic test of the Arakawa-Schubert cumulus parameterization. *Proc. of the Indo-U.S. seminar on parameterization of sub-grid scale processes in dynamical models of medium-range prediction and global climate.* Pune, India.

Betts, A. K., 1986: A new convective adjustment scheme. Part I: Observational and theoretical basis. *Quart. J. Roy. Meteor. Soc.***112**, 677–691.

_____ and M. J. Miller, 1986: A new convective adjustment scheme. Part I: Single column tests using GATE wave, BOMEX, ATEX and arctic air-mass data sets. *Quart. J. Roy. Meteor. Soc.*, **112**, 677–691.

_____ and P. L. Silva Dias, 1977: Modeling of convective downdrafts. Preprints, *11th Tech. Conf. on Hurricanes and Tropical Meteor.,* Miami, FL Amer. Met. Soc., 508-511.

Blanchard, D. O. and R. E. Lopez, 1984: Variability of the convective field pattern in South Florida and its relationship to the synoptic flow. NOAA Technical Memorandum ERL ESG-4. Environmental Sciences Group, Boulder, CO. 77 pp.

Bringi, V. N., I. J. Caylor, J. Turk and L. Liu, 1993a: Microphsyical and electrical evolution of a convective storm using multiparameter radar and aircraft data during CaPE. Preprints 26th Intl. Conf. on Radar Meteorology. *Amer. Met. Soc.* 312–314.

_____, A. Detweiler, V. Chandrasekar, P. L. Smith, L. Liu, I. J. Caylor and D. Musil, 1993: Multiparameter radar and aircraft study of the transition from early to mature storm during CaPE: The case of 9 August 1991 Preprints 26th Intl. Conf. on Radar Meteorology. *Amer. Met. Soc.* 318–320.

_____, K. Knupp, A. Detwiler, L. Liu, I.J. Caylor, and R. A. Black, 1995: Evolution of a Florida thunderstorm during the convection and precipitation/electrification experiment: The case of 9 August 1991. Submitted to MWR.

Burpee, R. W., 1979: Peninsula-scale convergence in the South Florida sea breeze. *Mon. Wea. Rev.*, **107**, 852–860.

_____ and L. N. Lahiff, 1983: Peninsula-scale rainfall variations on sea-breeze days in South Florida. *Mon. Wea. Rev.*, **111**, 520-534.

Caylor, I. J., V. Chandrasekar, V. N. Bringi and S. S. Minger, 1993: Multiparameter radar observations of lightning. Preprints 26th Intl. Conf. on Radar Meteorology. *Amer. Met. Soc.* 306–308.

Cotton, W. R. and R. A. Anthes, 1989: Storm and cloud dynaimcs. Academic Press, Inc. 883 pp.

Dalu, G. A. and R. A. Pielke, 1989: An analytical study of the sea breeze. *J. Atmos. Sci.*, **46**, 1815–1825.

Emanuel, K. A., 1991: A scheme for representing cumulus convection in large-scale models. *J. Atmos. Sci.*, **48**, 2313–2335.

Fritsch, J. M. and C. F. Chappell, 1980: Numerical prediction of convectively driven mesoscale pressure systems. Part I: Convective parameterization. *J. Atmos. Sci.*, **37**, 1722–1733.

Gannon, Sr. P.T., 1978: Influence of earth surface and cloud properties on the South Florida sea breeze. NOAA Technical Memorandum ERL 402 NHEML 2. U.S. Dept. of Commerce, Boulder, CO. 91 pp.

Gaudet, B. J. 1996: Statistical analysis of Winter orographic precipitation forecasts using a bulk microphysical model. Master's Thesis, Colorado State University, Fort Collins, CO.

Geisler, J. E. and F. P. Bretherton, 1969: The sea breeze front runner. *J. Atmos. Sci.*, **26**, 82-95.

Grasso, L. D. and W. R. Cotton, 1995: Numerical simulation of a tornado vortex. *J. Atmos. Sci.*, **52**, 1192-1203.

Pielke, R. A., 1973: An observational study of cumulus convective patterns in relation to the sea breeze over South Florida. NOAA Technical Memorandum ERL OD-16, U.S. Dept. of Commerce, Boulder, CO. 81 pp.

_____, 1974: A three-dimensional numerical model of the sea breezes over South Florida. *Mon. Wea. Rev.*, **102**, 115-139.

_____ and Y. Mahrer, 1978: Verification analysis of the University of Virginia three-dimensional mesoscale model prediction over South Florida for 1 July, 1973. *Mon. Wea. Rev.*, **106**, 1568–1589.

Hack, J. J., W. H. Schubert, and P. L. Silva Dias, 1984: A spectral cumulus parameterizations for use in numerical models of the tropical atmosphere. *Mon. Wea. Rev.*, **112**, 704-716.

Hallet, J., R. I. Sax, D. Lamb and A. S. R. Murty, 1978: Aircraft measurements of ice in Florida cumuli. *Quart. J. Roy. Meteor. Soc.*, **104**, 631–651.

Jiang, H., R. L. McAnelly and W. R. Cotton, 1996: The trigger function to activate an MCS parameterization scheme in GCM. *Proc. 7th Conf. on Mesoscale Processes.* Reading, UK.

Johnson, R. H. 1976: The role of convective-scale precipitation downdrafts in cumulus and synoptic-scale interactions. *J. Atmos. Sci.*, **33**, 1890–1910.

Kain and Fritsch, 1990: A one-dimensional entraining/detraining plume model and its application in convective parameterization. *J. Atmos. Sci.*, **47**, 2784-2802.

Keller, V. W. and R. I. Sax, 1980: Microphysical development of a pulsating cumulus tower: a case study. *Quart. J. Roy. Meteor. Soc.*, **107**, 679–697.

Kreitzberg, C. W. and D. J. Perkey, 1976: Release of potential instability: Part I. A sequential plume model within a hydrostatic primitive equation model. *J. Atmos. Sci.*, **33**, 456–475.

Kuo, H. L., 1965: On the formation and intensification of tropical cyclones through latent heat release by cumulus convection. *J. Atmos. Sci.*, **22**, 40–63.

Liu, L., V. N. Bringi, I. J. Caylor and V. Chandrasekar, 1993: Intercomparison of multiparameter radar signatures from Florida storms. Preprints 26th Intl. Conf. on Radar Meteorology. *Amer. Met. Soc.*, 733–735.

Lord and A. Arakawa, 1980: Interaction of a cumulus cloud ensemble with the large-scale environment, Part II. *J. Atmos. Sci.*, **37**, 2677–2692.

Nicholls, M. E. R. A. Pielke and W. R. Cotton, 1991: A two-dimensional numerical investigation of the interaction between sea breezes and deep convection over the Florida peninsula. *Mon. Wea. Rev.*, **119**, 298–323.

Olsson, P. Q. and W. R. Cotton, 1996: Rapid vortex generation in a simulated meso-scale convective system. *Proc. 7th Conf. on Mesoscale Processes*, Reading, U.K.

Pan, D. -M., 1995: Development and application of a prognostic cumulus parameterization. Ph.D. Dissertation. Colorado State University, 207pp.

Press, W. H., S. A. Teukolsky, W. T. Vettering, and B. P. Flannery, 1992: Numerical recipes in C. Cambridge University Press, 994 pp.

Randall, D. A., and D. -M. Pan, 1993: Implementation of the Arakawa-Schubert cumulus parameterization with a prognostic closure. *Cumulus Parameterization*, Meteorological Monograph published by the American Meteorological Society, K. Emanuel and D. Raymond, Eds., pp. 137 - 144.

Sax, R. I. and V. W. Keller, 1979: Water-ice and water-updraft relationships near $-10°C$ within populations of Florida Cumuli. *J. Atmos. Sci.*, **36**, 505–514.

Simpson, J. and V. Wiggert, 1969: Models of precipitating cumulus towers. *Mon. Wea. Rev.*, **97**, 471–489.

Stevens B. J., G. Feingold and W. R. Cotton, 1996: Elements of the microphysical structure of numerically simulated nonprecipitating stratocumulus. *J. Atmos. Sci.*, **53**, 980-1006.

Weisman, M. L and J. B. Klemp, 1982: The dependence of numerically simulated convective storms on vertical wind shear and buoyancy. *Mon. Wea. Rev.*, **110**, 504–520.

Weissbluth, M.J., 1991: Convective parameterization in mesoscale models. Ph.D. Dissertation, Colorado State University, 211 pp.

Weissbluth, M. J., and W. R. Cotton, 1993a: The representation of convection in mesoscale models. Part I: Scheme fabrication and calibration. *J. Atmos. Sci.*, **51**, 3852–3872.

Weissbluth, M. J., and W. R. Cotton, 1993b: Personal communication.

Williams, S. F., K. Caesar and K Southwick, 1992: The convection and precipitation electrification operations summary and data inventory. National Center for Atmospheric Research, Office of Field Project Support, Boulder, Colorado.

Xu, K. -M. 1991: The coupling of cumulus convection with large-scale processes. Ph.D. Dissertation, University of California, Los Angeles, 250 pp.

Xu, K. -M., and A. Arakawa, 1992: Semiprognostic tests of the Arakawa-Schubert cumulus parameterization using simulated data. *J. Atmos. Sci.*, **49**, 2421–2436.

Yanai, M., S. Esbensen and J. -H. Chu, 1973: Determination of bulk properties of tropical cloud clusters from large-scale heat and moisture budgets. *J. Atmos. Sci.*, **30**, 611–627.